MIT OpenCourseWare
http://ocw.mit.edu

Continuum Electromechanics

For any use or distribution of this textbook, please cite as follows:

Melcher, James R. *Continuum Electromechanics*. Cambridge, MA: MIT Press, 1981. Copyright Massachusetts Institute of Technology. ISBN: 9780262131650. Also available online from MIT OpenCourseWare at http://ocw.mit.edu (accessed MM DD, YYYY) under Creative Commons license Attribution-NonCommercial-Share Alike.

For more information about citing these materials or our Terms of Use, visit: http://ocw.mit.edu/terms.

8

Statics and Dynamics of Systems Having a Static Equilibrium

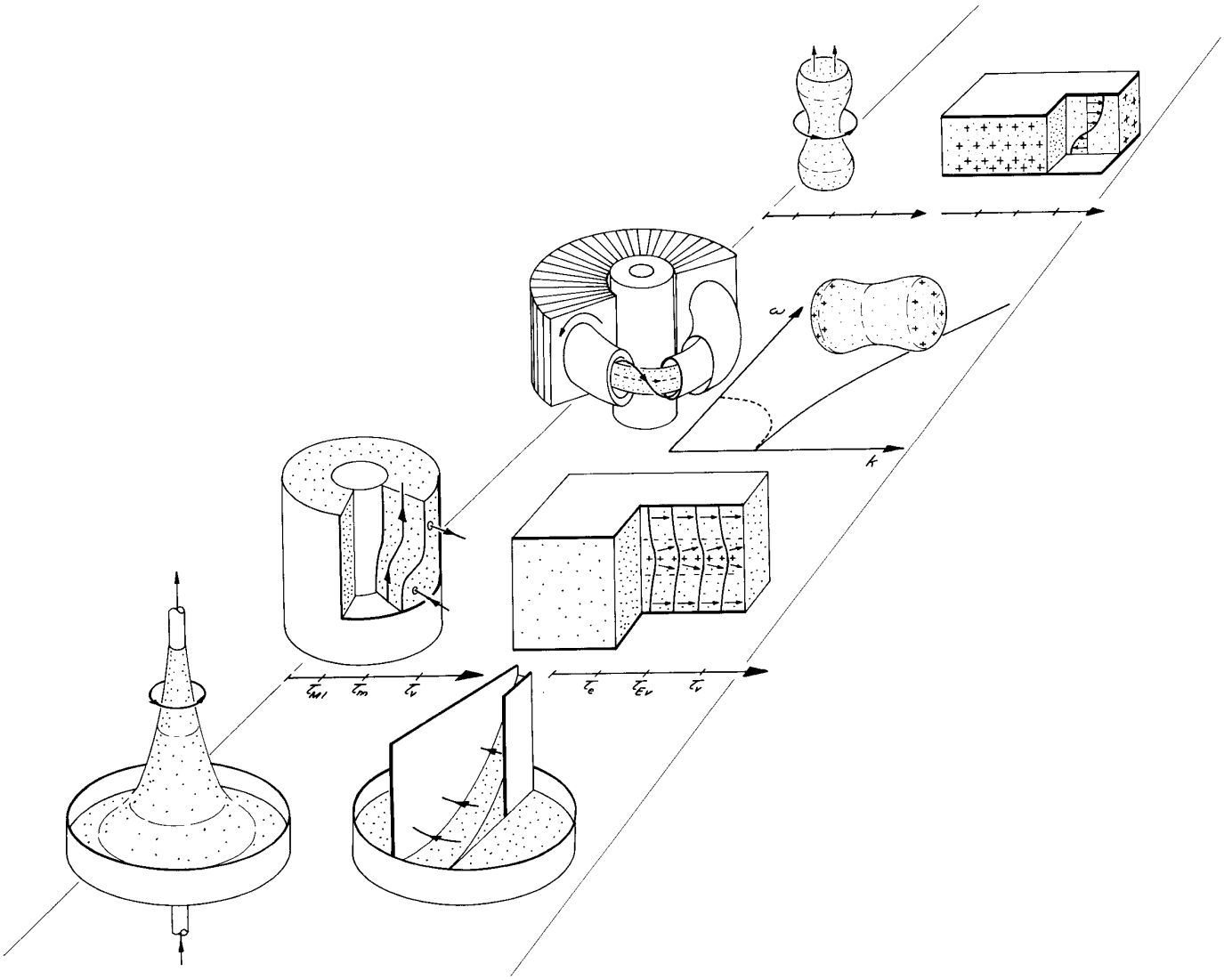

8.1 Introduction

In general, it is not possible for a fluid to be at rest while subject to an electric or magnetic force density. Yet, when a field is used to levitate, shape or confine a fluid, it is a static equilibrium that is often desired. The next section begins by identifying the electromechanical conditions required if a state of static equilibrium is to be achieved. Then, the following three sections exemplify typical ways in which these conditions are met. From the mathematical viewpoint, the subject becomes more demanding if the material deformations have a significant effect on the field. These sections begin with certain cases where the fields are not influenced by the fluid, and end with models that require numerical solution.

The magnetization and polarization static equilibria of Sec. 8.3 also offer the opportunity to explore the attributes of the various force densities from Chap. 3, to exemplify how entirely different distributions of force density can result in the same incompressible fluid response and to emphasize the necessity for using a consistent force density and stress tensor.

Given a static equilibrium, is it stable? This is one of the questions addressed by the remaining sections, which concern themselves with the dynamics that result if an equilibrium is disturbed. Some types of electromechanical coupling take place in regions having uniform properties. These are exemplified in Secs. 8.6-8.8. However, most involve inhomogeneities. The piecewise homogeneous models developed in Secs. 8.9-8.16 are chosen to exemplify the range of electromechanical models that can be pictured in this way.

The last sections, on smoothly inhomogeneous systems, serve as an introduction to a viewpoint that could equally well be exemplified by a range of electromechanical models. Once it is realized that the smoothly inhomogeneous systems can be regarded as a limit of the piecewise inhomogeneous systems, it becomes clear that all of the models developed in this chapter have counterparts in this domain.

The five electromechanical models that are a recurring theme throughout this chapter are summarized in Table 8.1.1.

Table 8.1.1. Electromechanical models.

Model	Approximation
Magnetization (MQS) or polarization (EQS)	No free current or charge Instantaneous magnetization or polarization
Flux conserving (MQS)	$\tau \ll \tau_m$
Charge conserving (EQS)	$\tau \ll \tau_e$ or τ_{mig}
Instantaneous magnetic diffusion (MQS)	$\tau \gg \tau_m$
Instantaneous charge relaxation (EQS)	$\tau \gg \tau_e$ or τ_{mig}

Magnetization and polarization models for incompressible motions require an inhomogeneity in magnetic or electric properties. The remaining interactions involve free currents or charges which generally bring in some form of magnetic diffusion or charge relaxation (or migration). How such rate processes come into the electromechanics is explicitly illustrated in the sections on homogeneous systems, Secs. 8.6 and 8.7. However, in the more complex inhomogeneous systems, the last four models of Table 8.1.1 not only result in analytical simplifications, but give insights that would be difficult to glean from a more general but complicated description. "Constant potential" continua fall in the category of instantaneous charge relaxation models.

STATIC EQUILIBRIA

8.2 Conditions for Static Equilibria

Often overlooked as an essential part of fluid mechanics is the subject of fluid statics. A reminder of the significance of the subject is the equilibrium between the gravitational force density and the hydrostatic fluid pressure involved in the design of a large dam. On the scale of the earth's surface, where g is essentially constant, the gravitational force acting on a homogeneous fluid obviously is of a type that can result in a static equilibrium.

Except for scale, electric and magnetic forces might well have been the basis for Moses' parting of the Red Sea. Fields offer alternatives to gravity in the orientation, levitation, shaping or

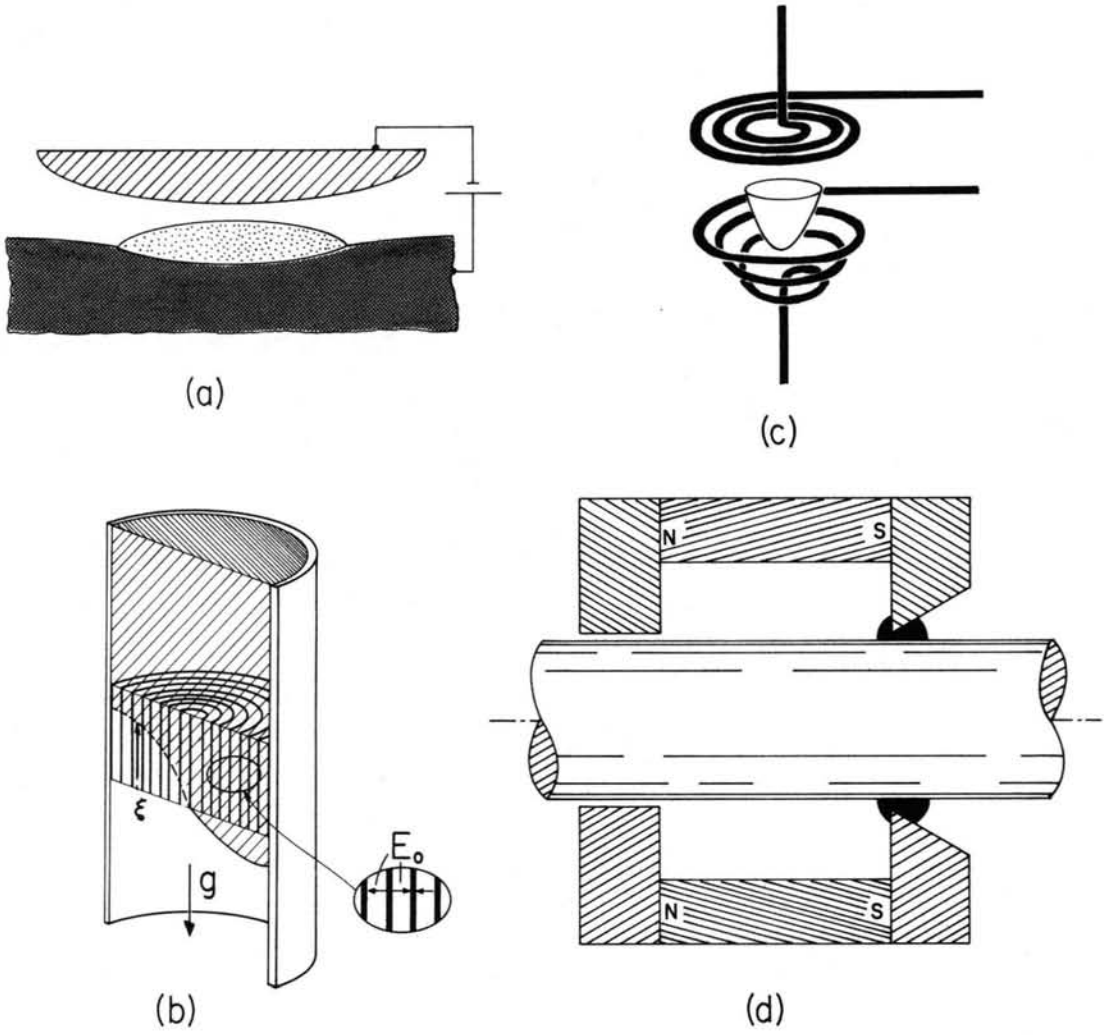

Fig. 8.2.1. (a) Electric field used to shape a "lens" of conducting liquid resting on a pool of liquid metal. Molten plastics and glass are sufficiently conducting that they can be regarded as "perfect" conductors. (b) Polarization forces used to orient a highly insulating liquid in the top of a tank regardless of gravity. The scheme might be used for providing an artificial bottom in cryogenic fuel storage tanks under the zero-gravity conditions of space. (c) Liquid metal levitator that makes used of forces induced by a time-varying magnetic field. At high frequencies, the flux is excluded from the metal, and hence the fields tend toward a condition of zero shearing surface force density. (d) Cross-sectional view of axisymmetric magnetic circuit and magnetizable shaft with magnetizable fluid used to seal penetration of rotating shaft through vacuum containment.

otherwise controlling of static fluid configurations. Examples are shown in Fig. 8.2.1.[1-3]

For what force distributions can each element of a fluid be in static equilibrium? If the external electric or magnetic force density is $\vec{F}^e$, then the force equation reduces to

$$-\nabla(p - \rho\vec{g}\cdot\vec{r}) = \vec{F}^e \qquad (1)$$

This expression is a limiting form of Eq. 7.4.4 with the velocity zero. Even if effects of viscosity

1. J. R. Melcher, D. S. Guttman and M. Hurwitz, "Dielectrophoretic Orientation," J. Spacecraft and Rockets 6, 25 (1969).
2. E. C. Okress et al., "Electromagnetic Levitation of Solid and Molten Metals," J. Appl. Phys. 23, 545 (1952).
3. R. E. Rosensweig, G. Miskolczy and F. D. Ezekiel, "Magnetic-Fluid Seals," Machine Design, March 28, 1968.

are included in the model, because $\vec{v} = 0$, Eq. 1 still represents the static equilibrium. Thus, it is also the static limit of Eq. 7.4.4. The curl of a gradient is zero. So, the curl of Eq. 1 gives a necessary condition on $\vec{F}^e$ for static equilibrium:

$$\nabla \times \vec{F}^e = 0 \tag{2}$$

To achieve a static equilibrium, the force density must be the gradient of a scalar, $-\nabla\mathcal{E}$. Then Eq. 1 becomes

$$\nabla(p - \rho\vec{g}\cdot\vec{r} + \mathcal{E}) = 0 \tag{3}$$

which will be recognized as Eq. 7.8.4 in the limit $\vec{v} = 0$.

More often than not, in an electromagnetic field a fluid does not reach a static equilibrium. Electromagnetic forces do not generally satisfy Eq. 2. Fields designed to achieve an irrotational force density are exemplified by Secs. 8.3-8.5.

These sections also illustrate that stress balance at interfaces is similarly restricted. A clean static interface is incapable of sustaining a net electrical shearing surface force density. Formally, this is seen from the interfacial stress balance, Eq. 7.7.6, which states that the normally directed pressure jump and surface tension surface force density must be balanced by the electrical force density. The last, $[\![T^e_{ij}]\!] n_j$, is in general not normal to the interface.

To be specific about what types of interfaces do satisfy this requirement, consider an interface having a normal vector in the x direction. Then, $n_j = \delta_{jx}$ and for the directions $i \neq x$ the surface force density is

$$\begin{aligned} [\![T_{ix}]\!] &= [\![E_i D_x]\!] = E_i [\![D_x]\!] \quad \text{(EQS)} \\ [\![T_{ix}]\!] &= [\![H_i B_x]\!] = B_x [\![H_i]\!] \quad \text{(MQS)} \end{aligned} \tag{4}$$

In writing the second equalities, advantage is taken of the continuity of tangential $\vec{E}$ (EQS) and normal $\vec{B}$ (MQS). From Eq. 4a, two EQS idealizations are distinguished for having no electrical shearing surface force density at the interface. First, the tangential electric field intensity can vanish, in which case (4a) is satisfied. The interface is "perfectly" conducting. Secondly, the jump in electric displacement at the interface can vanish, and again, there is no shear stress at the interface. The interface then supports no free surface charge density. Two MQS circumstances exist for achieving no shearing surface force density. First, the normal flux density can vanish at the interface. Physically, this is realized if the interface is perfectly conducting. Alternatively, the jump in tangential $\vec{H}$ can vanish, and this means that there is no surface current density on the interface.

The four static equilibria of Fig. 8.2.1 exemplify the four limiting situations in which there is no electrical shearing force density at an interface. In Fig. 8.2.1a, the lens is pictured as sufficiently highly conducting that it excludes the electric field, and hence behaves as a perfect conductor. Molten glass is more than conducting enough to satisfy this condition. Polarization forces are used to orient highly insulating fluids with no free charge density either on the interface or in the bulk, as illustrated in Fig. 8.2.1b. Metallurgists use high-frequency magnetic fields to make a crucible with magnetic walls, as shown in Fig. 8.2.1c. Here, because of the high frequency used, the magnetic field penetrates the liquid metal only slightly, and tends to the limit of no normal flux density. Thus, a static configuration with the melt levitated in mid-air is in principle possible. Magnetic fluids are being exploited as the basis for making vacuum seals for shaft penetrations as sketched in Fig. 8.2.1d. Here, the magnetic field is used to orient the liquid in the region between shaft and walls. Generally, the magnetizable fluids are highly insulating and so there is not only no surface current to produce a surface shearing force density, but also no volume force density due to $\vec{J} \times \vec{B}$.

In all of the examples in Fig. 8.2.1, the electromechanical forces can be regarded as confined to interfaces. This is clear for the free charge and free current interactions of parts (a) and (c) of that figure, because there are no fields inside the material. In the polarization and magnetization interactions, the properties are essentially uniform in the bulk. Thus, the force density expressed as Eq. 3.7.19 or 3.8.14 is concentrated at the interfaces.

Some common static configurations involving volume forces are evident from symmetry. For example, if the force density is in one direction and only depends on that direction, i.e., if

$$\vec{F}^e = F_x(x)\vec{i}_x \tag{5}$$

then it is clear that the force density is the gradient of $(-\mathcal{E})$:

$$\mathcal{E} = -\int F_x(x)dx \tag{6}$$

Similar arguments can be used if the force density is purely in a radial direction.

Other approaches to securing a static equilibrium using bulk force densities are illustrated in Sec. 8.4.

8.3 Polarization and Magnetization Equilibria: Force Density and Stress Tensor Representations

For an incompressible fluid, the pressure is a dangling variable. It only appears in the force equation. Its role is to be whatever it must be to insure that the velocity is solenoidal. As a consequence, those external forces which are gradients of "pressures" have no influence on the observable incompressible dynamics. Any "pressure" can be lumped with p and a new pressure defined. Although true for dynamic as well as static situations, this observation is now illustrated by two static equilibria.

The first of these illustrates polarization forces, and is depicted by Fig. 8.3.1. A pair of diverging conducting electrodes are dipped into a liquid having permittivity ε. A potential difference V_o applied between these plates results in the electric field

$$\vec{E} = \frac{V_o}{\alpha r}\vec{i}_\theta \tag{1}$$

in the interior region well away from the edges. At any given radius r, the situation is essentially the dielectric of Fig. 3.6.1, drawn into the region between parallel capacitor plates. Because the field increases to the left, so also does the liquid height. What is this height of rise, $\xi(r)$?

There are two reasons that this experiment is a classic one. The first stems from the lack of coupling between the fluid geometry and the electric field. The interface tends to remain parallel with the θ-direction, and as a result the electric field given by Eq. 1 remains valid regardless of the height of rise. As a result, the description is greatly simplified. The second reason pertains to its use as a counterexample against any contention that the polarization force density is $\rho_p\vec{E}$, where ρ_p is the polarization charge density. In this example, there is neither polarization charge in the liquid bulk (in the region between the electrodes and even in the fringing field near the lower edges of the electrodes in the liquid) nor is there surface polarization charge at the interface (where $\vec{E}$ is tangential). If $\rho_p\vec{E}$ were the force density, the liquid would not rise!

Illustrated now are two self-consistent approaches to determining the height of rise, the first using Kelvin's force density and the second exploiting the Korteweg-Helmholtz force density.

Kelvin Polarization Force Density: The force density and associated stress tensor are in this case (Table 3.10.1)

$$\vec{F} = \vec{P}\cdot\nabla\vec{E} \tag{2}$$

$$T_{ij} = E_iD_j - \frac{1}{2}\delta_{ij}\varepsilon_oE_kE_k \tag{3}$$

The liquid is modeled as electrically linear with $\vec{P}$ and $\vec{E}$ collinear,

$$\vec{P} = (\varepsilon - \varepsilon_o)\vec{E} \tag{4}$$

Throughout the liquid, ε is uniform. Hence, Eqs. 2 and 3 and the fact that $\vec{E}$ is irrotational combine to show that the force density is

$$(\vec{P}\cdot\nabla\vec{E})_i = (\varepsilon - \varepsilon_o)E_j\frac{\partial E_i}{\partial x_j} = (\varepsilon - \varepsilon_o)E_j\frac{\partial E_j}{\partial x_i} = (\varepsilon - \varepsilon_o)\frac{\partial}{\partial x_i}(\frac{1}{2}E_jE_j) \tag{5}$$

So long as the force density is only used where ε is constant (in the bulk of the liquid or of the air) Eq. 6 is in the form of the gradient of a pressure,

$$\vec{F} = -\nabla\mathcal{E};\quad \mathcal{E} \equiv -\frac{1}{2}(\varepsilon - \varepsilon_o)\vec{E}\cdot\vec{E} \tag{6}$$

This makes it clear that the polarization force density is irrotational throughout the bulk. In the bulk, Eq. 8.2.3 applies. With $\mathcal{E}$ evaluated using Eq. 1, it follows that in the bulk regions

$$p + \rho gz - \frac{(\varepsilon - \varepsilon_o)V_o^2}{2\alpha^2r^2} = \text{constant} \tag{7}$$

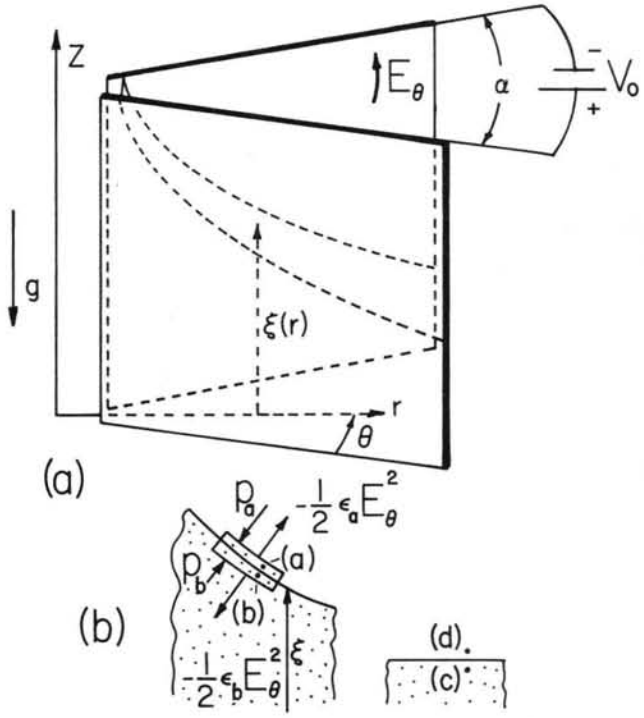

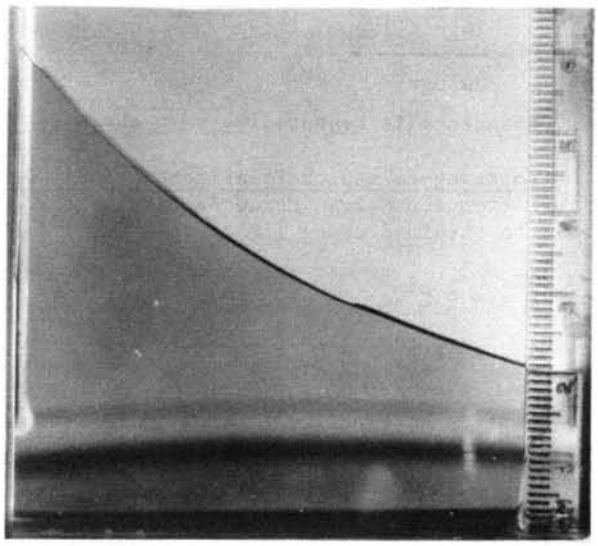

(c)

Courtesy of Education Development Center, Inc. Used with permission.

Fig. 8.3.1. (a) Diverging conducting plates with potential difference V_o are immersed in dielectric liquid. (b) Interfacial stress balance. (c) From Reference 12, Appendix C; corn oil ($\varepsilon = 3.7\ \varepsilon_o$) rises in proportion to local E^2. Upper fluid is compressed nitrogen gas ($\varepsilon \simeq \varepsilon_o$) so that E can approach 10^7 V/m required to raise liquid several cm. To avoid free charge effects, fields are 400 Hz a-c. The fluid responds to the time-average stress. The interface position is predicted by Eq. 12.

Thus, with the interface elevation, ξ, measured relative to the liquid level well removed from the electrodes, positions a and d in the air (where $\varepsilon = \varepsilon_o$ and $\rho \simeq 0$) and positions b and c (in the liquid) are joined by Eq. 7:

$$p_a = p_d \tag{8}$$

$$p_b + \rho g \xi - \frac{(\varepsilon - \varepsilon_o)V_o^2}{2\alpha^2 r^2} = p_c \tag{9}$$

To complete the formulation, account must be taken of any surface force densities at the interface that would make the pressure discontinuous at the interface. In general, the boundary condition is Eq. 7.7.6. As discussed in Sec. 8.2, there is no free surface charge, so there is no shearing component of the surface force density. If the electrodes are very close together, capillarity will contribute to the height of rise, as described by the example in Sec. 7.8. Here the electrodes are sufficiently far apart that the meniscus has a negligible effect.

If the local normal to the interface is in the x direction, the surface force density is $[\![T_{xx}]\!]$. Because the electric field is entirely perpendicular to x and is continuous at the interface, it follows from Eq. 3 that $[\![T_{xx}]\!] = [\![-\frac{1}{2}\varepsilon_o E_\theta^2]\!] = 0$, so that there is no surface force density. Hence, the stress equilibrium for the interface at locations a-b and c-d is simply represented by

$$p_a - p_b = 0 \tag{10}$$

$$p_c - p_d = 0 \tag{11}$$

The pressures are eliminated between the last four relations by multiplying Eq. 8 by (-1) and adding

the four equations. The resulting expression can then be solved for $\xi(r)$:

$$\xi = \frac{(\varepsilon - \varepsilon_o)V_o^2}{2\alpha^2\rho g r^2} \tag{12}$$

This dependence is essentially that shown in the photograph of Fig. 8.3.1.

Korteweg-Helmholtz Polarization Force Density: It is shown in Sec. 3.7 that this force density differs from the Kelvin force density by the gradient of a pressure. Thus, the same height of rise should be obtained using (from Table 3.10.1) the force density and stress tensor pair

$$\vec{F} = -\frac{1}{2}E^2\nabla\varepsilon \tag{13}$$

$$T_{ij} = \varepsilon E_i E_j - \frac{1}{2}\delta_{ij}\varepsilon E_k E_k \tag{14}$$

Now, there is no electrical force in the volume and the static force equation, Eq. 8.2.3, simply requires that

$$p + \rho g z = \text{constant} \tag{15}$$

Thus, points a and d and points b and c are joined through the respective bulk regions by Eq. 15 to obtain

$$p_a = p_d \tag{16}$$

$$p_b + \rho g \xi = p_c \tag{17}$$

By contrast with Eqs. 8 and 9 there is no bulk effect of the field. Now, the electromechanical coupling comes in at the interface where ε suffers a step discontinuity and hence a surface force density exists. At the interface, $[\![T_{xx}]\!] = -\frac{1}{2}(\varepsilon_o - \varepsilon)E_\theta^2$, so that the stress balances at the interface locations a-b and c-d are respectively

$$p_a - p_b = -\frac{(\varepsilon_o - \varepsilon)V_o^2}{2\alpha^2 r^2} \tag{18}$$

$$p_c - p_d = 0 \tag{19}$$

Multiplication of Eq. 16 by (-1) and addition of these last four equations eliminates the pressure and leads to the same deflection as obtained before, Eq. 12.

Korteweg-Helmholtz Magnetization Force Density: The force density and stress tensor pair appropriate if the fluid has a nonlinear magnetization are (from Table 3.10.1)

$$\vec{F} = \sum_{k=1}^{m} \frac{\partial W}{\partial \alpha_k}\nabla\alpha_k \tag{20}$$

$$T_{ij} = H_i B_j - \delta_{ij} W' \tag{21}$$

where $\vec{B}$ and $\vec{H}$ are collinear:

$$\vec{B} = \mu(\alpha_1, \alpha_2, \cdots, \alpha_m, H^2)\vec{H} \tag{22}$$

In the experiment of Fig. 8.3.2, the magnetic field

$$\vec{H} = \frac{I}{2\pi r}\vec{i}_\theta \tag{23}$$

is imposed by means of the vertical rod, which carries the current I. The ferrofluid in the dish has essentially uniform properties α_i throughout its bulk, but tends to saturate as the field exceeds about 100 gauss.

The Korteweg-Helmholtz force density has the advantage of concentrating the electromechanical coupling where the properties vary. In this example, this is at the liquid-air interface. Because

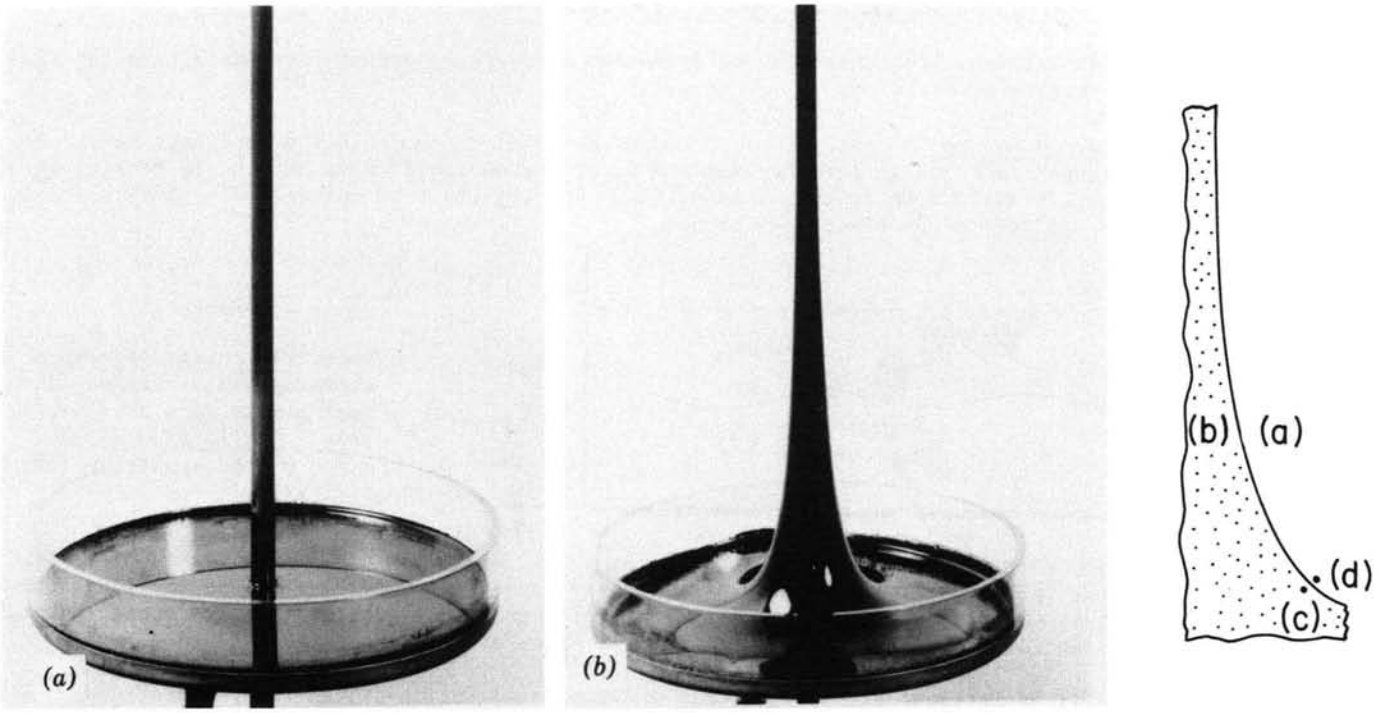

Courtesy of Textron Corporation. Used with permission.

Fig. 8.3.2. A magnetizable liquid is drawn upward around a current-carrying wire in accordance with Eq. 29. (Courtesy of AVCO Corporation, Space Systems Division.)

Eq. 20 is zero throughout the bulk regions, Eqs. 16 and 17 respectively pertain to these regions.

Stress balance at the interface is represented by evaluating the surface force density acting normal to the interface, to write

$$p_a - p_b = - [\![W']\!] \tag{24}$$

$$p_c - p_d = 0 \tag{25}$$

for locations a-b and c-d, respectively. The pressures are eliminated between Eqs. 16, 17, 24 and 25 to obtain

$$\xi = - \frac{[\![W']\!]}{\rho g} \tag{26}$$

To complete the evaluation of $\xi(r)$, the magnetization characteristic of the liquid must be specified. As an example, suppose that

$$\vec{B} = \frac{\vec{H}}{\alpha_1 \sqrt{\alpha_2^2 + H^2}} + \mu_o \vec{H} \tag{27}$$

where α_1 and α_2 are properties of the liquid. Then, the coenergy density (Eq. 2.14.13) is

$$W' = \int_o^{\vec{H}} \vec{B} \cdot \delta \vec{H} = \frac{1}{\alpha_1} \sqrt{\alpha_2^2 + H^2} - \frac{\alpha_2}{\alpha_1} + \frac{1}{2} \mu_o H^2 \tag{28}$$

and, in view of Eq. 23, Eq. 26 becomes

$$\xi = \frac{1}{\rho g} \left[\frac{1}{\alpha_1} \sqrt{\alpha_2^2 + \left(\frac{I}{2\pi r} \right)^2} - \frac{\alpha_2}{\alpha_1} \right] \tag{29}$$

As for the electric-field example considered previously, the relative simplicity of Eq. 26 originates in the independence of $\vec{H}$ and the liquid deformation. If there were a normal component of $\vec{H}$ at the interface, the field would in turn depend on the liquid geometry and a self-consistent solution would be more complicated.

8.4 Charge Conserving and Uniform Current Static Equilibria

A pair of examples now illustrate how the free-charge and free-current force densities can be arranged to give a static equilibrium.

Uniformly Charged Layers: A layer of fluid having uniform charge density q_b and mass density ρ_b rests on a rigid support and has an interface at $x = \xi$. A second fluid above has charge density q_a and mass density ρ_a. Gravity acts in the -x direction. The objective is control of $\xi(y)$ by means of the potential V(z) applied to the electrodes above.

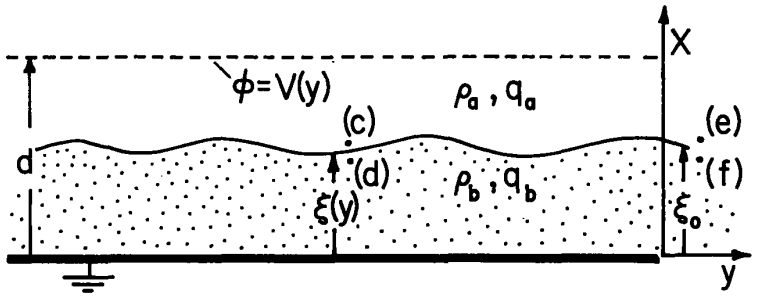

Fig. 8.4.1

Uniformly charged aerosols entrained in fluids of differing mass densities assume static equilibrium determined by the applied potential V(y).

As an example, the upper fluid might be air which is free of charge ($q_a = 0$) and the lower one a heavier gas such as CO_2 with entrained submicron particles previously charged by ion impact. Thus, the fluids have essentially the permittivity of free space and there is no surface tension.

The time-scales of interest are sufficiently short that migration of the charged particles relative to the fluids is inconsequential. Thus, the charge is frozen to the gas. Because the gas is incompressible ($\nabla\cdot\vec{v} = 0$), the charge density of a gas element is conserved. Regardless of the particular shape of the interface, the charge densities above and below remain uniform, q_a and q_b respectively. It is for this reason and because $\vec{E}$ is irrotational that the force density in each fluid is irrotational:

$$\vec{F} = q\vec{E} = -q\nabla\Phi = -\nabla(q\Phi) \tag{1}$$

Thus, Eq. 8.2.3 shows that within a given fluid region

$$p + \rho g x + q\Phi = \text{constant} \tag{2}$$

Evaluation of the constant at the points (e) and (f) adjacent to the interface where $\xi = \xi_o$ gives

$$\begin{aligned} p + \rho_a g x + q_a\Phi &= p^e + \rho_a g\xi_o + q_a\Phi(\xi_o);\ x > \xi \\ p + \rho_b g x + q_b\Phi &= p^f + \rho_b g\xi_o + q_b\Phi(\xi_o);\ x < \xi \end{aligned} \tag{3}$$

The force density suffers a step discontinuity at the interface. This means that there is no surface force density, so that the pressure is continuous at the interface. Continuity of p also follows formally from the stress jump condition, Eq. 7.7.6 with the surface tension $\gamma = 0$.

So that stability arguments can be made, an external surface force density $T_{ext}(y)$ is pictured as also acting on the interface. By definition $T_{ext} = 0$ at location (e-f):

$$p^c - p^d = T_{ext};\quad p^e - p^f = 0 \tag{4}$$

Subtraction of Eqs. 3a and 3b then gives

$$g(\xi - \xi_o)(\rho_b - \rho_a) + (q_b - q_a)[\Phi(\xi) - \Phi(\xi_o)] = T_{ext} \tag{5}$$

where $\Phi(\xi)$ is the potential evaluated at the interface.

Of course, the potential distribution is determined by the presently unknown geometry of the interface and the field equations. Here, the relation of field and geometry is simplified by considering long-wave distributions of the interface. The electric field is approximated as being dominantly in the x direction. Thus, Poisson's equation reduces to simply

$$\frac{\partial^2\Phi}{\partial x^2} = \frac{-q}{\varepsilon_o};\quad q = \begin{cases} q_a: x > \xi \\ q_b: x < \xi \end{cases} \tag{6}$$

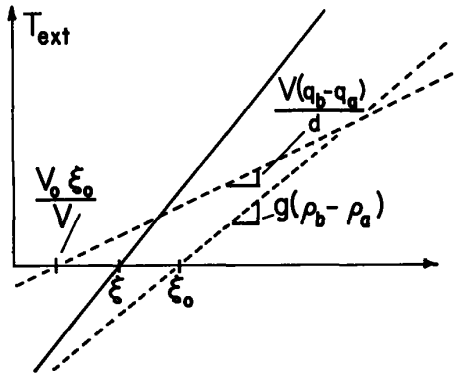

Fig. 8.4.2

Graphical representation of Eq. 9.

With the boundary conditions that $\Phi(d) = V(y)$, that $[\![\Phi]\!] = 0$ and $[\![\partial\Phi/\partial x]\!] = 0$ at the interface and that $\Phi(0) = 0$, it follows that

$$\Phi(\xi) = \frac{V\xi}{d} + \frac{q_a}{2\varepsilon_o d}\xi(d-\xi)^2 + \frac{q_b}{2\varepsilon_o d}\xi^2(d-\xi) \tag{7}$$

Thus, with $T_{ext} = 0$, Eq. 5 becomes a cubic expression that can be solved for $\xi(y)$ given $V(y)$

$$g(\xi-\xi_o)(\rho_b-\rho_a) + (q_b-q_a)\left(\frac{V\xi}{d} - \frac{V\xi_o}{d}\right) + (q_b-q_a)\left\{\frac{q_a}{2\varepsilon_o d}[\xi(d-\xi)^2 - \xi_o(d-\xi_o)^2] + \frac{q_b}{2\varepsilon_o d}[\xi^2(d-\xi)-\xi_o^2(d-\xi_o)]\right\} = T_{ext} \tag{8}$$

Given a desired $\xi(y)$, Eq. 8 can also be solved for the required $V(y)$. If the field imposed by the electrode potential $V(y)$ is large compared to the space charge field, the last term in Eq. 8 can be ignored. Then, the equilibrium is represented by

$$g(\xi-\xi_o)(\rho_b-\rho_a) + (q_b-q_a)\left(\frac{V\xi}{d} - \frac{V_o\xi_o}{d}\right) = T_{ext} \tag{9}$$

To picture how the interface responds to $V(y)$, it is helpful to use the graphical solution of Fig. 8.4.2. The interfacial deflection is given by $T_{ext} = 0$. Increasing V has the effect of decreasing the intercept and increasing the slope of the electrical "force" curve.

In this imposed field limit, Eq. 9 can be solved for the layer thickness as a function of the imposed potential:

$$\frac{\xi}{\xi_o} = \frac{1+\underline{V}_o}{1-\underline{V}}; \quad \underline{V} \equiv \frac{(q_b-q_a)}{gd(\rho_b-\rho_a)}V(y) \tag{10}$$

Illustrated in Fig. 8.4.3 is an example which represents what would happen if the potential shown were imposed on a light layer over a heavier layer, with the upper one uncharged and the lower one negatively charged.

Stability of the equilibrium can be argued from the dependence of T_{ext} on ξ. If

$$g(\rho_b-\rho_a) + \frac{V}{d}(q_b-q_a) > 0 \tag{11}$$

a positive force is required to produce a positive deflection, much as if the interface were equivalent to a spring with a positive spring constant. Thus, the condition of Eq. 11 is required for stability. In terms of the normalized voltage used in expressing Eq. 10, the interface is stable where $\underline{V} > -1$.

A more complete stability argument that includes the effects of space charge is given in Sec. 8.14.

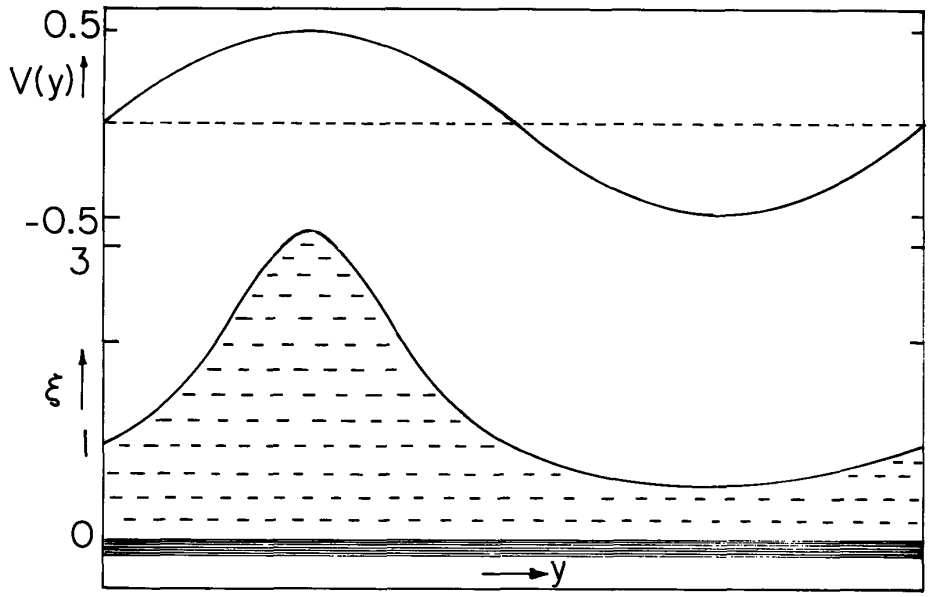

Fig. 8.4.3

Imposed field equilibrium with $\underline{V} = -0.7 \sin(y)$. Shape of charge layer is given by Eq. 10.

Uniform Current Density: Static equilibrium with the free-current force density $\vec{J}_f \times \mu_o \vec{H}$ distributed throughout the volume of a fluid is now illustrated. In the MQS system of Fig. 8.4.4, a layer of liquid metal rests on a rigid plane at $x = 0$ and has a depth $\xi(y)$. The system, including the fields and currents, is assumed to have a uniform distribution with the z direction, so that the view shown is any cross section.

The magnetic field is to be used in deforming the liquid interface. A d-c electromagnet produces a magnetic flux density with components in the x-y plane. In addition, a voltage source drives a uniform current density J_o in the z direction throughout the fluid volume. This current density interacts with the imposed flux density to produce a vertical component of magnetic force in the liquid, and a resultant deformation of the interface. Note that because the fields are static, there are no surface currents. Also, the liquid metal is not magnetizable, so there are no magnetization forces to consider. Finally, effects of surface tension are ignored. Therefore, the interface is in stress equilibrium, provided the pressure there is continuous.

The essential approximation in obtaining the irrotational force density throughout the volume is that the imposed magnetic flux density is very large compared to the flux density induced by the imposed current density J_o. Thus, the force density takes the approximate form

$$\vec{F} = J_o \vec{i}_z \times [B_x \vec{i}_x + B_y \vec{i}_y] \tag{12}$$

The vector potential is convenient for dealing with $\vec{B}$, because if the substitution is made $\vec{B} = \nabla \times \vec{A}$, then Eq. 12 becomes $\vec{F} = -\nabla \mathcal{E}$, wherein

$$\mathcal{E} = -J_o A(x,y) \tag{13}$$

The imposed field approximation and the uniform imposed current result in the irrotational force density required for static equilibrium. Given the particular field structure and the magnitude of the field excitation, $A(x,y)$ is known.

In an engineering application, the liquid metal might serve as a base for the casting of plastic or glass products.[1] The magnetic field can be controlled so that there is a ready means of altering the shape of the mold without a need for replacing the casting material. If a quiescent fluid state is desirable, conditions for a static equilibrium are essential. From Eq. 8.2.3 and Eq. 13

$$p + \rho g x - J_o A = \text{constant} \tag{14}$$

There is no current density in the gas above the interface, and hence no force density. The depth as $y \to -\infty$ is defined as ξ_∞, and A ($x = \xi$, $y \to -\infty$) is defined as A_∞. Then, Eq. 14 shows that for points

1. See U.S. Patent #3,496,736, "Sheet Glass Thickness Control Method and Apparatus," February 24, 1970, M. Hurwitz and J. R. Melcher.

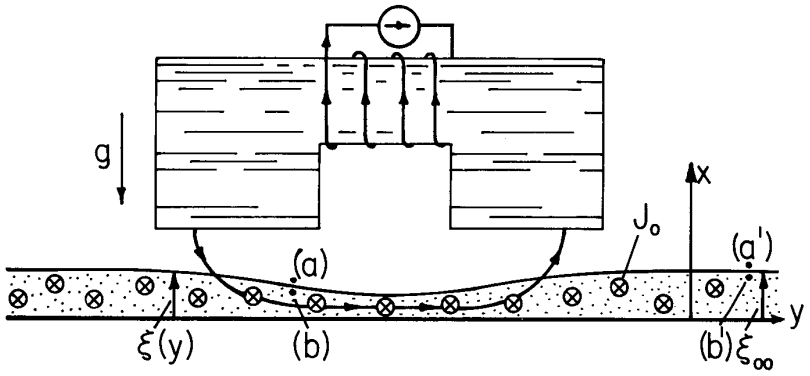

Fig. 8.4.4. Layer of liquid metal has the depth $\xi(y)$ which is controlled by the interaction of a uniform z-directed current density J_o and a magnetic flux density induced by means of the magnetic structure.

(a) and (a') of Fig. 8.4.4

$$p_{a'} + \rho_a g\xi_\infty = p_a + \rho_a g\xi \tag{15}$$

and for points (b) and (b')

$$p_{b'} + \rho_b g\xi_\infty - J_o A_\infty = p_b + \rho_b g\xi - J_o A \tag{16}$$

Because the hydrostatic pressures are the same at the primed and unprimed positions, subtraction of Eq. 15 from Eq. 16 gives a relation that can be solved for the height $\xi(y)$:

$$\xi = \xi_\infty - J_o(A_\infty - A)/g(\rho_b - \rho_a) \tag{17}$$

The vector potential has the physical significance of being a flux linkage per unit length in the z direction. To see this, define $\lambda(y)$ as the flux linked by a loop having one edge outside the field region to the right, the other edge at the position y and height ξ of the interface and unit depth in the z direction. Then the flux linked per unit length is

$$\lambda = \int_S \vec{B}\cdot\vec{n}da = \int_C \vec{A}\cdot d\ell = A_\infty - A(\xi,y) \tag{18}$$

and in terms of this flux, Eq. 18 becomes

$$\xi = \xi_\infty - \frac{J_o\lambda}{g(\rho_b - \rho_a)} \tag{19}$$

The flux passing through the interface to the right of a given point determines the depression at that point. Proceeding from right to left, the flux is at first increasing, and hence the depression is increasing. But near the middle, additions to the total flux reverse, and the net flux tends toward zero. Hence, ξ returns to ξ_∞, as sketched in Fig. 8.4.4. Even if used only qualitatively, Eq. 19 gives a picture of the interfacial deformation that is useful for engineering design. Measurements can be used to determine $\lambda(x,y)$.

8.5 Potential and Flux Conserving Equilibria

Typical of EQS systems in which an electric pressure is used to shape the interface of a somewhat conducting liquid is that shown in Fig. 8.5.1a. Provided that the region between the cylindrical electrode and the liquid is highly insulating compared to the liquid, the interface is an equipotential. Because the applied voltage is constant and the equilibrium is static, this is true even for what might be regarded as relatively insulating liquids. Certainly water, molten glass, plasticizers and even used transformer oil will behave as equipotentials with air insulation between electrodes and interface. The liquid is in a reservoir. By virtue of its surface tension, the interface attaches to the reservoir's edges at $y = \pm\ell$. Thus, continuity requires that the upward deflection of the interface under the electrode be compensated by a downward deflection to either side. To be considered in this section is how the static laws make it possible to account for such requirements of mass conservation.

In the MQS system of Fig. 8.5.1b, the liquid is probably a metal. To achieve the conditions for a static equilibrium, the driving flux source F_o is sinusoidally varying with a sufficiently high frequency that the skin depth is small compared to dimensions of interest. Thus, the normal flux density at the interface approaches zero. The liquid responds to the time average of the normal magnetic stress.

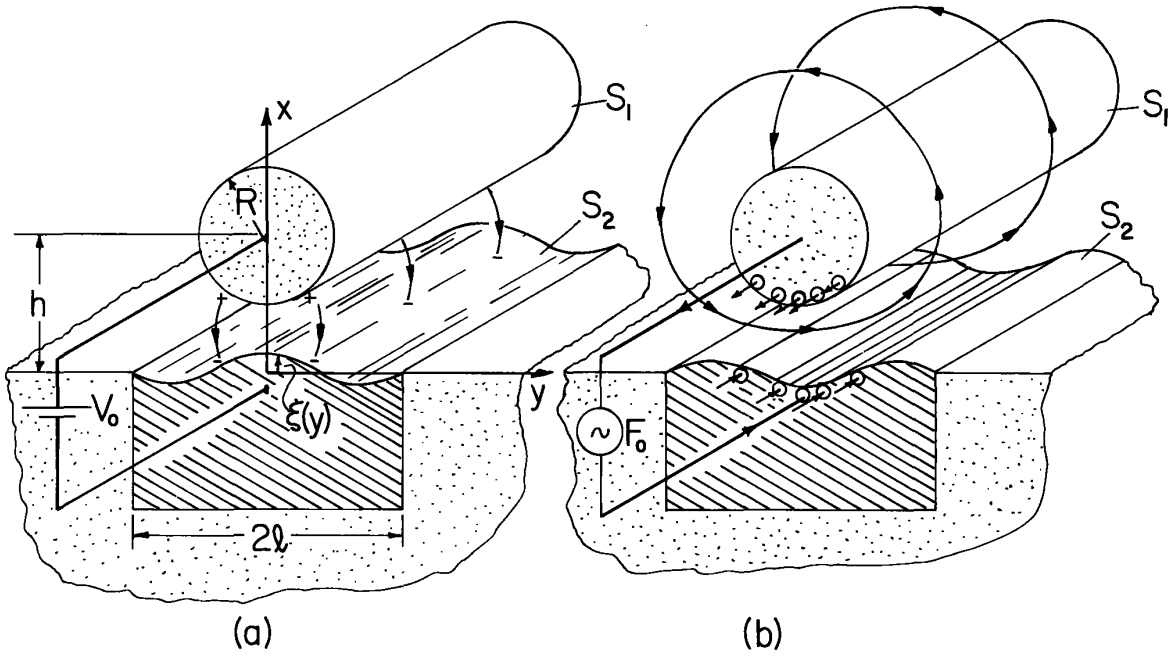

Fig. 8.5.1. (a) EQS system; liquid interface stressed by d-c field is equipotential. (b) MQS system; driving current has sufficiently high frequency that currents are on surfaces of liquid and electrode. Liquid responds to time average of magnetic pressure.

This pair of case studies exemplifies the free charge and free current static equilibria, from Sec. 8.2, involving electromagnetic surface force densities. The EQS static equilibrium is possible because there is no electric field tangential to the interface, while the MQS equilibrium results because there is essentially no normal magnetic flux density.

Antiduals: The two-dimensional fields in the two systems have an interesting relationship. For the moment, suppose that the geometry of the interfaces is known. Then, the electric field is represented by the potential, while the magnetic flux density is represented in terms of the z component of the vector potential, as summarized by Eqs. (a)-(c) of Table 2.18.1. Thus, in the regions between electrodes and interfaces,

$$\nabla^2\Phi = 0 \quad \Big| \quad \nabla^2 A = 0 \tag{1}$$

Boundary conditions on the respective systems are

$$\Phi = V_o \text{ on } S_1 \quad \Big| \quad A = F_o \text{ on } S_1 \tag{2}$$

$$\Phi = 0 \text{ on } S_2 \quad \Big| \quad A = 0 \text{ on } S_2 \tag{3}$$

where S_1 is the surface of the electrode or bus above the interface and S_2 is the interface and adjacent surface of the container. By definition, F_o is the flux per unit length (in the z direction) passing between the bus and the interface. Note that to make the magnetic field tangential to these surfaces, A is constant on the interface and on the surface of the bus.

With the understanding that n denotes the direction normal to the local interface, the electric and magnetic stresses on the interfaces are

$$T_{nn} = \frac{1}{2}\varepsilon_o E_n^2 = \frac{1}{2}\varepsilon_o\left(\frac{\partial\Phi}{\partial n}\right)^2 \quad \Big| \quad T_{nn} = -\frac{1}{2}\mu_o H_t^2 = -\frac{1}{2}\mu_o\left(\frac{1}{\mu_o}\frac{\partial A}{\partial n}\right)^2 \tag{4}$$

Thus, if the interface had the same geometry in the two configurations, the magnetic stress would "push"

on the interface to the same degree that the electric stress would "pull." The magnetic stress is the negative of the electric stress and can be formally found by replacing $\varepsilon_o \to \mu_o$ and $\partial\Phi/\partial n \to (\partial A/\partial n)/\mu_o$.

Although limited to two-dimensional fields, the antiduality makes it possible to extend the electromechanical description of one class of configurations to another by simply changing the sign of the electromechanical coupling term. Provided that charge can relax sufficiently rapidly on the EQS interface to render it an equipotential even under dynamic conditions, and provided that motions remain slow compared to the period of the sinusoidal excitation for the MQS system (so that the interface responds primarily to the time-average magnetic stress), the antiduality is valid for dynamic as well as static interactions.

Bulk Relations: Bernoulli's equation, Eq. 7.8.7, applied to the air and liquid bulk regions, shows that

$$p = \begin{cases} \Pi_a & ; \quad x > \xi \\ \Pi_b - \rho g x & ; \quad x < \xi \end{cases} \tag{5}$$

where Π_a and Π_b are constants. The mass density of the air is ignored compared to that of the liquid.

Stress Equilibrium: The normal component of the stress balance, Eq. 7.7.6, requires that

$$[\![p]\!] = T_{nn} - \gamma \nabla\cdot\vec{n} \tag{6}$$

Evaluation of the pressure jump using Eqs. 5 and of $\nabla\cdot\vec{n}$ with $\vec{n}$ given by Eq. 7.5.3 gives

$$(\Pi_a - \Pi_b) + \rho g \xi = T_{nn} + \gamma \frac{d}{dy}\left\{\frac{d\xi}{dy}\left[1 + \left(\frac{d\xi}{dy}\right)^2\right]^{-\frac{1}{2}}\right\} \tag{7}$$

Evaluation of Surface Deflection: Suppose that in the absence of a field, the interface is flat. Then, as the excitation V_o or F_o is raised, $\xi(y)$ increasingly departs from this initial state, $\xi = 0$. One way to compute $\xi(y)$ at a given excitation is to find the deflections as the excitation is raised, in stages, to this final value. Thus, $T_{nn}(y)$ in Eq. 7 is approximated by solving Eq. 1 with $\xi(y)$ approximated by its shape at the previous somewhat lower level of excitation. Thus, T_{nn} is a known function of y and the new $\xi(y)$ is approximated by integrating Eq. 7. Once this is done, the new $\xi(y)$ can be used to refine the determination of the fields. This interaction can be repeated until a desired accuracy is achieved. Then, the excitation can be incrementally raised and the process repeated.

For a system that is symmetric about the x axis boundary conditions appropriate to the solution of the second-order differential equation, Eq. 7, are

$$\frac{d\xi}{dy}(0) = 0 \tag{8}$$

$$\xi(-\ell) = 0 \tag{9}$$

In addition, mass conservation requires that

$$\int_{-\ell}^{0} \xi dy = 0 \tag{10}$$

This condition translates into a determination of the pressure jump. In view of Eqs. 8 and 10, integration of Eq. 7 between $y = -\ell$ and $y = 0$ shows that

$$\Pi_a - \Pi_b = \int_{-1}^{0} T_{nn} d_y - \frac{1}{W}\left(\frac{u}{\sqrt{1+u^2}}\right)_{y=-1} \tag{11}$$

where normalized variables and dimensionless parameters are

$$\begin{aligned} &y = \ell \underline{y}; \quad \Pi_a - \Pi_b = (\underline{\Pi}_a - \underline{\Pi}_b)(\tfrac{1}{2}\varepsilon_o V_o^2/\ell^2); \quad \xi = \ell\underline{\xi} \\ &T_{nn} = (\tfrac{1}{2}\varepsilon_o V_o^2/\ell^2)\underline{T}_{nn}; \quad W \equiv \tfrac{1}{2}\varepsilon_o V_o^2/\gamma\ell; \quad G \equiv \rho g \ell^2/\gamma \end{aligned} \tag{12}$$

and u is the slope of the interface, defined as

$$\frac{d\xi}{dy} = u \tag{13}$$

In terms of u, Eq. 7 is normalized and written as a first-order differential equation

$$\frac{du}{d\underline{y}} = (1 + u^2)^{3/2}[(\Pi_a - \Pi_b)W + G\underline{\xi} - WT_{nn}] \qquad (14)$$

This last pair of relations, equivalent to Eq. 7, take a form that is convenient for numerical integration. (The integration of systems of first-order nonlinear equations, given "initial conditions," is carried out using standard computer library subroutines. For example, in Fortran IV, see IMSL Integration Package DEVREK.) With $T_{nn}(y)$ given from the solution of Eqs. 1-3 (to be discussed shortly), the integration begins at $\underline{y} = -1$ where Eq. 9 provides one boundary condition. To make a trial integration of Eqs. 12 and 13, a trial value of u(-1) is assumed. Thus, from Eq. 11, the value of Π_a-Π_b that insures conservation of mass is determined. Integration of Eqs. 12 and 13 is then carried out and evaluated at y=0. Using u(-1) as a parameter, this process is repeated until the condition u(0) = 0 (boundary condition, Eq. 8) is satisfied. One way to close in on the appropriate value of u(-1) is by halving the separation of two u(-1)'s yielding opposite-signed slopes at y = 0.

Evaluation of Stress Distribution: To provide $T_{nn}(y)$ at each step in the determination of the surface deflection which has just been described, it is necessary to solve Eq. 1 using the boundary conditions of Eqs. 2 and 3. A numerical technique that is well suited to this task results in the direct evaluation of the surface charge density σ_f on the interface. Because $T_{nn} = \varepsilon_o E_n^2/2 = \sigma_f^2/2\varepsilon_o$, this is tantamount to a direct determination of the desired stress distribution.

In the two-dimensional configuration of Fig. 8.5.2, the solution of Laplace's equation can be represented by a potential (at the location $\vec{r}$) that is the superposition of potentials due to incremental line charges per unit length $\sigma_f ds'$:

$$\Phi(\vec{r}) = \frac{-1}{2\pi}\int \sigma_f(\vec{r}')\ \ln|\vec{r} - \vec{r}'|ds' \qquad (15)$$

This expression is normalized such that

$$\Phi = V_o\underline{\Phi};\quad \sigma_f = \frac{\varepsilon_o V_o}{\ell}\underline{\sigma}_f;\quad s = \ell\underline{s} \qquad (16)$$

Although $\ln|\vec{r} - \vec{r}| = \ln|\underline{\vec{r}} - \underline{\vec{r}}| + \ln \ell$, so long as the net charge in the system is zero, integration of the $\ln \ell$ term gives no contribution and so is omitted from Eq. 15. The desired (normalized) surface charge is $\underline{\sigma}_f$ and $d\underline{s}'$ is the (normalized) incremental segment of boundary.

The integral equation is solved numerically by approximating the integral by a sum over segments of the boundaries. These are denoted by the index n, as shown in Fig. 8.5.3. The first N segments are on the zero potential interface, the next 2M are on the surrounding zero potential plane and the remaining P segments are on the cylindrical electrode, and hence have the potential $\underline{\Phi} = 1$. Thus, the potential at the mth segment is the superposition of integrations over each of the charge segments. Because the latter have a length Δs that is small, the surface charge on each segment can be approximated as constant and the integration carried out analytically. For example, the contribution to the potential of the mth segment from the surface charge σ_n on the nth segment is (see Fig. 8.5.4),

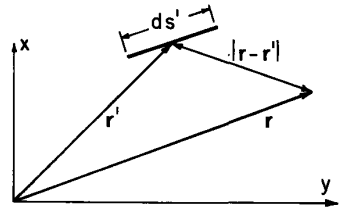

Fig. 8.5.2. Potential given by Eq. 15 at $\vec{r}$ is superposition of potentials due to line charges at $\vec{r}'$.

$$\Phi_m = -\frac{\sigma_n}{2\pi}\int_{s_n}^{s_n+\Delta s} \ln\sqrt{d_n^2 + s^2}\ ds \qquad (17)$$

Thus, Eq. 15 becomes

$$\Phi_m = \sum_{n=1}^{N+2M+P} a_{mn}\,\sigma_n \qquad (18)$$

where

$$a_{mn} = -\frac{1}{2\pi}\{\tfrac{1}{2}(\Delta s + s_n)\ln[(\Delta s + s_n)^2 + d_n^2] - \Delta s - \tfrac{1}{2}s_n \ln[s_n^2 + d_n^2] + d_n \tan^{-1}\left(\frac{\Delta s + s_n}{d}\right) - d_n \tan^{-1}\frac{s_n}{d}\} \qquad (19)$$

Now, Eq. 18 can be written for each of the N+2M+P segments. Thus, it represents a set of N+2M+P equations, linear in as many unknowns σ_n. These equations are then inverted to obtain the desired σ_n's. (Matrix inversion is carried out using standard computer library subroutines. For example, in Fortran IV see IMSL Matrix Inversion Routine LINV1F.)

Because $\underline{T}_{nn} = \underline{\sigma}_n^2/2$, the normalized stress distribution on each segment follows. So that the numerical integration of the surface equations, Eqs. 13 and 14, can be carried out with an arbitrary step size, the discrete representation of T_{nn} on the interface is conveniently converted to a smooth function by fitting a polynomial to the values of T_{nn}. (Polynomial fit can be carried out using a Least Square Polynomial Fit Routine such as the Math Library Routine LSFIT.)

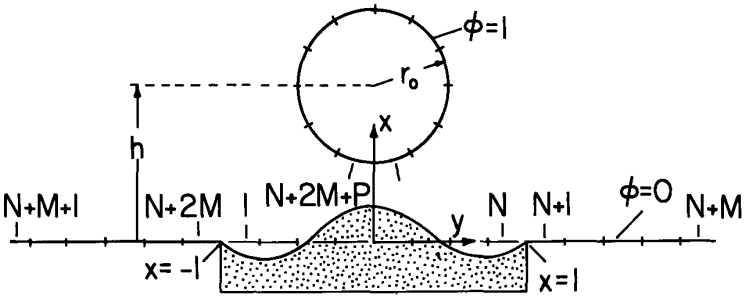

Fig. 8.5.3. Definition of segments and geometry for numerical solution.

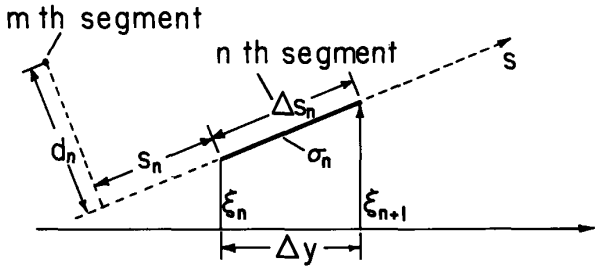

Fig. 8.5.4. Typical segment on interface.

Typical results of the combined numerical integration to determine $T_{nn}(y)$ and the interfacial deformation are shown in Fig. 8.5.5. (These computations were carried out by Mr. Kent R. Davey.) The procedure begins with a modest value of W and a flat interface and starts with a determination of T_{nn}. Then, Eqs. 13 and 14 are integrated and this integration repeated until the boundary condition $u(0) = 0$ is satisfied. Using this revised distribution of $\xi(y)$, the distribution of T_{nn} is recalculated, followed by a recalculation of the interface shape. This process is repeated until a desired accuracy is achieved.

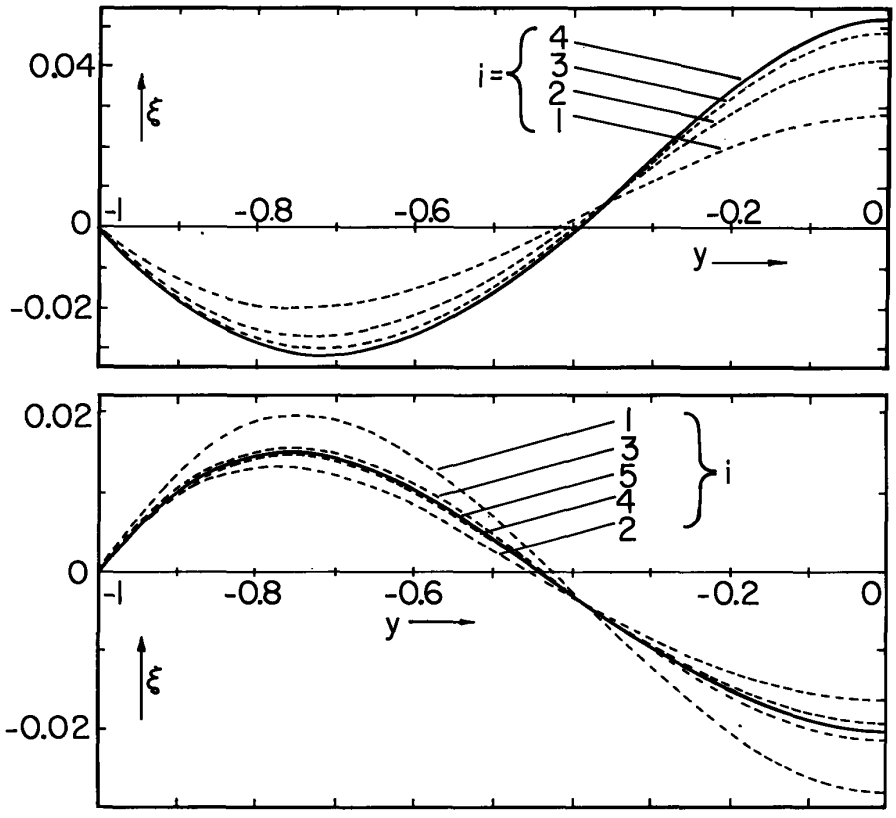

Fig. 8.5.5

Shape of interface with G = 3, $\underline{r}_o = 0.5$ and $\underline{h} = 1$. Broken curves are for successive iterations (i) with W fixed. (a) EQS system with W = 0.5. (b) MQS system with W = -0.5. Note that electric case converges monotonically, while magnetic one oscillates.

With W raised to a somewhat higher value, the previously determined shape is used as a starting point in repeating the iteration described.

8.6 Flux Conserving Continua and Propagation of Magnetic Shear Stress

Alfvén waves that propagate along magnetic field lines in the bulk of a highly conducting fluid result from the tendency for arbitrary fluid surfaces of fixed identity to conserve their flux linkage. The physical mechanisms involved are apparent in the one-dimensional motions of a uniformly conducting incompressible fluid permeated by an initially uniform magnetic field intensity $H_o\vec{i}_x$, as in Fig. 8.6.1a. By assumption, each fluid particle in a y-z plane executes the same motion.

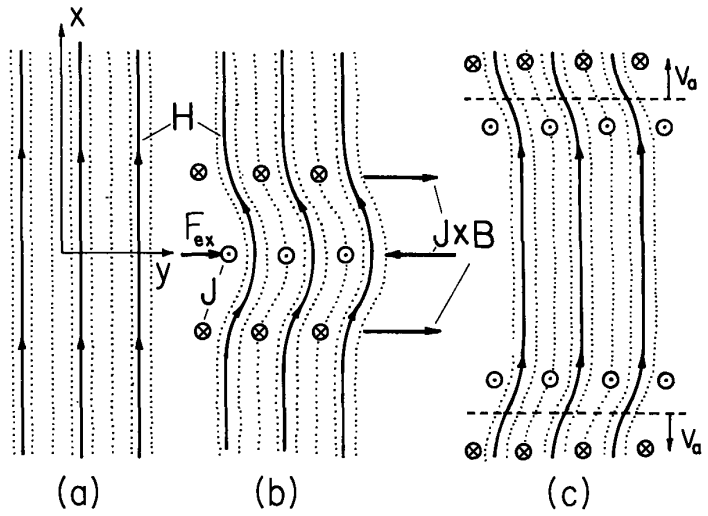

Fig. 8.6.1. (a)Perfectly conducting fluid initially at rest in uniform magnetic field. (b) For flux conservation of loops of fixed identity initially lying in x-z planes, translation of layer in y-z plane requires induced currents shown. (c) Force densities associated with currents induced by initial motion. (d) Translation of layers resolves into wave fronts propagating along magnetic field lines.

Consider the consequences of using an external force density $F_{ex}\vec{i}_y$ (Fig. 8.6.1b) to give a y-directed translation to a layer of fluid in one of these y-z planes. Because of the translation, fluid elements initially in any x-z plane form a surface that would be pierced twice by the initial field H_o. It is shown in Sec. 6.2 that if the fluid is perfectly conducting, the total flux linked by such a surface of fixed identity must be conserved. As a result of material deformation, a current density (sketched in Fig. 8.6.1b) is induced in just such a way as to create the y component of magnetic field required to maintain the net field tangential to each material surface initially in an x-y plane.

Note that because charge accumulation is inconsequential, the current density is solenoidal, so that current in the z direction must be returned in the -z direction in adjacent planes. The force density associated with these return currents is also shown in Fig. 8.6.1b. Because these currents are proportional to the displacement of a layer, the external force is retarded by a "spring-like" force proportional to the magnitude of the displacement. Similarly, the returning currents in adjacent y-z layers cause magnetic forces above and below, but here tending to carry these layers in the same direction as the original displacement. Thus, fluid layers to either side tend to move in the same direction as the layer subjected to the external force. Adjacent layers in the y-z planes are coupled by a magnetic shear stress representing the force associated with currents induced to preserve the constant flux condition.

In the absence of viscosity, the magnetic shear stress on adjacent layers is only retarded by inertia. There is some analogy to the viscous diffusion (Sec. 7.19), with the interplay between viscosity and inertia now replaced by one between magnetic field and inertia. The viscous shear stress of Sec. 7.19 is proportional to the shear-strain rate. By contrast, the magnetic shear stress in the perfect conductor is proportional to the shear strain (the spatial rate of change of the material displacement rather than velocity). Thus, rather than being diffusive in nature, the motion resulting from the magnetic shear stress in a perfect conductor is wave-like. As suggested by Fig. 8.6.1c, the motion propagates along the lines of magnetic field intensity as a transverse electromechanical wave. Just how perfectly the fluid must conduct and how free of viscosity it must be to observe these waves is now determined by a model that includes magnetic and viscous diffusion.

A layer of fluid having conductivity σ, viscosity η and thickness Δ is shown in Fig. 8.6.2. In static equilibrium, it is permeated by a uniform x directed magnetic field intensity H_o. Because the magnetic flux density is solenoidal, it is written in the form $\vec{B} = \mu H_o \vec{i}_x + \nabla \times \vec{A}$, where $\vec{A}$ is governed by the magnetic diffusion equation, Eq. 6.5.3. Fluid deformations that are now considered are independent of z and confined to x-y planes, and so only the z component of $\vec{A}$ exists; $\vec{A} = A\vec{i}_z$. Moreover, motions are taken as independent of y, so $\vec{v} = v_y(x,t)\vec{i}_y$ and $A = A(x,t)$. Thus,

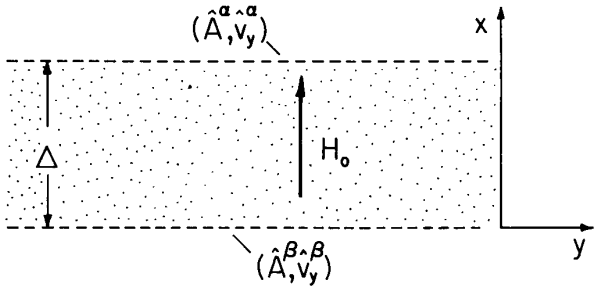

Fig. 8.6.2. Layer of liquid metal or plasma with ambient magnetic field H_o.

$$\frac{1}{\mu\sigma}\frac{\partial^2 A}{\partial x^2} = \frac{\partial A}{\partial t} + \mu H_o v_y \qquad (1)$$

where [Eq. (b) of Table 2.18.1]

$$H_y = -\frac{1}{\mu}\frac{\partial A}{\partial x} \qquad (2)$$

The fact that motions are independent of y and that $\vec{B}$ is solenoidal combine to show that B_x is independent of x, and hence $B_x = \mu H_o$ even as the motion occurs. There is no linearization implied by the last term of Eq. 1.

For the one-dimensional incompressible motions, conservation of mass is identically satisfied and only the y component of the force equation is pertinent. With the magnetic stress substituted into Eq. 7.16.1, it follows from Eq. 2 that

$$\rho\frac{\partial v_y}{\partial t} = -H_o\frac{\partial^2 A}{\partial x^2} + \eta\frac{\partial^2 v_y}{\partial x^2} \qquad (3)$$

where the magnetic shear stress is $T_{yx} = \mu H_o H_y$ and the viscous shear stress is

$$S_{yx} = \eta\frac{\partial v_y}{\partial x} \qquad (4)$$

The self-consistent coupling between field and fluid is expressed by Eqs. 1 and 3. These represent the one-dimensional response of the layer shown in Fig. 8.6.2. Given the amplitudes $[\hat{A}^{\alpha},\hat{A}^{\beta},\hat{v}_y^{\alpha},\hat{v}_y^{\beta}]$ at the boundaries, what are the transfer relations for the amplitudes $[\hat{H}_y^{\alpha},\hat{H}_y^{\beta},\hat{S}_{yx}^{\alpha},\hat{S}_{yx}^{\beta}]$ in these same planes? (Note that these relations are the limit $k \to 0$ of more general transfer relations for traveling wave dependences on y. For the two-dimensional motions implied by such a dependence, v_x becomes an additional variable, and the normal stress S_{xx} is its complement. Thus, the more general two-dimensional transfer relations relate two potentials and four velocity components to two tangential fields and four stress components, evaluated at the α and β surfaces.)

For complex amplitude solutions of the form $A = \mathrm{Re}\,\hat{A}(x)\exp(j\omega t)$, Eqs. 1 and 3 become differential laws for the x dependence:

$$\frac{1}{\mu\sigma}\frac{d^2\hat{A}}{dx^2} - j\omega\hat{A} - \mu H_o\hat{v}_y = 0 \qquad (5)$$

$$\eta\frac{d^2\hat{v}_y}{dx^2} - j\omega\rho\hat{v}_y - H_o\frac{d^2\hat{A}}{dx^2} = 0 \qquad (6)$$

These constant coefficient expressions admit solutions $\hat{A} \propto \exp(\gamma x)$ and $\hat{v}_y \propto \exp(\gamma x)$. Substitution shows that γ must satisfy the relation ($\gamma\Delta = \underline{\gamma}$):

$$(\gamma^2 - j\omega\tau_m)(\gamma^2 - j\omega\tau_v) - \left(\frac{\tau_m\tau_v}{\tau_{MI}^2}\right)\gamma^2 = 0 \qquad (7)$$

Thus, the spatial distribution with x is determined by the magnetic diffusion time, τ_m, the viscous diffusion time, τ_v, and the magneto-inertial time, τ_{MI}:

$$\tau_m \equiv \mu\sigma\Delta^2; \quad \tau_v \equiv \rho\Delta^2/\eta; \quad \tau_{MI} = \Delta\sqrt{\rho/\mu H_o^2} \qquad (8)$$

In the absence of the equilibrium magnetic field ($H_o = 0$), Eq. 7 shows that what remains is viscous diffusion (Secs. 7.18 and 7.19) and magnetic diffusion (Secs. 6.5 and 6.6). The parameter expressing the coupling in Eq. 7, the ratio of the geometric mean of the magnetic and viscous diffusion times to the magneto-inertial time is defined as the Magnetic Hartmann number $H_m = \sqrt{\tau_m \tau_v}/\tau_{MI} = \Delta\mu H_o\sqrt{\sigma/\eta}$. With the coupling, there are three characteristic times that determine the dynamics.

Even so, the biquartic form of Eq. 7 shows that there are still only four solutions to Eqs. 5 and 6, $\gamma = \pm\gamma_1$ and $\gamma = \pm\gamma_2$, where

$$\frac{\gamma_1}{2} = \left\{\frac{1}{2}\left[H_m^2 + j\omega(\tau_m + \tau_v)\right] \pm \frac{1}{2}\sqrt{\left[H_m^4 - \omega^2(\tau_m - \tau_v)^2\right] + 2j\omega(\tau_m + \tau_v)H_m^2}\right\}^{1/2} \tag{9}$$

Thus, in terms of coefficients $\hat{A}_1 \cdots \hat{A}_4$, the solution is

$$\hat{A} = \hat{A}_1 \sinh \gamma_1 x + \hat{A}_2 \sinh \gamma_1(x - \Delta) + \hat{A}_3 \sinh \gamma_2 x + \hat{A}_4 \sinh \gamma_2(x - \Delta) \tag{10}$$

Equation 5 shows how to find $\hat{v}_y$ in terms of these same four coefficients:

$$\hat{v}_y = \frac{1}{\mu^2 H_o \sigma}\left(\frac{d^2\hat{A}}{dx^2} - j\omega\mu\sigma\hat{A}\right) \tag{11}$$

Given the potential and velocity in the α and β planes, Eqs. 10 and 11 become four expressions that can be inverted to determine $\hat{A}_1 \cdots \hat{A}_4$. Fortunately, $\hat{A}_1$ and $\hat{A}_3$ are determined by the α variables alone, and A_2 and A_4 by the β variables alone, so this task is not all that difficult. In fact, with a bit of hindsight, the desired linear combination of solutions can be written by inspection:

$$\begin{aligned}\hat{A} = \Bigg\{&\left[-(\gamma_2^2 - j\omega\mu\sigma)\hat{A}^\alpha + \mu^2 H_o \sigma \hat{v}_y^\alpha\right]\frac{\sinh \gamma_1 x}{\sinh \gamma_1 \Delta} + \left[(\gamma_2^2 - j\omega\mu\sigma)\hat{A}^\beta - \mu^2 H_o \sigma \hat{v}_y^\beta\right]\frac{\sinh \gamma_1(x-\Delta)}{\sinh \gamma_1 \Delta} \\ &+ \left[(\gamma_1^2 - j\omega\mu\sigma)\hat{A}^\alpha - \mu^2 H_o \sigma \hat{v}_y^\alpha\right]\frac{\sinh \gamma_2 x}{\sinh \gamma_2 \Delta} + \left[-(\gamma_1^2 - j\omega\mu\sigma)\hat{A}^\beta + \mu^2 H_o \sigma \hat{v}_y^\beta\right]\frac{\sinh \gamma_2(x-\Delta)}{\sinh \gamma_2 \Delta}\Bigg\}/(\gamma_1^2 - \gamma_2^2)\end{aligned} \tag{12}$$

Now, by use of Eqs. 11 and 12 in 2 and 4, the transfer relations follow:

$$\begin{bmatrix} \hat{H}_y^\alpha \\ \hat{H}_y^\beta \\ \hat{S}_{yx}^\alpha \\ \hat{S}_{yx}^\beta \end{bmatrix} = \left[M_{ij}\right] \begin{bmatrix} \hat{A}^\alpha \\ \hat{A}^\beta \\ \hat{v}_y^\alpha \\ \hat{v}_y^\beta \end{bmatrix} \tag{13}$$

where with $\gamma_k \equiv \gamma_k \Delta$ and $q_k^2 \equiv \gamma_k^2 - j\omega\mu\sigma\Delta^2$, k = 1 or 2:

$$M_1\binom{1}{2} = -M_2\binom{2}{1} = \frac{1}{\mu}\left[\gamma_1 q_2^2 \begin{pmatrix}\cosh \gamma_1 \\ -1\end{pmatrix}\sinh \gamma_2 - \gamma_2 q_1^2 \begin{pmatrix}\cosh \gamma_2 \\ -1\end{pmatrix}\sinh \gamma_1\right]/F$$

$$M_1\binom{3}{4} = -M_2\binom{4}{3} = \mu H_o \sigma \Delta^2\left[\gamma_1 \begin{pmatrix}\cosh \gamma_1 \\ -1\end{pmatrix}\sinh \gamma_2 - \gamma_2 \begin{pmatrix}\cosh \gamma_2 \\ -1\end{pmatrix}\sinh \gamma_1\right]/F$$

$$M_3\binom{1}{2} = -M_4\binom{2}{1} = \frac{\eta}{\mu^2 H_o \sigma \Delta^2} q_1^2 q_2^2\left[\gamma_1 \sinh \gamma_2 \begin{pmatrix}-\cosh \gamma_1 \\ 1\end{pmatrix} - \gamma_2 \sinh \gamma_1 \begin{pmatrix}-\cosh \gamma_2 \\ 1\end{pmatrix}\right]/F$$

$$M_3\binom{3}{4} = -M_4\binom{4}{3} = \eta\left[\gamma_1 q_2^2 \begin{pmatrix}\cosh \gamma_2 \\ -1\end{pmatrix}\sinh \gamma_1 - \gamma_1 q_1^2 \begin{pmatrix}\cosh \gamma_1 \\ -1\end{pmatrix}\sinh \gamma_2\right]/F$$

$$F = \Delta(\gamma_1^2 - \gamma_2^2)\sinh \gamma_1 \sinh \gamma_2$$

Temporal Modes: Suppose that the layer is excited in the α and β planes by perfectly conducting rigid boundaries that (perhaps by dint of a displacement in the y direction) provide excitations $(\hat{v}_y^{\alpha}, \hat{v}_y^{\beta})$. The perfect conductivity assures $\hat{A}^{\alpha} = 0$ and $\hat{A}^{\beta} = 0$ (Eq. 6.7.6). Thus, the electrical and mechanical variables on the right in Eq. 13 are determined. The temporal modes for this system (that represent the homogeneous response to initial conditions and underlie the driven response) are then given by F = 0. The roots of this equation are simply

$$\gamma_1 = jn\pi; \quad \gamma_2 = jn\pi, \quad n = 1,2,\cdots \tag{14}$$

With these values of γ, Eq. 7 can be solved for the eigenfrequencies

$$\omega_n = j\frac{(n\pi)^2}{2}\left[\frac{1}{\tau_m} + \frac{1}{\tau_v}\right] \pm \sqrt{(n\pi)^2\left[\frac{1}{\tau_{MI}^2} - \frac{(n\pi)^2}{4}\left(\frac{1}{\tau_m} - \frac{1}{\tau_v}\right)^2\right]} \tag{15}$$

In the extreme where τ_m and τ_v are long compared to τ_{MI},

$$\omega_n = \pm\frac{n\pi}{\tau_{MI}} \tag{16}$$

This oscillatory natural frequency is the result of an Alfven wave resonating between the boundaries. The wave transit time is $\tau_{MI} = \Delta/v_a$, so $v_a = \sqrt{\mu H_o^2/\rho}$ is the velocity of this Alfvén wave.

Typical of an experiment using a sodium-based liquid metal are the parameters

$$\left.\begin{array}{ll} \sigma = 10^6 \text{ mhos/m} & \Delta = 0.1 \text{ m} \\ \rho = 10^3 \text{ kg/m}^3 & \mu H_o = 1 \text{ tesla} \\ \eta = 10^{-3} \text{ newton-sec/m}^2 & \end{array}\right\} \quad \begin{array}{l} \tau_v = 10^4 \text{ sec} \\ \tau_m = 1.25 \times 10^{-2} \text{ sec} \\ \tau_{MI} = 3.53 \times 10^{-3} \text{ sec} \end{array} \tag{17}$$

Thus, the characteristic times have the ordering $\tau_{MI} < \tau_m < \tau_v$ with the magnetic diffusion time far shorter than the viscous diffusion time. (The ratio of these times is sometimes defined as the magnetic Prandtl number $P_m = \tau_m/\tau_v = \eta\mu\sigma/\rho$. For the numbers given by Eq. 17, $P_m = 1.25 \times 10^{-6}$.) Thus, in Eq. 15, $1/\tau_v$ can be neglected compared to $1/\tau_m$ and it is seen that the natural frequency will display an oscillatory part if

$$\frac{\tau_m}{\tau_{MI}} > \frac{n\pi}{2} \tag{18}$$

That the transit time for the Alfvén wave be short compared to the time for appreciable magnetic diffusion underscores the flux-conserving nature of the wave dynamics. For the numbers of Eq. 17, $\tau_m/\tau_{MI} = 3.54$. As a practical matter, Alfvén waves observed in the laboratory are relatively damped. Note that as Δ increases, the inequality of Eq. 18 is better satisfied. The dependence of the natural frequency on the mode number n reflects how damping increases with the wave number $j\gamma$ in the x direction. Near the origin in Fig. 8.6.3, the linear relation of frequency and mode number is typical of nondispersive wave phenomena. As the mode number increases, magnetic (and possibly viscous) diffusion damps the oscillations, which then give way to totally damped modes. The oscillatory modes would of course appear as resonances in the sinusoidal steady-state driven response.

Spatial Structure of Sinusoidal Steady-State Response: The penetration of a sinusoidal excitation from the surfaces into the bulk is determined by γ_1 and γ_2, Eq. 9. As the magnetic field is raised, the viscous and magnetic skin effect are taken over by the electromechanical coupling. In Fig. 8.6.4, the transition of these complex wave numbers is shown, with the magnetic Hartmann number H_m representing the magnetic field. In terms of characteristic times, H_m is increased until the magneto-inertial time becomes sufficiently short that the Alfvén wave can penetrate the layer before the flux diffuses to its original uniform distribution. The magnetic shear stress is then able to penetrate the layer (tending to set the whole of it into motion) to a greater extent than would be possible via the magnetic or viscous diffusion alone. This is indicated by the lower of the roots shown, which has an imaginary part $\gamma \to \pm\sqrt{\tau_m\tau_v}/\Delta H_m = \pm\omega\tau_{MI}/\Delta$ as H_m becomes large. In this same limit of large H_m, the other branch becomes strongly decaying, with value $\gamma = \pm H_m/\Delta$. The physical nature of the dynamics represented by this mode is recognized by observing that $H_m = \sqrt{\tau_m/\tau_{MV}}$, where τ_{MV} is the magneto-viscous time. The electrical analogue of this time, which expresses the rate at which a process occurs involving a competion of viscous and magnetic stresses, will play an essential role in the next section. An experiment demonstrating Alfvén waves is sketched in Fig. 8.6.5.[1]

1. See also J. R. Melcher and E. P. Warren, "Demonstration of Magnetic Flux Constraints and a Lumped Parameter Alfvén Wave," IEEE Transactions on Education, Vol. E-8, Nos. 2 and 3, June-September, 1965, pp. 41-47.

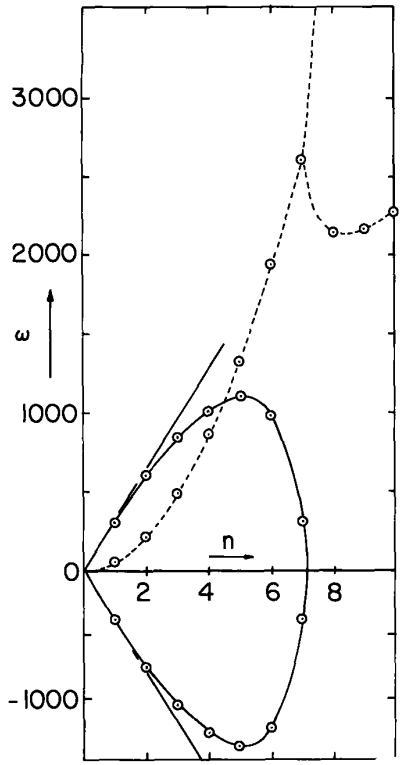

Fig. 8.6.3. Eigenfrequencies of temporal modes as a function of mode number for $\tau_{MI} = 0.01$, $\tau_m = 0.1$, and $\tau_v = 1$. ω_r ———, ω_i -----. H_m=31.6.

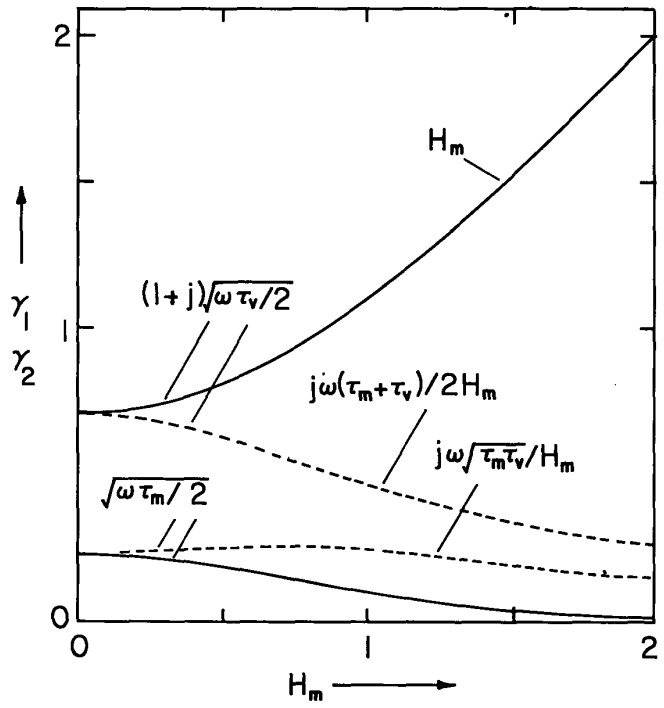

Fig. 8.6.4. Real (——) and imaginary (---) parts of γ_1 and γ_2 (Eq. 9) as functions of $H_m \equiv \Delta\mu H_o\sqrt{\sigma/\eta}$. Low- and high-$H_m$ approximations are shown. Note that the Alfvén wave branch is represented by $j\omega\sqrt{\tau_m\tau_v}/H_m = j\omega\tau_{MI}$.

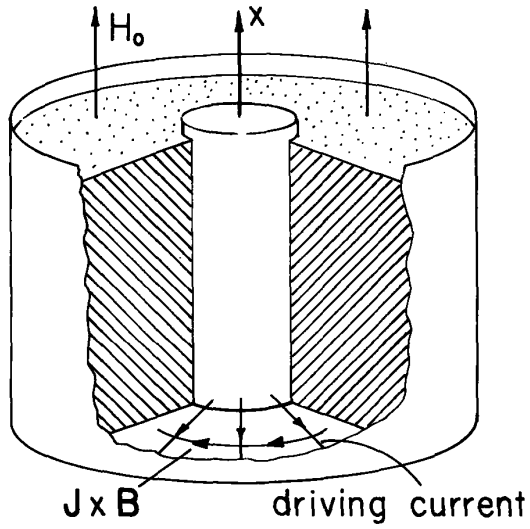

Fig. 8.6.5

Alfvén wave, as demonstrated by Shercliff in film "Magnetohydrodynamics" (Reference 7, Appendix C). Liquid NaK (sodium-potassium eutectic) fills conducting circular metal container having coaxial inner and outer walls. Wave is excited at bottom by radial driving current and detected at middle by coil that senses the change in magnetic field accompanying the passage of the upward-propagating electromechanical wave. As viewed radially inward, layers of liquid metal undergo shearing motions depicted by Fig. 8.6.1.

8.7 Potential Conserving Continua and Electric Shear Stress Instability

In an electric counterpart to the magnetic flux conserving fluid introduced in Sec. 8.6, a fluid element having fixed identity tends to retain its potential even as it moves. Under what physical circumstances could a homogeneous continuum tend to conserve its potential in this way? Figure 8.7.1 gives a schematic illustration (see Prob. 5.12.1 for charge relaxation in anisotropic conductors).

Initially, the volume is filled with static layers of miscible fluid having the same mechanical properties. Alternate layers are rendered conducting, perhaps by doping the same fluid as used for the other layers. At the upper and lower extremities, the conducting layers make electrical contact with

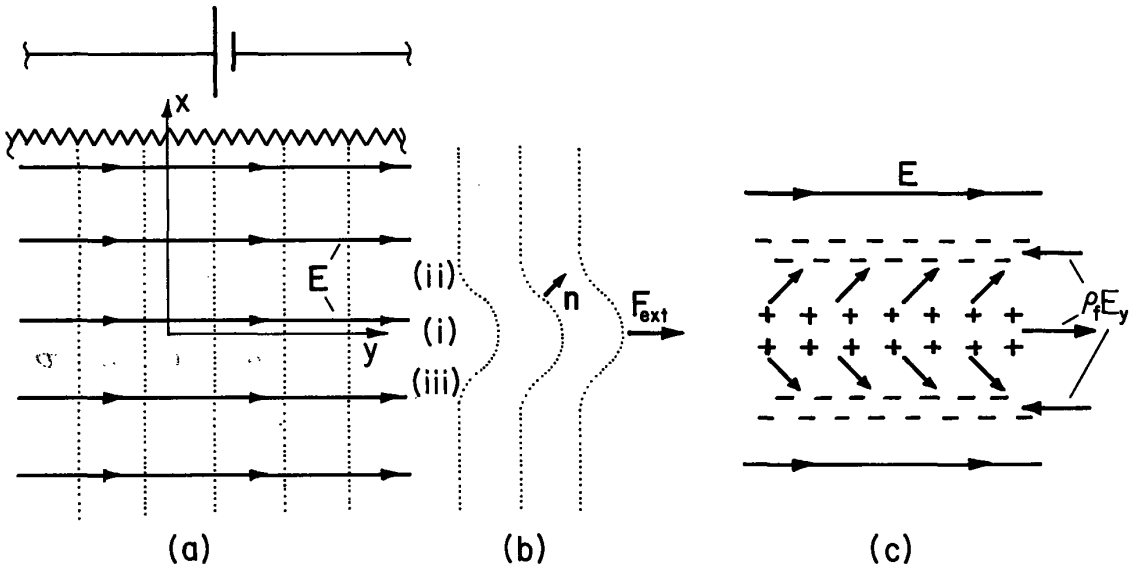

Fig. 8.7.1. (a) Example of potential conserving fluid made from numerous conducting layers buffered by relatively insulating layers. On a macroscale, a given fluid region tends to retain its potential as it deforms. (b) Shearing displacement causing elevation of potential in plane (i) relative to that at the same position y in planes (ii) and (iii). (c) Charge density implied by potential conservation, showing electrical force induced by the motion in adjacent layers.

surfaces having a linear potential distribution in the y direction. Thus, there is an initial ambient electric field $\vec{E} = E_0\vec{i}_y$ throughout the volume. What would be termed an isotropic inhomogeneous system on a microscale typified by the interlayer dimensions, is an anisotropic homogeneous system on the macroscale considered here. On this macroscale, a material element tends to retain its initial potential. In the model considered here, the conducting layers are of finite conductivity, but the layers between are considered perfect insulators. Just how faithfully the potential is conserved therefore depends on the electrical relaxation time of the composite.

By way of forming an intuitive impression of why the electric field induces instability, consider motions that are purely y-directed but depend on x. Suppose that the external force density $F_{ext}\vec{i}_y$ is used to translate a fluid layer in the y-z plane, denoted by (i) in Fig. 8.7.1b. To begin with, the potential of this and the adjacent layers decreases linearly in the y direction. So, at a given position along the y axis, the translation results in the potential in the plane (i) becoming elevated with respect to that of the adjacent layers (ii) and (iii). The adjacent layers form capacitor plates with the (i) layer which, in accordance with the relative potentials, are charged as sketched in Fig. 8.7.1c.

The field- and deformation-induced charge of the initially displaced layer, (i), are such that it is subject to an electrical force tending to further encourage the deformation. Thus, with the adjacent layer fixed, the external force would act against a negative spring constant. However, the adjacent layers are not fixed and experience electrical forces tending to carry them in a direction opposite that of the original displacement. There is an electrical shear stress acting between adjacent layers that is proportional to the <u>negative</u> of the strain. By contrast with the magnetic shear stress that gives rise to Alfvén waves, the electric stress tends to cause instability.

The laws needed to formulate a model begin with a constitutive law for the conduction. With $\vec{n}$ defined as a unit normal to a material surface of fixed identity that is initially in an x-z plane, as shown in Fig. 8.7.1b, the component of the electric field that is tangential to this surface is $-\vec{n} \times \vec{n} \times \vec{E}$. Thus, if the average conductivity in the plane of the conducting layer is σ, the current density in a stationary sample of the anisotropic material is

$$\vec{J}_f' = -\sigma\vec{n} \times \vec{n} \times \vec{E} \tag{1}$$

Because $\vec{J}_f = \vec{J}_f' + \rho_f\vec{v}$, it follows that the statement of charge conservation, Eq. 2.3.25a, is

$$\nabla\cdot[-\sigma(\vec{n} \times \vec{n} \times \vec{E}) + \rho_f\vec{v}] + \frac{\partial\rho_f}{\partial t} = 0 \tag{2}$$

The normal vector can be eliminated from this expression by first expressing it in terms of the surface $y = \xi(x,t)$

$$\vec{n} = [\vec{i}_y - \frac{\partial \xi}{\partial x}\vec{i}_x][1 + (\frac{\partial \xi}{\partial x})^2]^{-\frac{1}{2}} \tag{3}$$

and then recognizing that because this surface is of fixed identity, the function $F = y - \xi$ must have a convective derivative that is zero (Sec. 7.5):

$$v_y = \frac{\partial \xi}{\partial t} + v_x \frac{\partial \xi}{\partial x} \tag{4}$$

In Eq. 2, $\vec{n}$ can be replaced by Eq. 3, where ξ is in turn related to $\vec{v}$ by Eq. 4.

Before carrying out this elimination for the case at hand, note that because the electric field is irrotational and the perturbation quantities only depend on x, the electric field in the y direction is not a function of x. Pinned at E_o in any y-z plane, E_y remains this value even as the fluid deforms: $\vec{E} = E_o\vec{i}_y - (\partial\Phi/\partial x)\vec{i}_x$. As a result, Gauss' Law becomes

$$\frac{\partial^2 \Phi}{\partial x^2} = -\frac{\rho_f}{\varepsilon} \tag{5}$$

The motions considered are only in the y direction: $\vec{v} = v_y(x,t)\vec{i}_y$. With this understanding, Eqs. 2, 3 and 4 are linearized and combined to eliminate ξ, and Eq. 5 is substituted for ρ_f, to obtain

$$\frac{\partial^2}{\partial x^2}[E_o v_y - \frac{\partial}{\partial t}(\Phi + \frac{\varepsilon}{\sigma}\frac{\partial \Phi}{\partial t})] = 0 \tag{6}$$

This statement of the effect of the motion on the fields reduces to the linearized version of $D\Phi/Dt = 0$ in the limit where the charge relaxation time, ε/σ, is short compared to times of interest. If the charge can relax instantaneously, the potential of an element of fluid is conserved even as it deforms.

The y component of the force equation, Eq. 7.16.6 with $\nabla\cdot\vec{v} = 0$ and $\vec{F}_{ex}$ represented by the divergence of the stress tensor (given with Eq. 3.7.22 of Table 3.10.1), is

$$\rho \frac{\partial v_y}{\partial t} = -\varepsilon E_o \frac{\partial^2 \Phi}{\partial x^2} + \eta \frac{\partial^2 v_y}{\partial x^2} \tag{7}$$

The x-component simply determines the pressure distribution required to equilibrate the x component of the electrical force density. Equations 6 and 7 represent the electromechanical coupling.

The quantity in brackets in Eq. 6 is zero throughout the volume when the fluid is in static equilibrium. Hence, the two constants resulting from integrating Eq. 6 twice on x are zero. Then, with the substitutions $v_y = \mathrm{Re}\hat{v}_y(x)e^{j\omega t}$ and $\Phi = \mathrm{Re}\hat{\Phi}(x)e^{j\omega t}$, Eqs. 6 and 7 become

$$E_o\hat{v}_y = j\omega[1 + \frac{j\omega\varepsilon}{\sigma}]\hat{\Phi} = 0 \tag{8}$$

$$(j\omega\rho - \eta\frac{d^2}{dx^2})\hat{v}_y + \varepsilon E_o \frac{d^2\hat{\Phi}}{dx^2} = 0 \tag{9}$$

By contrast with the magnetohydrodynamic system represented by Eqs. 8.6.5 and 8.6.6, the system is only second order in x, so that there are only two boundary conditions that can be imposed on a layer having the thickness Δ (Fig. 8.6.2). Imposing a boundary condition on $\hat{\Phi}$ is (through Eq. 8) tantamount to a condition on v_y. Substitution into Eqs. 8 and 9 of solutions having the form $\hat{v}_y = \exp(\gamma x)$ and $\hat{\Phi} = \exp(\gamma x)$ gives a pair of homogeneous relations

$$\begin{bmatrix} E_o & -j\omega\left(1 + \frac{j\omega\varepsilon}{\sigma}\right) \\ j\omega\rho - \eta\gamma^2 & \varepsilon E_o\gamma^2 \end{bmatrix}\begin{bmatrix} \hat{v}_y \\ \hat{\Phi} \end{bmatrix} = 0 \tag{10}$$

and the requirement that the determinant of the coefficients vanish gives an expression for the allowed values of γ:

$$\gamma = \pm\gamma_1; \quad \gamma_1 \equiv \sqrt{\frac{j\omega\rho}{\eta + \dfrac{j\varepsilon E_o^2}{\omega(1 + \dfrac{j\omega\varepsilon}{\sigma})}}} \tag{11}$$

The situation is now no different than in dealing with Laplace's equation, where solutions take the form of Eq. 2.16.15 with $\gamma \to \gamma_1$. Thus, the transfer relation for the layer is (Table 2.16.1):

$$\begin{bmatrix} \hat{D}_x^\alpha \\ \hat{D}_x^\beta \end{bmatrix} = \frac{\gamma_1\varepsilon}{\sinh(\gamma_1\Delta)} \begin{bmatrix} -\cosh(\gamma_1\Delta) & 1 \\ -1 & \cosh(\gamma_1\Delta) \end{bmatrix} \begin{bmatrix} \hat{\Phi}^\alpha \\ \hat{\Phi}^\beta \end{bmatrix} \tag{12}$$

In terms of these variables, the mechanical variables follow from Eq. 8 as

$$\hat{v}_y = \frac{j\omega}{E_o}\left[1 + \frac{j\omega\varepsilon}{\sigma}\right]\hat{\Phi} \tag{13}$$

$$\hat{S}_{yx} = \eta\frac{d\hat{v}_y}{dx} = \frac{j\omega\eta}{E_o}\left[1 + \frac{j\omega\varepsilon}{\sigma}\right]\frac{d\hat{\Phi}}{dx} \tag{14}$$

Temporal Modes: Because the system is unstable, the temporal modes are of most interest. For a system bounded by planes maintaining the linear equilibrium distribution in potential (constrained to zero perturbation potential), the condition on ω resulting from there being a finite solution $(\hat{D}_x^\alpha, \hat{D}_x^\beta)$ with $(\hat{\Phi}^\alpha, \hat{\Phi}^\beta) = 0$ is $\sinh(\gamma_1\Delta) = 0$. Thus, the eigenvalues are

$$\gamma_1\Delta = jn\pi, \quad n = 1,2,3\cdots \tag{15}$$

The eigenfrequencies follow by substituting γ_1 from this expression into Eq. 11. The result is a cubic equation which determines the allowed frequencies ω:

$$\omega^3 - \omega^2 j\left[\frac{(n\pi)^2}{\tau_v} + \frac{1}{\tau_e}\right] - \omega\frac{(n\pi)^2}{\tau_v\tau_e} - \frac{j(n\pi)^2}{\tau_e\tau_v\tau_{EV}} = 0 \tag{16}$$

$$\tau_v \equiv \frac{\rho\Delta^2}{\eta}; \quad \tau_e \equiv \frac{\varepsilon}{\sigma}; \quad \tau_{EV} = \frac{\eta}{\varepsilon E_o^2}$$

As a function of the mode number $n\pi$, the solutions $s_n = j\omega$ of this expression are illustrated in Fig. 8.7.2. For each sinusoidal distribution represented by a given n, there are three temporal modes, one unstable and two decaying.

Typical of a 2-cm liquid layer having 50 times the viscosity of water, the density of water, an electrical relaxation time of 10^{-2} sec and $E_o = 2 \times 10^{+5}$ V/m are the times given in the caption. Note that $\tau_e < \tau_{EV} < \tau_v$.

The roots to Eq. 16 in the limit $\tau_e \to 0$ give a good idea of what is happening on time scales long compared to τ_e. The quadratic limit of Eq. 16 can then be solved to give

$$s = \frac{(n\pi)^2}{2\tau_v}\left[-1 \pm \sqrt{1 + \frac{4\tau_v}{\tau_{EV}(n\pi)^2}}\right] \tag{17}$$

Thus, there are roots $s_n > 0$ representing an exponentially growing instability. The fastest growing modes are those having the largest number of wavelengths in the x direction. In the limit $n\pi \to \infty$, this mode has a growth rate τ_{EV}. (In fact, there would be a finite mode exhibiting the maximum rate of growth, since wavelengths in the x direction shorter than the distance between layers are not described by the model.) By contrast with the electro-viscous nature of the short-wavelength instability, the long wavelengths (small mode numbers) are electro-inertial in nature. In the limit $n\pi \to 0$, Eq. 17 reduces to $s_n = 1/\tau_{EI}$, where $\tau_{EI} = \sqrt{\tau_v\tau_{EV}} = \Delta\sqrt{\rho\varepsilon E^2}$. Until its rate of decay becomes comparable to τ_e, the decaying mode can also be approximated using Eq. 17. At short wavelengths, the basically viscous diffusion mode and charge relaxation mode couple to produce a pair of modes that are damped in a sinusoidal fashion.

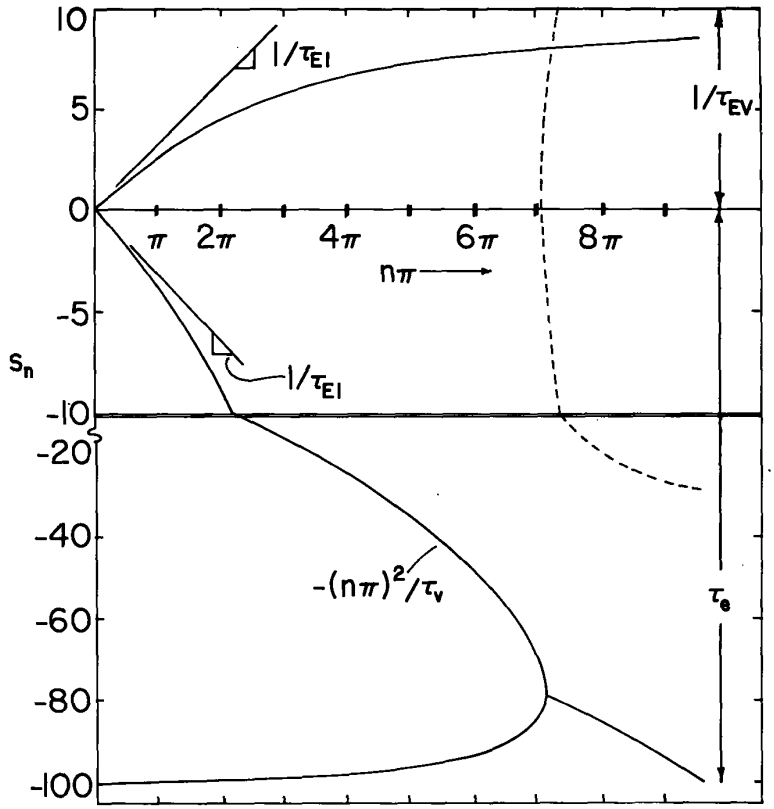

Fig. 8.7.2. Frequencies of temporal eigenmodes, $s_n = j\omega$; --- $(s_n)_r$, —— $(s_n)_i$. For each n there are three modes. $\tau_e = 10^{-2}$ sec, $\tau_{EV} = 0.1$ sec, $\tau_v = 10$ sec.

The instability is fundamental to many situations where electric fields are used to augment mass, heat and momentum transfer. Usually a more complicated model is required even to recognize the linear stages of instability. Shown in Fig. 8.7.3 is an example for which the illustration given in this section is itself a useful model. The Couette mixer exploits a rotating inner cylinder to promote large scale mixing. Two liquids entering at the bottom are typically the highly viscous components of a polymer. Because of the rotation, these form laminae of relatively insulating and conducting liquids that work their way upward to the exit. With the application of a radial electric field, instability leads to mixing. The electrohydrodynamic instability provides mixing on a length scale that bridges the gap between what can be efficiently produced by the mechanical stirring and what is required to insure

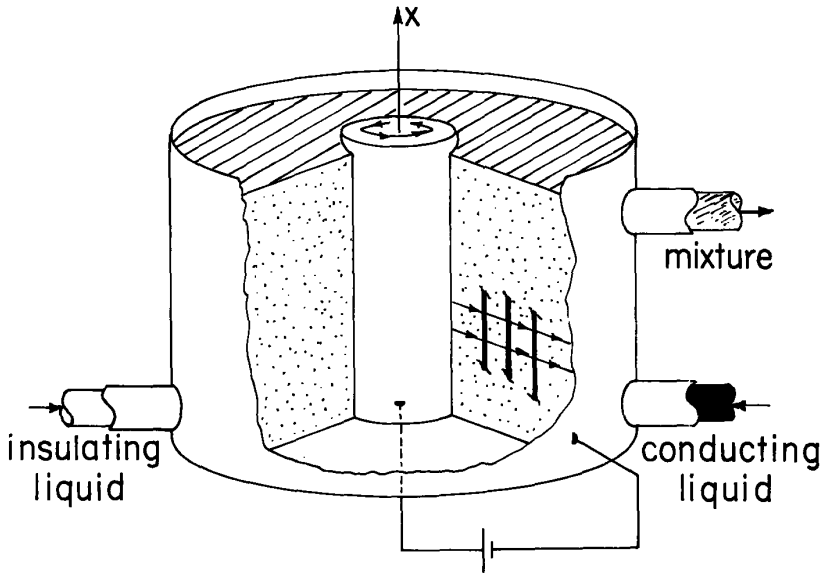

Fig. 8.7.3

Couette mixer exploiting instability of components stressed by electric field.

genuine molecular scale mixing.[1] For successful operation the residence time of the liquids must at least exceed $\tau_{EV} = \eta/\epsilon E_o^2$. Even in its nonlinear stages and on length scales shorter than the distance between layers, τ_{EV} is found to scale the rate at which mixing processes occur.[2,3] In practical applications, the "insulating" component actually is itself semi-insulating so the growth rate for instability is reduced by a factor reflecting the ratio of the component conductivities.

8.8 Magneto-Acoustic and Electro-Acoustic Waves

Electromechanical coupling through dilatational deformation is illustrated in this section. First considered as one-dimensional examples are perfectly conducting limits of the MQS and EQS continua of Secs. 8.6 and 8.7, respectively. Then, the incremental motions of a system of magnetizable particles randomly suspended in a uniform magnetic field are modeled.

Both the MQS and EQS configurations are shown in Fig. 8.8.1. Also shown in each case are the distributed elements that embody the same physical phenomena as represented by the continuum models. Without electromechanical coupling, the one-dimensional acoustic wave propagates through a continuum of masses (represented by the perfectly conducting plates) interconnected by layers of fluid comprising the springs.

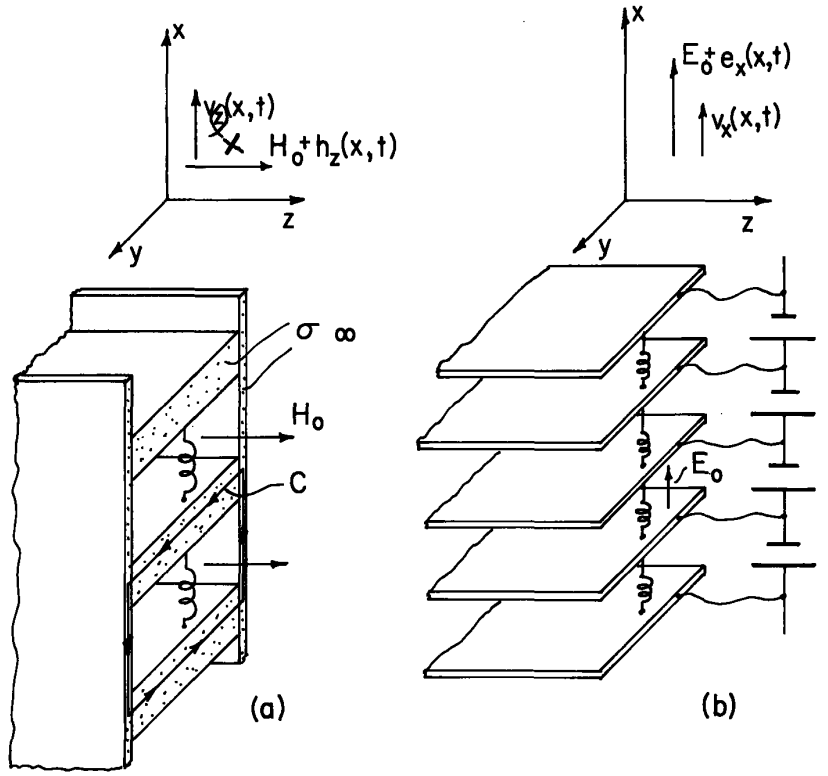

Fig. 8.8.1. One-dimensional compressional motions. (a) Magneto-acoustic waves in perfectly conducting liquid across uniform magnetic field. (b) electro-acoustic waves in potential conserving continuum along uniform electric field. Lumped models emphasize salient features of dynamics.

In the magnetohydrodynamic case, the fluid is uniform and perfectly conducting. When at rest, it is permeated by a uniform magnetic field H_o directed transverse to the direction of propagation. Compression of the fluid results in a decrease in enclosed area for a contour such as C which is attached to the fluid. To retain the same flux linkage, a current is induced around this contour. The associated force density tends to counteract the dilatation, thus having the effect of a magnetic spring between elements. It is not surprising that the magnetic field tends to increase the velocity of propagation of waves.

---

1. C. A. Rotz, "A Generalized Approach to Increased Mixing Efficiency for Viscous Liquids," S.M. Thesis, Department of Mechanical Engineering, Massachusetts Institute of Technology, Cambridge, Mass., 1976.

2. J. H. Lang, J. F. Hoburg and J. R. Melcher, "Field Induced Mixing Across a Diaphragm," Phys. Fluids 19, 917 (1976).

3. J. F. Hoburg and J. R. Melcher, "Electrohydrodynamic Mixing and Instability Induced by Collinear Fields and Conductivity Gradients," Phys. Fluids 20, 903 (1977).

In the electrohydrodynamic case, a given element of fluid conserves its potential, as described in Sec. 8.7. Either the fluid is a stratification of insulating and conducting components, or it actually consists of thin conducting sheets dispersed through the fluid. Because the motions are compressional, such sheets would not inhibit the motions. The equivalent distributed lumped parameter system, shown in Fig. 8.7.1b, consists of perfectly conducting layers constrained to have the same potential difference even as their relative spacing changes. As a "plate" approaches one of its neighbors, the intervening electric field increases. So also does the electric force associated with the charge on that side of the plate. Thus, the electric field is equivalent in its effect to a spring with a negative spring constant. It has the effect of diminishing the stiffness of the "spring" separating a pair of plates. The field is expected to reduce the velocity of a wave propagating in the x direction.

Now, consider the interactions in analytical terms. In both cases, the linearized longitudinal force equation is simply

$$\rho_o \frac{\partial v_x}{\partial t} + \frac{\partial p'}{\partial x} = \frac{\partial T_{xx}}{\partial x} \tag{1}$$

where ρ_o is the equilibrium mass density, p' is the perturbation pressure, and T_{xx} is the Maxwell stress. With the assumption that pressure is only a function of density, Eq. 7.11.3 can be used to replace the perturbation pressure with the perturbation density,

$$p' = a^2\rho' \tag{2}$$

where a is the acoustic velocity. The permeability and permittivity in the respective situations are taken as constant. Thus, with $\vec{h}$ and $\vec{e}$ the perturbations in $\vec{H}$ and $\vec{E}$ respectively, to linear terms, T_{xx} becomes simply (Table 3.10.1, Eqs. 3.7.22 and 3.8.14)

$$T_{xx} \simeq -\frac{\mu}{2}(H_o+h_z)^2 \simeq -\frac{1}{2}\mu H_o^2 - \mu H_o h_z \quad \Big| \quad T_{xx} \simeq \frac{1}{2}\epsilon(E_o+e_x)^2 \simeq \frac{1}{2}\epsilon E_o^2 + \epsilon E_o e_x \tag{3}$$

These last three equations combine to become

$$\rho_o \frac{\partial v_x}{\partial t} + a^2 \frac{\partial \rho'}{\partial x} = -\mu H_o \frac{\partial h_z}{\partial x} \quad \Big| \quad \rho_o \frac{\partial v_x}{\partial t} + a^2 \frac{\partial \rho'}{\partial x} = \epsilon E_o \frac{\partial e_x}{\partial x} \tag{4}$$

To linear terms, conservation of mass, Eq. 7.2.3, requires that

$$\frac{\partial \rho'}{\partial t} + \rho_o \frac{\partial v_x}{\partial x} = 0 \tag{5}$$

These last two statements represent the mechanics, including the effect of the fields.

The reciprocal effects of the deformation on the fields follow from

the requirement that the flux linked by a surface of fixed identity be constant, Eq. 8.6.1. To linear terms

$$H_o \frac{\partial v_x}{\partial x} = -\frac{\partial h_z}{\partial t}$$

the requirement that the potential, Φ, of an element of fixed identity be constant, Eq. 8.7.1. To linear terms

$$\frac{\partial \Phi'}{\partial t} - E_o v_x = 0 \tag{6}$$

where $e_x = -\nabla\Phi'$

To combine these last three statements, take the time derivative of Eq. 4 and the space derivative of Eqs. 5 and 6 and eliminate p and h_z or e_x:

$$\frac{\partial^2 v_x}{\partial t^2} = a_m^2 \frac{\partial^2 v_x}{\partial x^2} \quad \Big| \quad \frac{\partial^2 v_x}{\partial t^2} = a_e^2 \frac{\partial^2 v_x}{\partial x^2} \tag{7}$$

These wave equations make it clear that the effect of the fields is to replace the acoustic velocity with a magneto-acoustic velocity:

$$a_m = \sqrt{a^2 + \frac{\mu H_o^2}{\rho_o}} \quad \Big| \quad a_e = \sqrt{a^2 - \frac{\epsilon E_o^2}{\rho_o}} \tag{8}$$

Acoustic velocities, given in Table 7.11.1, are typically 300 m/sec in gases and 1500 m/sec in liquids. In gases, the Alfvén velocity, $\sqrt{\mu H_o^2/\rho_o}$, can be made to dominate in its contribution to the magneto-acoustic velocity. In liquid metals the magnetic contribution to a_m is greatly reduced by the increased mass density, although it is still possible for it to be significant. But in the electro-acoustic wave, electrical breakdown limits the effect of the electric field to a level that would make it difficult to even measure the effect.

Magnetization Dilatational Waves: Although electromechanical effects on dilatational motions in natural materials are likely to be small, continua formed from "molecules" that are actually macroscopic in their dimensions can give rise to significant electromechanical effects. As an example, magnetizable spheres are suspended in a random array, with the voidage a gas or even vacuum. Interest is confined to deformations characterized by lengths that are large compared to the distance between particles. Unperturbed, the system is uniform on the macroscopic scale, and is subjected to a uniform z-directed magnetic field intensity H_o. Because the spheres can interact with each other only through the magnetic field, the pressure is taken as zero.

Perhaps determined experimentally, the effective permeability of the continuum has been related to the mass density through a constitutive law, $\mu = \mu(\rho)$. Thus, the force density of Eq. 3.8.17 from Table 3.10.1 is applicable. With perturbations from the equilibrium mass density and magnetic field, ρ_o and $H_o\vec{i}_z$, denoted by ρ' and $\vec{h}$, respectively, this force density is linearized to become

$$\vec{F} = \rho_o \nabla[H_o(\frac{\partial \mu}{\partial \rho})_o h_z + \frac{1}{2} H_o^2 (\frac{\partial^2 \mu}{\partial \rho^2})_o \rho'] \tag{9}$$

Because there are no free currents, $\vec{H}$ is irrotational and hence $\vec{H} = H_o\vec{i}_z - \nabla\psi$. Thus, the force equation, Eq. 7.4.4 written with $p = 0$, is

$$\rho_o \frac{\partial \vec{v}}{\partial t} = -\rho_o H_o (\frac{\partial \mu}{\partial \rho})_o \nabla(\frac{\partial \psi}{\partial z}) + \frac{\rho_o}{2} H_o^2 (\frac{\partial^2 \mu}{\partial \rho^2})_o \nabla\rho' \tag{10}$$

Mass conservation is represented by a linearized version of Eq. 7.2.3:

$$\frac{\partial \rho'}{\partial t} + \rho_o \nabla\cdot\vec{v} = 0 \tag{11}$$

In terms of the scalar potential, ψ, the linearized statement that $\mu\vec{H}$ is solenoidal is

$$-\mu(\rho_o)\nabla^2\psi + H_o(\frac{\partial \mu}{\partial \rho})_o \frac{\partial \rho'}{\partial z} = 0 \tag{12}$$

To obtain an expression for ρ' alone, the divergence of Eq. 10 is taken. Then Eq. 11 eliminates $\nabla\cdot\vec{v}$, while the $\partial(\ )/\partial z$ of Eq. 12 can be used to eliminate ψ. Thus, the expressions combine to give

$$\frac{\partial^2 \rho'}{\partial t^2} = \frac{\rho_o H_o^2}{\mu(\rho_o)} (\frac{\partial \mu}{\partial \rho})_o^2 \frac{\partial^2 \rho'}{\partial z^2} - \frac{\rho_o}{2} H_o^2 (\frac{\partial^2 \mu}{\partial \rho^2})_o \nabla^2\rho' \tag{13}$$

A possible relation between permeability and mass density is the Clausius-Mossotti law:[1]

$$\frac{(\frac{\mu}{\mu_o} - 1)}{(\frac{\mu}{\mu_o} + 2)} = C\rho \Rightarrow \frac{\partial \mu}{\partial \rho} = \frac{\mu_o}{3}(\frac{\mu}{\mu_o} + 2)(\frac{\mu}{\mu_o} - 1)\rho^{-1} \Rightarrow \frac{\partial^2 \mu}{\partial \rho^2} = \frac{2\mu_o}{9}(\frac{\mu}{\mu_o} - 1)^2(\frac{\mu}{\mu_o} + 2)\rho^{-2} \tag{14}$$

where C is determined by the nature of the spheres.

It follows from Eqs. 13 and 14 that compressional motions across the field lines (in the x direction) are unstable, while those in the direction of the field propagate with the velocity

$$a_M = \sqrt{\frac{\mu_o H_o^2}{\rho_o} \frac{2}{9} (\frac{\mu}{\mu_o} + 2)(\frac{\mu}{\mu_o} - 1)^2 \frac{\mu_o}{\mu}} \tag{15}$$

---

1. J. A. Stratton, Electromagnetic Theory, McGraw-Hill Book Company, New York, 1941, p. 140.

8.9 Gravity-Capillary Dynamics

The incompressible dynamics of fluids that are inhomogeneous in mass density are as commonplace as wave motions in a teacup or at the interface between sea and atmosphere. At the interface, the mass density suffers a step discontinuity. Fundamentally, the pertinent laws express the fact that the mass density in the neighborhood of a particle of fixed identity remains constant, Eq. 7.2.4, that mass is conserved, Eq. 7.2.5, and that inertial and pressure forces balance. For the present purposes the fluid is represented as being inviscid, and hence the pertinent force law is Eq. 7.4.4 with the external force density that due to gravity, $\vec{f}_{ex} = \rho\vec{g}$.

Because inhomogeneities in electrical properties are often accompanied by variations in mass density, electromechanical interactions with inhomogeneous systems are commonly interwoven with the fluid mechanics resulting from effects of gravity. In this section, the mechanics of a fluid interface illustrates effects of gravity in systems that are inhomogeneous in mass density. If the interface is between immiscible fluids, effects of capillarity are also important.

In the configuration shown in Fig. 8.9.1, planar layers of fluid each have uniform properties designated by the subscripts "a" (above) and "b" (below), respectively, and a common interface at $x = \xi(y,z,t)$. The lower fluid rests on a rigid boundary while the upper one consists of a deformable structure. The system is driven from this structure by the traveling-wave excitation shown in the figure. What is the response of the fluids, and in particular of their interface?

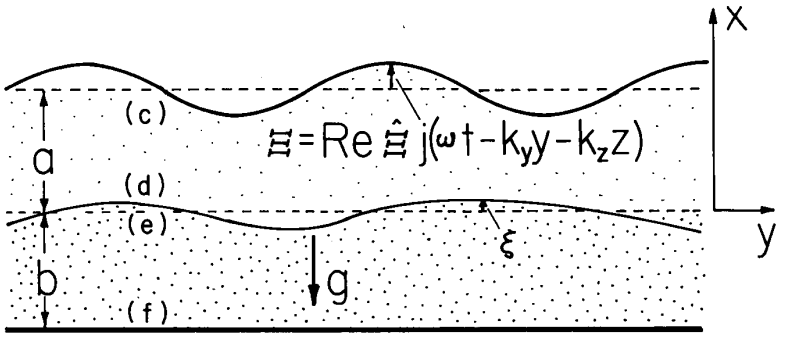

Fig. 8.9.1. Fluids of differing mass densities have interface at ξ and are driven by structure at Ξ.

In the absence of the excitation, the fluids are in static equilibrium with the gravitational force density. Thus, the fluid velocity $\vec{v} = 0$ and the pressure balances the gravitational force density. From the force equation, Eq. 7.8.3, applied to each region:

$$p = \begin{cases} -\rho_a g x + \Pi_a; & x > 0 \\ -\rho_b g x + \Pi_b; & x < 0 \end{cases} \tag{1}$$

Perturbations from this static equilibrium are represented in terms of complex amplitudes. To linear terms the pressure and velocity are

$$p = -\rho g x + \Pi + p'(x,y,z,t);\ p' = \mathrm{Re}\hat{p}(x)\exp j(\omega t - k_y y - k_z z) \tag{2}$$

$$\vec{v} = \mathrm{Re}\hat{\vec{v}}(x)\exp j(\omega t - k_y y - k_z z) \tag{3}$$

Within a given fluid region the mass density is uniform. Thus, the complex amplitudes in the respective planes designated in Fig. 8.9.1 are related by the transfer relations for an inviscid fluid given by Eq. (c) of Table 7.9.1:

$$\begin{bmatrix} \hat{p}^c \\ \hat{p}^d \end{bmatrix} = \frac{j\omega\rho_a}{k}\begin{bmatrix} -\coth(ka) & \frac{1}{\sinh(ka)} \\ \frac{-1}{\sinh(ka)} & \coth(ka) \end{bmatrix}\begin{bmatrix} \hat{v}_x^c \\ \hat{v}_x^d \end{bmatrix};\quad \begin{bmatrix} \hat{p}^e \\ \hat{p}^f \end{bmatrix} = \frac{j\omega\rho_b}{k}\begin{bmatrix} -\coth(kb) & \frac{1}{\sinh(kb)} \\ \frac{-1}{\sinh(kb)} & \coth(kb) \end{bmatrix}\begin{bmatrix} \hat{v}_x^e \\ \hat{v}_x^f \end{bmatrix} \tag{4}$$

Complex amplitudes are evaluated in the equilibrium planes. But, the jump conditions apply wherever the interface is actually located and that location is in fact yet to be determined! This difficulty is sidestepped by linearizing the jump conditions in such a way that they are expressed in terms of perturbation variables evaluated at the equilibrium positions of the boundaries.

Taking boundary and jump conditions from top to bottom, observe first that the position of the deformable upper structure is related to the velocity of the adjacent fluid by Eq. 7.5.5, which to linear terms is

$$\hat{v}_x^c = j\omega\hat{\Xi} \tag{5}$$

where it is appropriate to use the complex amplitude evaluated at the equilibrium position because the difference between that and $\hat{v}_x$ $(x = a + \Xi)$ is second order in the perturbation amplitude, Ξ.

Similarly, at the interface the velocities are related to the interfacial deformation by

$$\hat{v}_x^d = j\omega\hat{\xi}; \quad \hat{v}_x^e = j\omega\hat{\xi} \tag{6}$$

Again, this jump condition, which expresses mass conservation for the interface, has been written in terms of amplitudes evaluated at the equilibrium interfacial position. Stress balance for the interface is represented by Eq. 7.7.6, which has only a normal component. To linear terms, this is represented by the i = x component

$$[-\rho_a g\xi + \Pi_a + p'^d(x=\xi)]-[-\rho_b g\xi + \Pi_b + p'^e(x=\xi)] = \gamma\left(\frac{\partial^2\xi}{\partial y^2} + \frac{\partial^2\xi}{\partial z^2}\right) \tag{7}$$

where the surface tension force density is given by Eq. (c) of Table 7.6.1. For static equilibrium, $\Pi_a-\Pi_b = 0$. Also, to linear terms the perturbation pressures evaluated at the perturbed position ξ are equal to these pressures evaluated at the equilibrium position of the interface. Thus, Eq. 7 reduces to

$$\hat{p}^d - \hat{p}^e = g\hat{\xi}(\rho_a - \rho_b) - \gamma k^2\hat{\xi} \tag{8}$$

It is because the fluid is inviscid that the other two components of the interfacial stress balance equation are, to linear terms, identically satisfied. Finally, on the rigid lower boundary

$$\hat{v}_x^f = 0 \tag{9}$$

The boundary and jump conditions, Eqs. 5, 6, 8 and 9, are now used to "splice" together the bulk solutions represented by Eqs. 4. Of the four equations summarized by these relations, the expressions for $\hat{p}^c$ and $\hat{p}^f$ simply serve to determine these pressures once the fluid motions have been determined. The other two, Eqs. 4b and 4d, are evaluated using the boundary conditions, Eqs. 6, 7 and 10, and substituted into the stress balance condition, Eq. 9, to obtain

$$-\frac{\omega^2}{k}[\rho_a \coth(ka) + \rho_b \coth(kb)]\hat{\xi} + [\gamma k^2 + g(\rho_b - \rho_a)]\hat{\xi} = -\frac{\omega^2\rho_a}{k\sinh(ka)}\hat{\Xi} \tag{10}$$

This relation has the same form as would be used to describe the deflections of a spring attached to a mass at one end and to a displacement source at the other. The "mass" reflects the inertia of the fluids to either side of the interface while the "spring" results from the combined gravitational and capillary forces.

From Eq. 10, it follows that the complex amplitude of the interfacial response is

$$\hat{\xi} = -\frac{\omega^2\rho_a}{k\sinh(ka)}\frac{\hat{\Xi}}{D(\omega,k)} \tag{11}$$

where the dispersion equation, $D(\omega,k)$, is

$$D(\omega,k) = -\frac{\omega^2}{k}[\rho_a \coth(ka) + \rho_b \coth(kb)] + [\gamma k^2 + g(\rho_b - \rho_a)] \tag{12}$$

Driven Response: The response having the same wave number and frequency as the drive would represent all of the motions if the system were reentrant in the direction of the traveling wave and sufficient time had elapsed for a temporal sinusoidal state to be established. (This presumes that the temporal natural modes are stable.) Under the assumption that $\gamma k^2+g(\rho_b - \rho_a) > 0$ (which is assured regardless of wavelength if the lower fluid is the heavier), the frequency response of the interface is as shown in Fig. 8.9.2. Because there are no dissipation mechanisms included in the model, the interface is either in phase or 180° out of phase with the excitation.

Gravity-Capillary Waves: The resonance comes at that frequency that gives synchronism between the phase velocity ω/k of the drive and phase velocity of a gravity-capillary wave propagating on the interface. Solution for ω/k of Eq. 13 set equal to zero identifies the phase velocity of these waves as

$$v_p = \sqrt{\frac{\gamma k + g(\rho_b - \rho_a)/k}{\rho_a \coth(ka) + \rho_b \coth(kb)}} \qquad (13)$$

Long waves are dominated by gravity while short ones are of a capillary nature. Often, the waves are short enough that effects of the transverse boundaries are not significant, $|ak| >> |bk| >> 1$. Then, Eq. 13 reduces to

$$v_p = \sqrt{\frac{\gamma k}{\rho_a + \rho_b} + \frac{g(\rho_b - \rho_a)}{k(\rho_b + \rho_a)}} \qquad (14)$$

This makes it evident that there is a wave number for minimum phase velocity, found by setting the derivative with respect to k of Eq. 14 equal to zero. The wavelength, $2\pi/k$, of this minimum will be termed the Taylor wavelength, λ_T:

$$\lambda_T = 2\pi \sqrt{\frac{\gamma}{g(\rho_b - \rho_a)}} \qquad (15)$$

At wavelengths longer than λ_T, gravity waves prevail, while shorter wavelengths represent capillary ripples. For an air-water interface, $\lambda_T = 1.7$ cm.

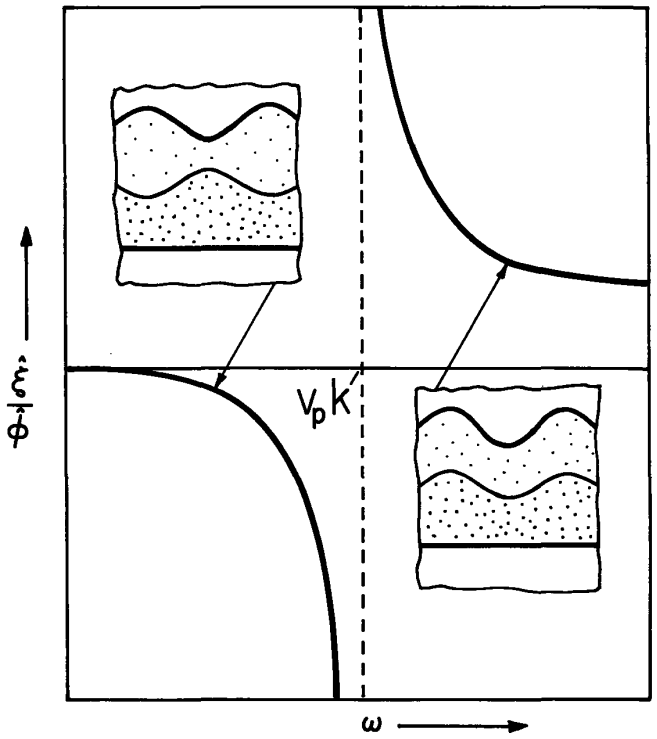

Fig. 8.9.2. Driven response of gravity-capillary wave system.

In the opposite limit of long waves, $|ka| << 1$ and $|kb| << 1$, the phase velocity becomes

$$v_p = \sqrt{\frac{\gamma k^2 + g(\rho_b - \rho_a)}{[(\rho_a/a) + (\rho_b/b)}} \qquad (16)$$

and the gravity wave (which is likely to dominate in a long-wave situation) propagates without dispersion. A quasi-one-dimensional model for long gravity waves results in the wave equation with a velocity given by Eq. 16 without the capillary term.

Temporal Eigenmodes and Rayleigh-Taylor Instability: Temporal transients, initiated from conditions that are periodic in the horizontal plane, are described by $D(\omega,k) = 0$ with k real and $j\omega$ the eigenfrequencies s_n. The role of the temporal modes in this chapter is very much as introduced in Sec. 5.15. The roots of $D(s_n,k) = 0$ are either purely real or imaginary. Resonance in the driven response results from the coincidence of the natural frequency and the driving frequency. Of most interest is the instability resulting from having the heavier fluid on top and sufficiently long wavelengths that

$$\gamma k^2 < g(\rho_a - \rho_b) \qquad (17)$$

Note that this condition prevails for wavelengths longer than the Taylor wavelength defined with Eq. 15. The eigenfrequencies can be pictured as poles in the complex s plane, with the density difference $\rho_b - \rho_a$ a variable parameter. For $\rho_b > \rho_a$, the poles are conjugates on the imaginary axis. With decreasing density difference and long enough wavelength, the poles migrate to the origin, and as the condition of Eq. 17 prevails, the poles separate on the real axis. The instability is incipient at zero frequency. In general, there might be an infinite set of eigenfrequencies. If all pass into the right-half s plane through the origin, the principle of exchange of stabilities applies. That is, the incipient condition could be identified by setting $\omega = 0$ at the outset and asking for the condition on $\rho_b - \rho_a$ that makes it possible for all of the fluid mechanics laws to be satisfied. Here, as in Sec. 5.15 where the charge relaxation eigenfrequencies for a step discontinuity in electrical properties is considered, there are a finite number of eigenfrequencies (two). There it is shown that a smooth distribution of electrical properties leads to an infinite set of temporal modes. It should come as no surprise that a smoothly distributed density distribution similarly leads to an infinite set of eigenmodes. In that case, taken up in Sec. 8.18, the principle of exchange of stabilities also applies.

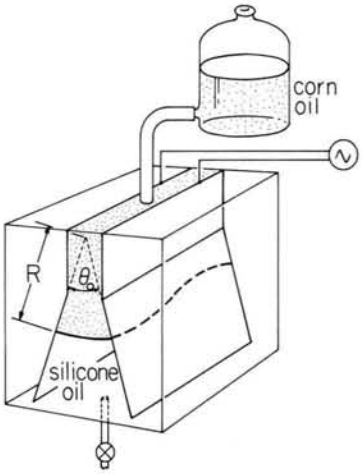

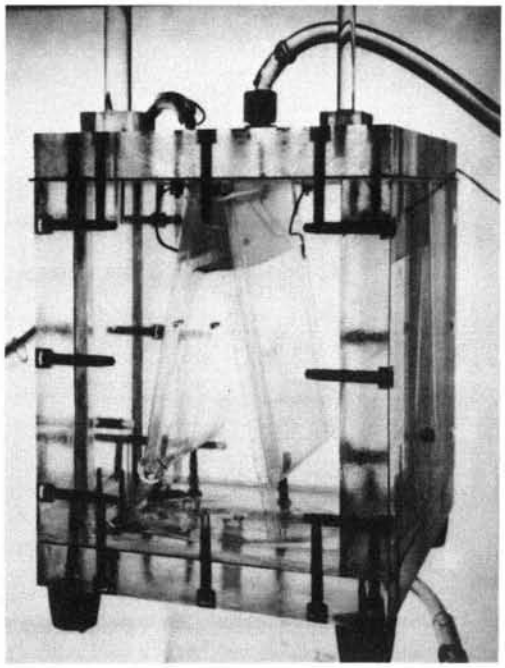

Fig. 8.9.3a. Heavy liquid is stabilized on top of lighter fluid by means of polarization forces induced by applying potential difference to the diverging glass plates. These plates have a thin transparent coating that renders them conducting.

The inviscid model is especially justified for predicting the incipience, because there are then no temporal rates involved. Thus the effects of viscosity vanish.

In the example of this Rayleigh-Taylor instability shown in Fig. 8.9.3,[1] polarization forces are used to stabilize a static equilibrium with a heavy liquid on top of a lighter one. (The electromechanics is developed in Sec. 8.11.) When the field is removed, the unstable temporal eigenmode is evident. Some fluid rises so that some can fall. The sinusoidal deflection predicted by the linear theory gives way to a plume extending into the lighter liquid. It is characteristic of this purely mechanical instability that the nonlinear "process" initiated by the instability becomes blunted in its advanced stages. The bulbous plume can itself be unstable if the viscosity is low. This characteristic appearance, which is commonly seen "upside down" as warm air rises into the atmosphere, is in sharp contrast with the electromechanical forms of Rayleigh-Taylor instability considered in the following sections.

Spatial Eigenmodes: Spatial modes are introduced in Sec. 5.17. With longitudinal boundary conditions, the sinusoidal steady-state response consists not only of a part having the same wave number as the transverse drive, but an infinite set of eigenmodes having the same frequency as the drive, each with its own wave number. These are in general complex, $k = k_r + jk_i$, and found by solving the dispersion equation $D(\omega,k) = 0$ for k, given that ω is the same as for the drive. In general this expression is transcendental, so that it must be solved numerically. Here, an infinite set of eigenvalues can be identified by a simple graphical solution. First, there are the two propagating modes in which $k = k_r$ and the dispersion equation becomes

$$\omega^2 = \frac{[\gamma k_r^2 + g(\rho_b - \rho_a)]k_r}{\rho_a \coth(k_r a) + \rho_b \coth(k_r b)} \tag{18}$$

A graphical solution is obtained by finding the intersection of curves representing the right and left sides of this expression as a function of (ak_r). This is shown in Fig. 8.9.4a. An infinite set of modes are evanescent, $k = jk_i$. With k purely imaginary, the dispersion equation is again purely real ($\coth jx = -j \cot x$):

$$\omega^2 = \frac{[\gamma k_i^2 - g(\rho_b - \rho_a)]k_i}{\rho_a \cot(k_i a) + \rho_b \cot(k_i b)} \tag{19}$$

so that graphical solution gives rise to an infinite set of k_i's, as illustrated in Fig. 8.9.4b. The functions on the right in these last two expressions are even in the wave number, so for each positive root there is a negative one as well. The two propagating modes have an exponential dependence on depth, while the evanescent modes are sinusoidal in their depth dependence, with a number of zero crossings in the x direction that increases with the mode number.

---

1. See J. R. Melcher and M. Hurwitz, "Gradient Stabilization of Electrohydrodynamically Oriented Liquids," J. Spacecraft and Rockets 4, 864-881 (1967).

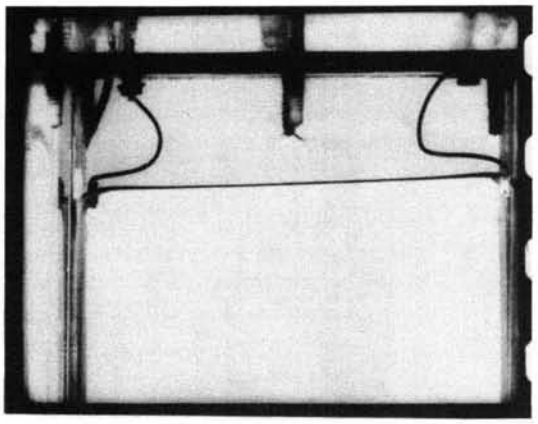

(a)

Fig. 8.9.3b. Side view of apparatus shown in Fig. 8.9.3a. (a) Equilibrium with field on. (b)-(e) Sequential view of developing instability. (From Complex Waves II, Reference 11, Appendix C.)

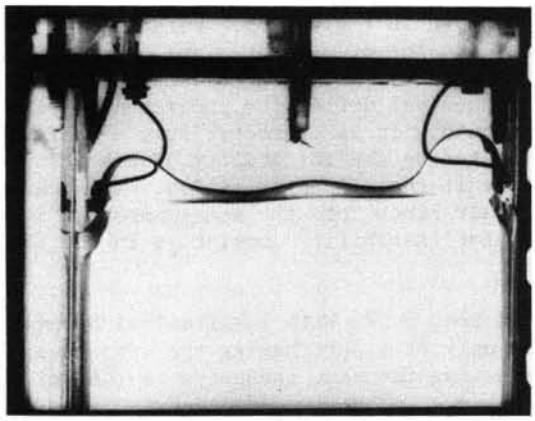

(b)

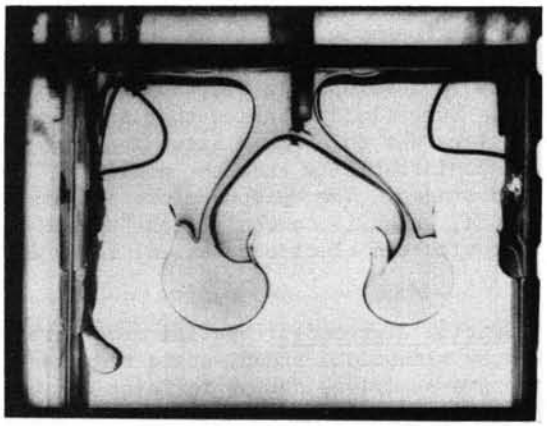

(d)

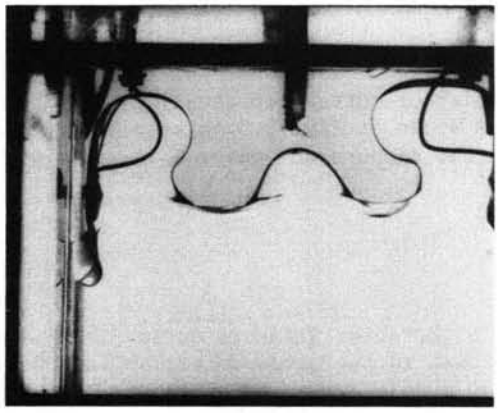

(c)

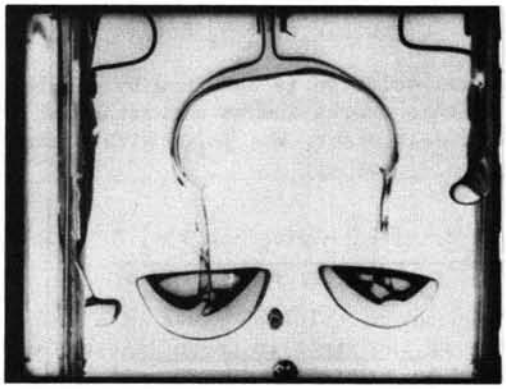

(e)

Courtesy of Education Development Center, Inc. Used with permission.

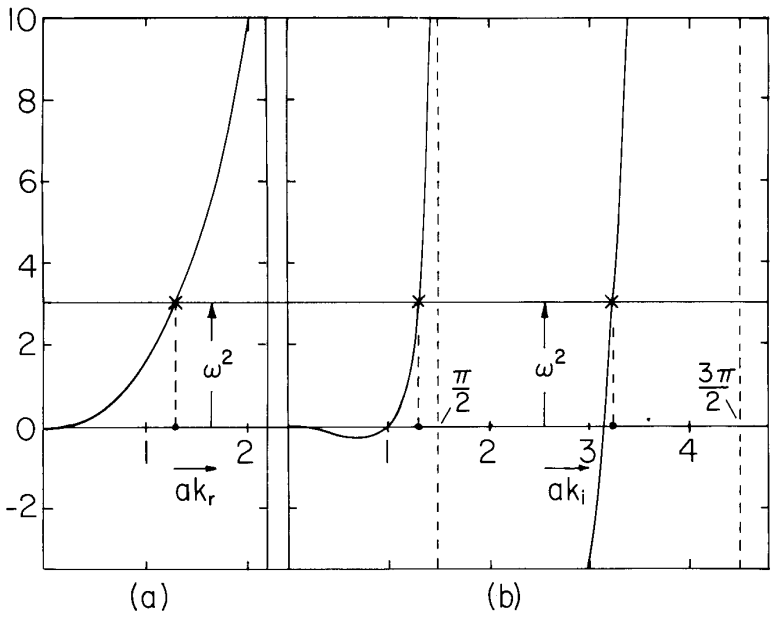

Fig. 8.9.4

Graphical solution for spatial eigenmodes. (a) Equation 18 for propagating modes. (b) Equation 19 for evanescent modes. For case shown, $\rho_a = 0$ and $\gamma/\rho_b g a^2 = 1$.

As an example, a gravity-capillary resonator might be constructed with rigid walls in the planes $y = 0$ and $y = \ell_y$ and $z = 0$ and $z = \ell_z$. These propagating and evanescent modes would in general also be excited by the transverse drive. In general, the evanescent modes are required to insure there being no normal velocity on the longitudinal boundaries. With the surface tension comes still another boundary condition. For example, by virtue of the surface tension, the interface can cling to a sharp edge. Note that for $\rho_b > \rho_a$ the lowest evanescent mode in fact exists because of the surface tension. It represents the effect of the surface tension reaching out into the interfacial region from the longitudinal boundary. The higher order modes are more closely connected with the inertia and mass conservation represented by Laplace's equation in the fluid bulk.

8.10 Self-Field Interfacial Instabilities

If a magnet is held over or under the free surface of a ferrofluid so that the field is normal to the interface, sprouts of liquid will be seen to extend into the air. With the magnet fixed, the sprouts are fixed. Even if stressed by an initially perfectly uniform magnetic field (so that hydrostatic pressure can balance the magnetic forces to maintain a static equilibrium with the interface flat), the sprouts represent a new static equilibrium preferred by the fluid. The electromechanical form of Rayleigh-Taylor instability that takes place as the planar interface, stressed by a uniform magnetic field, gives way to the new configuration, is one of the results from the model now developed. The configuration, shown in Fig. 8.10.1a, consists of planar layers having different permeabilities (μ_a,μ_b), mass densities (ρ_a,ρ_b) and equilibrium thicknesses (a,b). The common interface is at $x = \xi$, while rigid boundaries (infinitely permeable pole faces) bound the layers from above and below. The liquids are water based or even hydrocarbon based ferrofluids. Hence, in MQS terms, the materials are essentially insulating. Only the magnetization force density, Eq. 3.8.14 with $\vec{J}_f = 0$, is responsible for the electromechanical coupling.

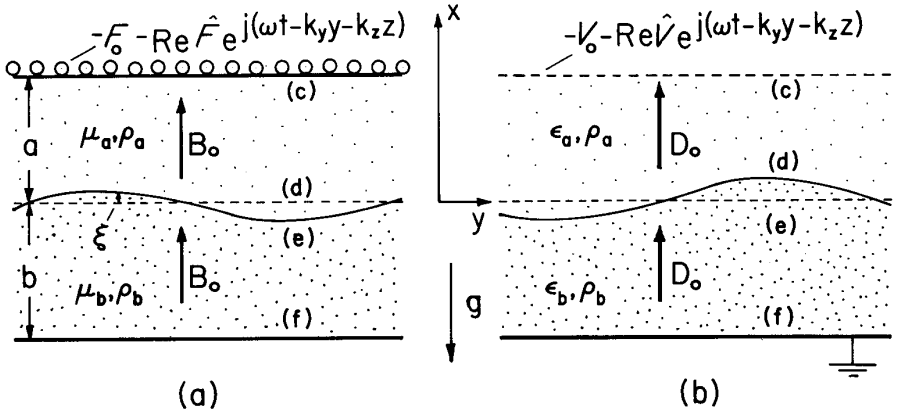

Fig. 8.10.1. (a) Layers of magnetizable fluid are stressed by a uniform normal magnetic flux density, B_o. Polarizable liquid layers are stressed by a normal electric displacement, D_o.

The time and space-varying drive is taken as imposed on the upper transverse boundary by means of a coil structure. Thus, the magnetic potential in this surface is an equilibrium value $\mathcal{F}_o$ (relative to the lower surface) representing the magnet field plus a traveling wave having the complex amplitude $\hat{\mathcal{F}}$.

The EQS system, consisting of layers of insulating polarizable fluid as shown in Fig. 8.10.1b, is described with the same model by simply identifying $\mu \to \varepsilon$, $B_o \to D_o$ and $\mathcal{F} \to \mathcal{V}$. There is an important physical difference between the two systems. To obtain a purely polarization coupling, it is necessary to use an alternating electric field having a high enough frequency to guarantee that free charge does not enter into the electromechanics. This field can be considered as being essentially static provided the frequency is also high enough to insure that the fluid responds to its rms value. In the respective regions the magnetic field is taken as having the form of an equilibrium plus a perturbation:

$$\vec{H} = \begin{Bmatrix} H_a \\ H_b \end{Bmatrix} \vec{i}_x + \vec{h}; \quad \vec{h} = -\nabla\Psi \tag{1}$$

The equilibrium magnetic flux density in each region is related to the equilibrium magnetic potential difference between the pole faces by

$$B_o = \mu_a H_a = \mu_b H_b = \frac{\mathcal{F}_o}{[(a/\mu_a) + (b/\mu_b)]} \tag{2}$$

The magnetization force density is confined to the interface, where it acts on the equilibrium interface as a normal surface force density. The equilibrium pressure difference $\Pi_a - \Pi_b$ then holds the interface in static equilibrium. In the bulk regions, the magnetic field is uncoupled from the fluid nechanics. Thus, the perturbation mechanics of each layer is described by the inviscid pressure-velocity relations from Table 7.9.1, Eqs. 8.9.4. Similarly, the perturbation magnetic field is described by the flux-potential transfer relations, Eqs. (a) of Table 2.16.1 ($k \equiv \sqrt{k_y^2 + k_z^2}$)

$$\begin{bmatrix} \hat{h}_x^c \\ \hat{h}_x^d \end{bmatrix} = k \begin{bmatrix} -\coth(ka) & \frac{1}{\sinh(ka)} \\ \frac{-1}{\sinh(ka)} & \coth(ka) \end{bmatrix} \begin{bmatrix} \hat{\Psi}^c \\ \hat{\Psi}^d \end{bmatrix}; \quad \begin{bmatrix} \hat{h}_x^e \\ \hat{h}_x^f \end{bmatrix} = k \begin{bmatrix} -\coth(kb) & \frac{1}{\sinh(kb)} \\ \frac{-1}{\sinh(kb)} & \coth(kb) \end{bmatrix} \begin{bmatrix} \hat{\Psi}^e \\ \hat{\Psi}^f \end{bmatrix} \tag{3}$$

The essence of the electromechanics is in the boundary conditions, which must be consistent with the electromagnetic and mechanical laws used in the model. Proceeding from top to bottom in Fig. 8.10.1a, the magnetic potential must be that of the drive at the upper boundary. The boundary is rigid, so

$$\hat{\Psi}^c = \hat{\mathcal{F}} \tag{4}$$

$$\hat{v}_x^c = 0 \tag{5}$$

At the interface, continuity requires that

$$\hat{v}_x^d = \hat{v}_x^e = j\omega\hat{\xi} \tag{6}$$

The x component of the stress balance jump condition, Eq. 7.7.3, is to linear terms equivalent to the normal component of the stress balance. With i = x, that jump condition is evaluated using the stress tensor with Eq. 3.8.14 in Table 3.10.1:

$$[-\rho_a g x + \Pi_a + p'^d]_{x=\xi} - [-\rho_b g x + \Pi_b + p'^e]_{x=\xi} \simeq [\tfrac{1}{2}\mu_a (H_a + h_x^d) - \tfrac{1}{2}\mu_b (H_b + h_x^e)^2]_{x=\xi} + \gamma\left(\frac{\partial^2\xi}{\partial y^2} + \frac{\partial^2\xi}{\partial z^2}\right) \tag{7}$$

where, remember, all quantities are evaluated at the actual position of the interface. The normal vector is written in terms of ξ by means of Eq. (a) from Table 7.6.1. Terms from the stress that are nonlinear in the perturbation amplitudes have already been dropped in writing Eq. 7. To linear terms, the perturbation quantities evaluated at $x = \xi$ are the same as if evaluated at the equilibrium interfacial position $x = 0$. Also, the equilibrium magnetic field is uniform (not a function of x like the equilibrium pressure), so these terms are the same at $x = 0$ as at $x = \xi$. The equilibrium part of Eq. 7 expresses the condition for static equilibrium,

$$\Pi_a - \Pi_b = \tfrac{1}{2}(\mu_a H_a^2 - \mu_b H_b^2) = \tfrac{1}{2} B_o (H_a - H_b) \tag{8}$$

and the perturbation part becomes the required jump condition representing stress balance at the interface:

$$(\hat{p}^d - \hat{p}^e) + \hat{\xi}g(\rho_b - \rho_a) = B_o(\hat{h}_x^d - \hat{h}_x^e) - k^2\gamma\hat{\xi} \tag{9}$$

The conditions of Eqs. 6 and 9 guarantee that the mechanical laws are satisfied through the interface. Similarly, on the magnetic side, $\vec{H}$ is irrotational and $\vec{B}$ is solenoidal, so $\vec{n} \times [\![\vec{H}]\!] = 0$ and $\vec{n} \cdot [\![\mu\vec{H}]\!] = 0$ (Eqs. 21 and 22 of Table 2.10.1). With $\vec{n}$ again given by Eq. (a) of Table 7.6.1, either the y or z components of the condition that tangential $\vec{H}$ be continuous reduces to

$$\hat{\Psi}^d - \hat{\Psi}^e = \hat{\xi}(H_a - H_b) \tag{10}$$

while the continuity of normal flux density is to linear terms given by

$$\mu_a\hat{h}_x^d = \mu_b\hat{h}_x^e \tag{11}$$

Finally, there are the mechanical and magnetic conditions at the lower rigid and infinitely permeable boundary:

$$\hat{v}_x^f = 0 \tag{12}$$

$$\hat{\Psi}^f = 0 \tag{13}$$

With the objective of finding the driven response and in the process deducing the dispersion equation, the stress and field continuity conditions, Eqs. 9, 10 and 11, are now written with the p's and h_x's substituted from the bulk equations, Eqs. 8.9.4 and 3. These latter relations are themselves first written using the remaining simple boundary conditions. Thus, Eqs. 9, 10 and 11 respectively become

$$\begin{bmatrix} \frac{\omega^2}{k}[\rho_a\coth(ka) + \rho_b\coth(kb) - g(\rho_b-\rho_a) - k^2\gamma & kB_o\coth(ka) & kB_o\coth(kb) \\ H_a - H_b & -1 & +1 \\ 0 & \mu_a k\coth(ka) & \mu_b k\coth(kb) \end{bmatrix} \begin{bmatrix} \hat{\xi} \\ \hat{\Psi}^d \\ \hat{\Psi}^e \end{bmatrix} = \begin{bmatrix} \frac{B_o k\hat{\mathscr{F}}}{\sinh(ka)} \\ 0 \\ \frac{\mu_a k\hat{\mathscr{F}}}{\sinh(ka)} \end{bmatrix} \tag{14}$$

Solution for $\hat{\xi}$ gives

$$\hat{\xi} = -\frac{kB_o(\mu_b - \mu_a)\coth(kb)\,\hat{\mathscr{F}}}{\sinh(ka)[\mu_b\coth(kb) + \mu_a\coth(ka)]}\,\frac{1}{D(\omega,k)} \tag{15}$$

where

$$D(\omega,k) = -\frac{\omega^2}{k}[\rho_a\coth(ka) + \rho_b\coth(kb)] + [\gamma k^2 + g(\rho_b - \rho_a)] - \frac{kB_o^2(\mu_b - \mu_a)^2}{\mu_a\mu_b[\mu_b\tanh(ka) + \mu_a\tanh(kb)]} \tag{16}$$

The many types of information that can be gleened from Eq. 15 are illustrated in Sec. 8.9. Concerning the driven response, it is here simply observed that its frequency dependence is similar to that illustrated by Fig. 8.9.2, with the frequency of the resonance occurring as the excitation phase velocity coincides with that of a field coupled surface wave having the phase velocity

$$v_p = \sqrt{\frac{\gamma k + g(\rho_b-\rho_a)/k - B_o^2(\mu_b-\mu_a)^2/\mu_a\mu_b[\mu_b\tanh(ka) + \mu_a\tanh(kb)]}{\rho_a\coth(ka) + \rho_b\coth(kb)}} \tag{17}$$

The effect of the field is to reduce the gravity-capillary phase velocity and hence the frequency. This phenomenon is a "self-field" effect, in the sense that a deformation of the interface distorts the magnetic field and this in turn creates a magnetization perturbation surface force density that tends to further increase the deflection.[1]

---

1. For experimental documentation of resonance frequency shift with magnetic field, see R. E. Zelazo and J. R. Melcher, "Dynamics and Stability of Ferrofluids: Surface Interactions," J. Fluid Mech. 39, 1 (1969).

The tendency for this self-field coupling to precipitate instability makes the temporal modes of particular interest. In the short-wave limit ka << 1 and kb << 1, solution of the dispersion equation $D(\omega,k) = 0$ for ω^2 results in

$$\omega^2 = \frac{gk(\rho_b - \rho_a)}{\rho_a + \rho_b} + \frac{k^3\gamma}{\rho_a + \rho_b} - \frac{k^2B_o^2(\mu_b - \mu_a)^2}{\mu_a\mu_b(\mu_a + \mu_b)(\rho_a + \rho_b)} \tag{18}$$

Even with the lighter fluid on top (say air over a ferroliquid) so $\rho_b > \rho_a$, the magnetic field can make $\omega^2 \to 0$ and hence one of the eigenmodes unstable. Figure 8.10.2 shows ω^2 as given by Eq. 18 as a function of k. As B_o is raised, there is a critical value at which the curve just kisses the $\omega^2 = 0$ axis. Under this condition, instability impends at the wave number k^*. For greater values of B_o, wave numbers between the roots of Eq. 18 with $\omega^2 = 0$, k_u and k_ℓ, are unstable. These roots coalesce as the discriminant of the quadratic formula vanishes. Thus, the incipient condition is

$$\left[\frac{B_o^2(\mu_b - \mu_a)^2}{\mu_a\mu_b(\mu_a+\mu_b)\gamma}\right]^2 = \frac{4g(\rho_b - \rho_a)}{\gamma} \tag{19}$$

The critical wave number is what remains from the quadratic formula, which in view of Eq. 19 is

$$k^* = \sqrt{\frac{g(\rho_b - \rho_a)}{\gamma}} \tag{20}$$

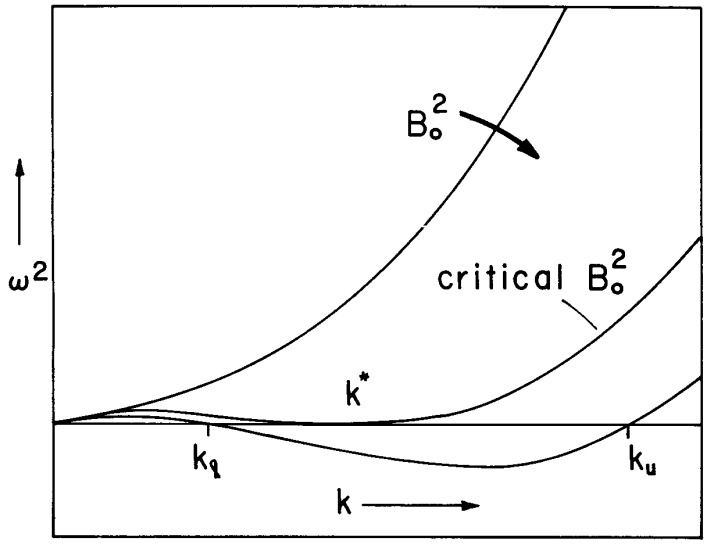

Fig. 8.10.2

Dependence of $\omega^2(k)$ as given by Eq. 18 with B_o^2 as a parameter.

Note that the first perturbations to become unstable as the field reaches the level predicted by Eq. 19 have the Taylor wavelength given by Eq. 15.[2]

What happens if the field is raised above the value consistent with Eq. 19? The initial rate of growth is given by the linear theory, although because a rate process is now involved, this may be strongly influenced by the viscosity. But, the ultimate state will depend on the nature of the electromechanical coupling. In the magnetization example at hand, the interface typically reaches a new state of static equilibrium. The protrusions shown in Fig. 8.10.3 are typical. Consistent with the fact that the interface is always free of a shearing surface force density, they are perfectly static.

As discussed in the introduction to this section, to obtain a similar instability in the EQS polarization configuration of Fig. 8.10.1b, it is usually necessary to use an alternating field.[3] If the frequency of this field is low enough that the natural modes can interact with its pulsating component, parametric instabilities can also result. By contrast with the coupling described here, these instabilities

2. Conditions for instability are studied by M. D. Cowley and R. E. Rosensweig, J. Fluid Mech. 30, 721 (1969).

3. E. B. Devitt and J. R. Melcher, "Surface Electrohydrodynamics with High-Frequency Fields," Phys. Fluids 8, 1193 (1965).

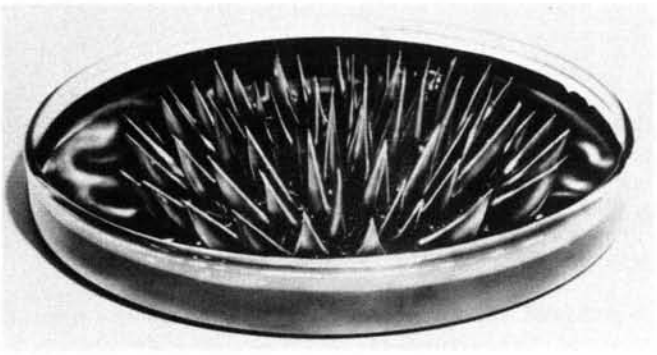

Courtesy of Ferrotec USA Corp., Bedford, NH. Used with permission.

Fig. 8.10.3. System of static fluid sprouts represents a new static equilibrium formed once planar interface in perpendicular field becomes unstable. (Courtesy of Ferrofluidics Corp., Burlington, Mass.)

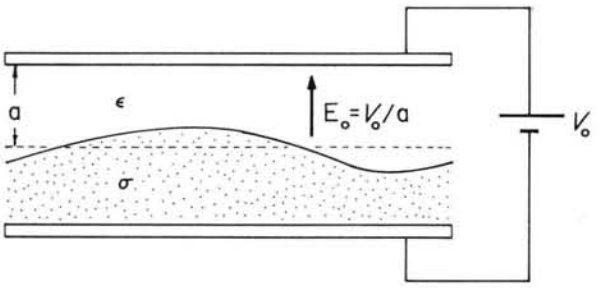

Fig. 8.10.4. Rigid plane-parallel electrodes bound liquids having common interface. The upper liquid is insulating relative to the lower one.

are dynamic in character and can result in splattering or atomization of the interface.[4]

To appreciate the perfectly static equilibrium of the polarization sprouts resulting from the instability of the flat interface, consider by contrast some of the possibilities resulting when the interface of a conducting fluid bounded by a relatively insulating one is stressed by a normal electric field E_o. The configuration is shown in Fig. 8.10.4. For example, the upper fluid might be air and the lower one water (or any other liquid having a charge relaxation time ϵ/σ short compared to times of interest).[5]

The boundary condition at the interface is that it sustains no tangential electric field. This is formally equivalent to the (analogous) magnetic field situation in the limit where the lower fluid is infinitely permeable. That is, in the limit $\mu_b \to \infty$, the interfacial tangential magnetic field just above the interface of Fig. 8.10.1a must vanish. The magnetic field above this infinitely permeable fluid then satisfies the same boundary conditions as the electric field does in the physically very different situation of Fig. 8.10.4.

It follows from Eq. 19 with the substitution $\mu_a \to \epsilon$, $\mu_b \to \infty$ and $B_o \to E_o/\epsilon = \mathscr{V}_o/a$ that the voltage required to just induce instability of the interface is

$$\mathscr{V}_o = a\left[\frac{4g(\rho_b - \rho_a)\gamma}{\epsilon^2}\right]^{1/4} \qquad (21)$$

The danger in exploiting the formal equivalence of the infinitely permeable and the "infinitely" conducting lower fluid is that the physics of the two situations will be confused. In the case now considered, the surface force density acting upward on the interface is due to free surface charges. That these are free to conduct accounts for the diverse processes that can be triggered by the instability.

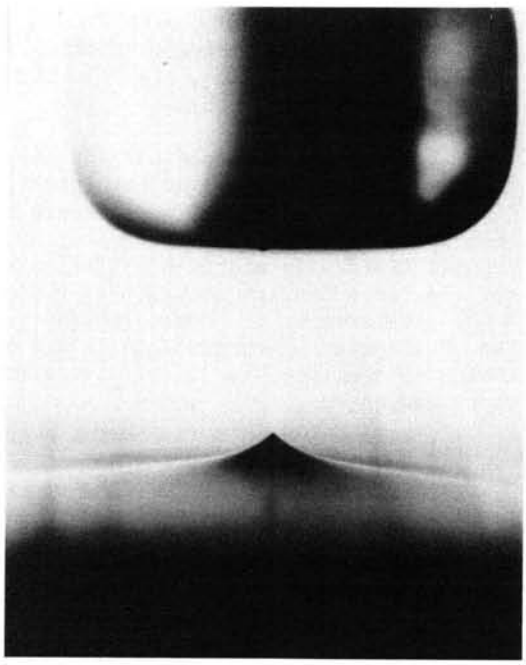

Fig. 8.10.5. Nonlinear stages of surface instability caused by applying 30 kV d-c between electrode above and glycerine interface below. Insulation is mixture of air and gaseous Freon.

A typical appearance shortly after incipience is shown in Fig. 8.10.5. An extremely sharp spike has formed. In the neighborhood of this point, the nonlinear stages of instability are generally dynamic, and often involve dielectric breakdown in some region of the insulating fluid. Depending on properties and breakdown strength, it is very likely that simultaneous spraying and corona discharge will be observed.

4. T. B. Jones, "Interfacial Parametric Electrohydrodynamics of Insulating Dielectric Liquids," J. Appl. Phys. 43, 4400 (1972).

5. For experiments and a more general treatment of stability conditions, see J. R. Melcher, Field-Coupled Surface Waves, The M.I.T. Press, Cambridge, Mass., 1963, Chaps. 3 and 4.

8.11 Surface Waves with Imposed Gradients

The electromechanical coupling exemplified in Sec. 8.10 is entirely caused by the distortion of the initially uniform field that results from a deformation of the interface. It is this perturbation field that creates the change in surface force density tending to destabilize the interface. The "self-field" origin of the coupling is reflected in the dependence of the coupling on the square of the jump in electrical properties [$(\mu_a - \mu_b)^2$ in the last term of Eq. 8.10.16]. The perturbation self-field is proportional to $\mu_a - \mu_b$ and the surface force density is proportional to this field multiplied by $(\mu_a - \mu_b)$. The net effect is proportional to the product of these and hence to $(\mu_a - \mu_b)^2$.

The surface force density can also vary simply because the interface moves in a nonuniform equilibrium field. Because the change in field experienced by the deforming interface is independent of the jump in property, it can be expected that this imposed field type of coupling is linearly proportional to the property jump.

To exemplify imposed field effects and at the same time highlight electromechanical surface waves that propagate along field lines, the electromechanics of the configuration shown in Fig. 8.9.3 is now considered. Both fluids can be regarded as perfectly insulating so that the relevant force density is given by Eq. 3.7.22 of Table 3.10.1. How is it that the polarization interaction can stabilize the initial equilibrium with the heavier liquid on top? What is the role of self-field effects when the equilibrium electric field is tangential to the interface?

The cross section of the system is shown in Fig. 8.11.1. Diverging transparent electrodes (which are tin oxide coated glass in Fig. 8.9.3a) are used to impose the field

$$\vec{E} = \vec{i}_\theta \frac{\mathscr{V}_o}{\theta_o r} \tag{1}$$

on fluids with an interface essentially at r = R. Note that Eq. 1 gives the exact solution, provided that the interface approximately has this equilibrium radius.

Because gravity does not act exactly in the radial direction, the equilibrium geometry of the interface is in fact somewhat field dependent. The essential physics are retained in a Cartesian model that pictures the interface as flat, but subject to a nonuniform imposed field. In static equilibrium the x-directed polarization surface force density is balanced by the jump in equilibrium pressure $[\![\Pi]\!]$. In terms of the coordinates defined in Fig. 8.11.1, r = R - x. The equilibrium electric field in the neighborhood of the interface (which is the only seat of electromechanical coupling) is therefore approximated by

$$\vec{E} = \vec{i}_y E_o (1 + \frac{x}{R}); \quad E_o \equiv \frac{\mathscr{V}_o}{\theta_o R} \tag{2}$$

Because of the quasi-Cartesian approximation, this equilibrium field is not irrotational.

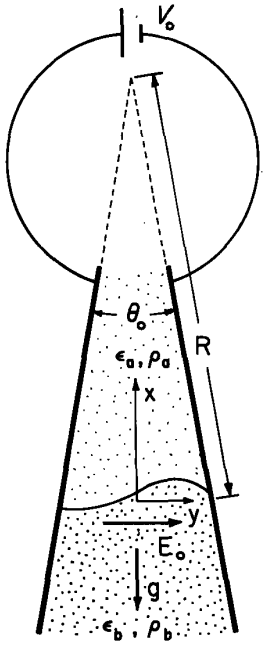

Fig. 8.11.1. Cross section of experiment shown in Fig. 8.9.3a with Cartesian coordinates for planar model.

Bulk Relations: Perturbations in the electric field are both irrotational and solenoidal in the uniform bulk of the fluids. In applying the flux-potential transfer relations representing Laplace's equation above and below the interface (Eqs. (a) of Table 2.16.1), perturbations on the interface having wave number $k \equiv \sqrt{k_y^2 + k_z^2}$ are assumed short enough that boundaries above and below the interface can be considered as being at $x = \pm \infty$. Thus, with the understanding that Rek > 0, perturbation fields evaluated at the equilibrium interfacial position are related by

$$\hat{e}_x^a = k\hat{\Phi}^a \tag{3}$$

$$\hat{e}_x^b = -k\hat{\Phi}^b \tag{4}$$

In the bulk regions, the pressure balances the gravitational force density. Hence, in each region the pressure takes the form

$$p = \Pi - \rho g x + p'(x,y,z,t) \tag{5}$$

From the inviscid pressure-velocity transfer relations (Eqs. (c) of Table 7.9.1) the perturbation part of Eq. 5 evaluated at the equilibrium interfacial position is related to the velocity there by

$$\hat{p}^a = \frac{j\omega\rho_a}{k}\hat{v}_x^a \tag{6}$$

$$\hat{p}^b = -\frac{j\omega\rho_b}{k}\hat{v}_x^b \tag{7}$$

Jump Conditions: To assure that the laws defining the model prevail through the interface, there are two electrical boundary conditions. First, $\vec{n} \times [\![\vec{E}]\!] = 0$ is evaluated at the interface using $\vec{n}$ expressed in terms of ξ (Eq. (a) of Table 7.6.1) and $\hat{e}_y = jk_y\hat{\Phi}$ or $\hat{e}_z = jk_z\hat{\Phi}$ to obtain

$$\hat{\Phi}^a - \hat{\Phi}^b = 0 \tag{8}$$

Second, by assumption there is no free surface charge so $\vec{n} \cdot [\![\varepsilon\vec{E}]\!] = 0$, which to linear terms requires that

$$\varepsilon_a\hat{e}_x^a - \varepsilon_b\hat{e}_x^b + jk_y\hat{\xi}E_o(\varepsilon_a - \varepsilon_b) = 0 \tag{9}$$

In addition, two mechanical conditions are required, the first representing continuity

$$\hat{v}_x^a = j\omega\hat{\xi} = \hat{v}_x^b \tag{10}$$

and the second force equilibrium. To linear terms, the normal force balance is the x component of Eq. 7.7.6 with the surface tension contribution given by Eq. (b) of Table 7.6.1,

$$[\Pi_a - \rho_a g\xi + p'^a(x=0)] - [\Pi_b - \rho_b g\xi + p'^b(x=0)]$$

$$= -\frac{1}{2}\varepsilon_a[E_o(1+\frac{\xi}{R}) + e_y^a(x=0)]^2 + \frac{1}{2}\varepsilon_b[E_o(1+\frac{\xi}{R}) + e_y^b(x=0)]^2 - \gamma\left[\frac{\partial^2\xi}{\partial y^2} + \frac{\partial^2\xi}{\partial z^2}\right] \tag{11}$$

The balance of the equilibrium surface force density by the equilibrium pressure is represented by the equilibrium part of Eq. 11:

$$\Pi_a - \Pi_b = -\frac{1}{2}(\varepsilon_a - \varepsilon_b)E_o^2 \tag{12}$$

so that in terms of complex amplitudes evaluated at the equilibrium position of the interface, the perturbation stress balance requires that

$$\hat{p}^a - \hat{p}^b + g(\rho_b - \rho_a)\hat{\xi} = (\varepsilon_b - \varepsilon_a)\frac{E_o^2}{R}\hat{\xi} - jk_yE_o(\varepsilon_a\hat{\Phi}^a - \varepsilon_b\hat{\Phi}^b) - \gamma k^2\hat{\xi} \tag{13}$$

Dispersion Equation: Of the possible types of information about the dynamics that can be gleaned from this model, it is the temporal modes that are of interest here. One way that they can be identified is to find the response to a transverse drive in the form of Eq. 8.9.11 for example. Then the condition is $D(\omega,k) = 0$. Here, there is no drive and the temporal modes are identified by asking for the relation between ω and k that makes it possible for surface distortions to exist, consistent with all the laws, but with homogeneous boundary conditions. To this end, Eqs. 3 and 4, 6 and 7 and 9 are substituted into Eq. 13 using Eqs. 8 and 10 in the process. The resulting expression is of the form $D(\omega,k)\hat{\xi} = 0$. If $\hat{\xi}$ is to be finite, it follows that $D(\omega,k) = 0$. This relation,

$$\omega^2(\rho_a+\rho_b) = gk(\rho_b-\rho_a) + \gamma k^3 + (\varepsilon_a-\varepsilon_b)\frac{kE_o^2}{R} + k_y^2E_o^2\frac{(\varepsilon_a - \varepsilon_b)^2}{(\varepsilon_a + \varepsilon_b)} \tag{14}$$

is an expression of the fact that the inertia of the fluid above and below the interface is equilibrated by forces due to gravity, surface tension, imposed fields and self-fields.

Temporal Modes: In addition to the now familiar gravity and capillary contributions to the phase velocity, ω/k, there are now the polarization contributions. In the absence of an imposed gradient the effect of the field is to stabilize perturbations with peaks and valleys running perpendicular to the electric field. To see why, consider the perturbation fields resulting from the deformation of the interface shown in Fig. 8.11.2a. With $\varepsilon_a < \varepsilon_b$, the equilibrium field, E_o induces polarization surface charges. As shown, these in turn give rise to the perturbation fields. Remember that the polarization surface force density on an interface stressed by a tangential field acts in the direction of decreasing permittivity. Thus, at the downward peaks where the perturbation field reinforces the applied field there is an increase in the upward directed surface force density, and this tends to restore the inter-

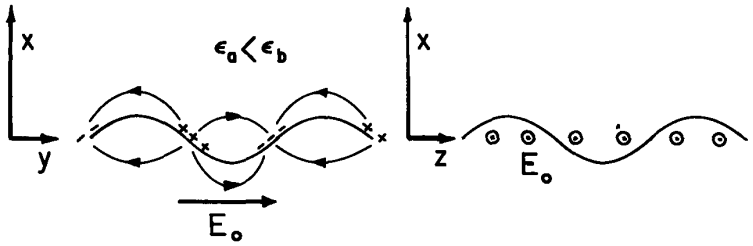

Fig. 8.11.2. (a) Perturbation fields for waves propagating along lines of electric field. (b) Perturbation fields are absent for waves propagating across $\vec{E}$ lines.

face to its equilibrium position. That perturbations propagating in the z direction are not influenced by the self-fields is evident from the fact that the equilibrium field remains unaltered by such deformations of the interface.

Note that the self-field stiffening cannot stabilize the interface with the heavy fluid on top; modes appearing as in Fig. 8.11.2b, sometimes called exchange modes because the fluid can be displaced without an associated change in stored electric energy, are unstable despite a uniform imposed field.

However, the imposed gradient can be used to stabilize all wavelengths. Regardless of wave number, the interface is stable provided that

$$(\epsilon_a - \epsilon_b)\frac{E_o^2}{R} > g(\rho_a - \rho_b) \qquad (15)$$

So, by making the upper fluid have the greater permittivity, the equilibrium can be made stable even with the heavier fluid on top.

In the experiment of Fig. 8.9.3, the region between the electrodes is sealed. Thus, hydrostatic pressure maintains the equilibrium, while the electric field stabilizes it. If too much of the upper fluid is run into the region between the electrodes, it simply breaks through the interface until enough is lost to satisfy Eq. 15.[1]

Considerations of stability are essential to the design of systems for orienting liquids. An example is the use of polarization forces for orienting liquid fuels in the zero gravity environments of space.[2] Magnetization interactions with ferrofluids are analogous to those described here.[3]

8.12 Flux Conserving Dynamics of the Surface Coupled z-θ Pinch

The magnetic field levitation of a liquid metal, sketched in Fig. 8.2.1c, is based on time-average forces caused by currents induced because the field is oscillating with a period short compared to a magnetic diffusion time. Transient, rather than steady-state forces, are similarly induced if the field is abruptly switched on. The confinement of a highly ionized gas in many fusion experiments[1] is based on this tendency for the plasma to behave as a "perfect conductor" over several magnetic diffusion times. Not only does the magnetic field "bottle up" the plasma, but it can also be the means of compressing the gas. The stability of the pinch configuration shown in Fig. 8.12.1 is examined in this section.

An axial current on the surface of the cylindrical conductor gives an azimuthal magnetic field, H_a, and hence a surface force density that compresses the conductor radially inward. An example is shown in Fig. 8.12.2.[2] If the conductor is an ionized gas, this pressure will evidence itself in the constriction of the conducting volume, thereby producing an increase in the plasma density and local conductivity. In turn, because the magnetic field intensity in the neighborhood of the conducting path is inversely proportional to the radius of the conductor, the magnetic pressure is itself increased. As a scheme for heating of plasmas for thermonuclear experiments, the magnetic field serves the dual purpose of compressing and confining the plasma column.

---

1. J. R. Melcher and M. Hurwitz, "Gradient Stabilization of Electrohydrodynamically Oriented Liquids," J. Spacecraft and Rockets 4, 864 (1967).

2. J. R. Melcher, D. S. Guttman and M. Hurwitz, "Dielectrophoretic Orientation," ibid., 6, 25 (1969).

3. R. E. Zelazo and J. R. Melcher, "Dynamics and stability of ferrofluids: surface interactions," J. Fluid Mech. 39, 1-24 (1969).

1. See, for example, D. J. Rose and M. Clarke, Jr., Plasmas and Controlled Fusion, The MIT Press and John Wiley & Sons, New York, 1961, p. 336.

2. See F. C. Jahoda. E. M. Little, W. E. Quinn, F. L. Ribe and G. A. Sawyer,"Plasma Experiments with a 570-kJ Theta-Pinch," J. Appl. Phys. 35, 2351-2363 (1964).

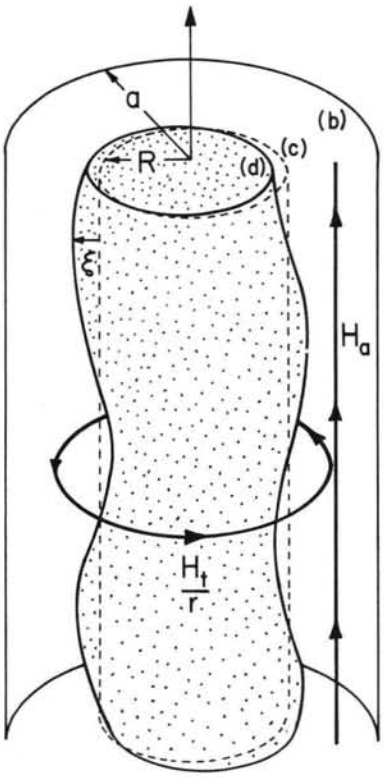

Fig. 8.12.1. Plasma column showing equilibrium radius R and equilibrium magnetic fields.

Image removed due to copyright restrictions.
Four images taken at 2.4 sec., 3.6 sec., 4.9 sec. and 6.1 sec.
As the plasma cross-section compresses, the number of dark and light rings decreases

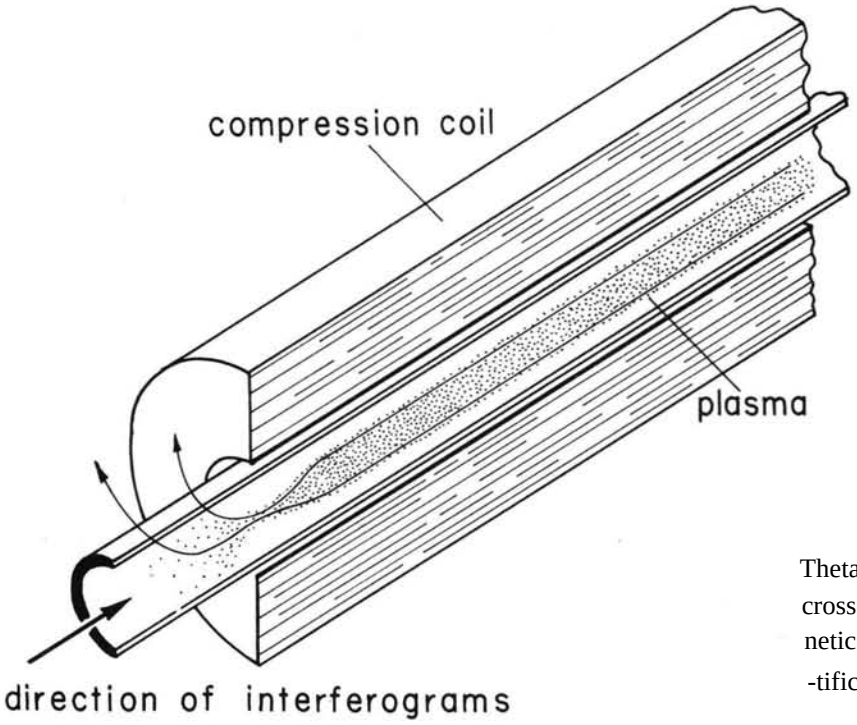

Fig.8.12.2

Theta-pinch experiment showing magnetic compression of plasma cross section as viewed by means of interferometer. Peak magnetic field is about 100 kgauss. (Courtesy of Los Alamos Scien -tificLaboratory.)

The axial or z pinch, with the current in the direction of the columnar axis and the induced magnetic field azimuthally directed, is inherently unstable: a fact that emphasized early in the fusion effort that the stability of confinement schemes was of primary importance. The theta pinch of Fig. 8.12.2 avoids the inherent tendency toward instability by using currents that flow azimuthally around the column. These are induced by a magnetic field applied suddenly in the axial direction. The applied magnetic field has the virtue of being uniform in the region around the plasma, and thus the magnetic stress at the surface of the column is independent of the radial position of the interface. As will be seen, it is the 1/r dependence of the equilibrium magnetic field that makes the axial pinch naturally unstable. The imposed field gradient is destabilizing. The combined axial and theta pinch configuration, shown in Fig. 8.12.1, is sometimes termed the "screw pinch" because of the helical shape of the magnetic field lines.

Equilibrium: The plasma column is modeled as a perfectly conducting cylinder of incompressible and inviscid fluid. Although the equilibrium is pictured as static, the fields are nevertheless applied and the column motion of interest completed in times that are short compared to the time for the field to diffuse into the column. Thus, surface currents are just those required to shield the applied fields from the column:

$$\vec{H} = \frac{R}{r} H_t \vec{i}_\theta + H_a \vec{i}_z \tag{1}$$

where H_a and H_t are, respectively, the axial and theta fields at the equilibrium surface of the column. The equilibrium surface current on the column is therefore

$$\vec{K} = -H_a \vec{i}_\theta + H_t \vec{i}_z \tag{2}$$

Stress equilibrium requires that the equilibrium pressure jump balance the magnetic surface force density:

$$\Pi_c - \Pi_d = -\frac{1}{2}\mu_o(H_t^2 + H_a^2) \tag{3}$$

Bulk Relations: With the column surface represented in the complex amplitude form $\xi = \mathrm{Re}\hat{\xi}\exp j(\omega t - m\theta - kz)$, perturbations in the magnetic field around the column, $\vec{h} = -\nabla\Psi$, where Ψ satisfies Laplace's equation. Thus, the flux potential relations, Eq. (c) of Table 2.16.2, pertain to the region between column and wall:

$$\begin{bmatrix} \hat{\Psi}^b \\ \hat{\Psi}^c \end{bmatrix} = \begin{bmatrix} F_m(R,a) & G_m(a,R) \\ G_m(R,a) & F_m(a,R) \end{bmatrix} \begin{bmatrix} \hat{h}_r^b \\ \hat{h}_r^c \end{bmatrix} \tag{4}$$

There is no perturbation magnetic field inside the column.

The perturbation mechanics of the column are represented by the inviscid model of Sec. 7.9. The pressure-velocity relations, Eq. (f) of Table 7.9.1 in the limit where $\beta \to 0$, show that

$$\hat{p}^d = j\omega\rho F_m(0,R)\hat{v}_r^d \tag{5}$$

That the region surrounding the column is essentially vacuum means that it is filled with fluid of negligible density and hence zero perturbation pressure: $\hat{p}^c \simeq 0$.

Boundary and Jump Conditions: Because the equilibrium $\vec{H}$ is nonuniform, the field evaluated at the perturbed position of the interface is to linear terms

$$\begin{aligned} \vec{H} &= \frac{R}{R+\xi} H_t \vec{i}_\theta + H_a \vec{i}_z + \vec{h}(r = R + \xi) \\ &\simeq H_t \vec{i}_\theta + H_a \vec{i}_z - \frac{\xi}{R} H_t \vec{i}_\theta + \vec{h}(r = R) \end{aligned} \tag{6}$$

The effect of the mechanics on the magnetic field is represented by the condition that there be no magnetic flux linked by contours lying in the deforming perfectly conducting interface. With the normal vector related to ξ by Eq. (e) of Table 7.6.1, it follows that to linear terms

$$\hat{h}_r^c = -j\left(\frac{mH_t}{R} + kH_a\right)\hat{\xi} \tag{7}$$

where $\hat{h}_r^c$ is evaluated at the unperturbed position of the interface.

The physical nature of the outer wall will be left open. For now, it is presumed that there is some normal magnetic field at the outer wall having the complex amplitude $\hat{\mathscr{H}}$:

$$\hat{h}_r^b = \hat{\mathscr{H}} \tag{8}$$

To express the effect of the fields on the mechanics, continuity requires that

$$\hat{v}_r^d = j\omega\hat{\xi} \tag{9}$$

Then, stress equilibrium is represented by Eq. 7.7.6. As applied to plasmas, the model need not include the surface tension. Of the three components of the stress condition, only the normal component is appropriate. Fundamentally, this is because a perfectly conducting interface sustains no magnetic shear stress (see Sec. 8.2). To linear terms, it is the radial component of the stress condition that represents the normal stresses. Thus, in view of Eq. 6 ($\hat{n}_z = jk\hat{\Psi}$, $\hat{n}_\theta = jm\hat{\Psi}/R$)

$$-\hat{p}^d = \frac{\mu_o H_t^2}{R}\hat{\xi} - j\mu_o\left(\frac{m}{R}H_t + kH_a\right)\hat{\Psi}^c \tag{10}$$

where $\hat{p}^c = 0$.

Dispersion Equation: Equations 4b and 5 are evaluated using Eqs. 7, 8 and 9 and substituted into Eq. 10 to obtain

$$\omega^2\rho F_m(0,R)\hat{\xi} = \frac{\mu_o H_t^2}{R}\hat{\xi} - \mu_o\left(\frac{m}{R}H_t + kH_a\right)^2 F_m(a,R)\hat{\xi} - j\mu_o\left(\frac{m}{R}H_t + kH_a\right)G_m(R,a)\hat{\mathscr{H}} \tag{11}$$

In particular, if the outer wall is perfectly conducting, Eq. 11 shows that the appropriate dispersion equation is

$$-\omega^2\rho F_m(0,R) = -\frac{\mu_o H_t^2}{R} + \mu_o\left(\frac{m}{R}H_t + kH_a\right)^2 F_m(a,R) \tag{12}$$

It is shown in Sec. 2.17 that $F_m(0,R) = 1/f_m(0,R) < 0$ (see Fig. 2.16.2b for typical behavior) and $F_m(a,R) > 0$.

The first term on the right in Eq. 12 arises from the imposed gradient in azimuthal magnetic field. That it tends to make the equilibrium unstable is not surprising because the inward directed magnetic surface force density associated with the imposed θ field decreases as the interface moves outward. The question of stability hinges on whether or not the self-field coupling represented by the last term in Eq. 12 "saves the day."

Certainly, the self-fields stiffen the interface. However, for deformations having azimuthal and axial wave numbers related by $(m/R)/k = -H_a/H_t$, this stiffening is absent. To appreciate the origins of this result, observe that a vector perpendicular to crests and valleys of the surface perturbation is $\vec{p} = (m/R)\vec{i}_\theta + k\vec{i}_z$, as shown in Fig. 8.12.3. Also, as a vector in the $(\theta R,z)$ plane, the equilibrium magnetic field is given by Eq. 1. The perturbations that produce no self-field effect have $\vec{p}\cdot\vec{H} = 0$ in the surface of the column. Thus the modes that cause no perturbation in $\vec{H}$ propagate across the lines of equilibrium field. If the equilibrium field circles the z axis in the clockwise direction shown in Fig. 8.12.3, the perturbations that produce no self-fields have crests and valleys that also follow these helical lines, as shown in Fig. 8.12.3b. Note that for the z pinch, where $H_a = 0$, these are the sausage modes $m = 0$. These modes that have no self-fields, sometimes called exchange modes, are similar to the polarization and magnetization modes of Sec. 8.11.

From another point of view, it is Alfvén surface waves propagating along the lines of magnetic field intensity that are described by Eq. 12. The flux conserving dynamics is similar to that for the bulk interactions. However, the phase velocity of waves is now dependent on k, the surface waves are dispersive.

The theta pinch ($H_t = 0$) is at worst neutrally stable. Only the self-field remains on the right in Eq. 12. However, for "exchange" perturbations with crests running in the axial direction, this term is zero, so that the frequency is zero, and the system is on the verge of instability. In fact, the theta pinch has been found to be a useful approach to obtaining confinement for extremely short periods

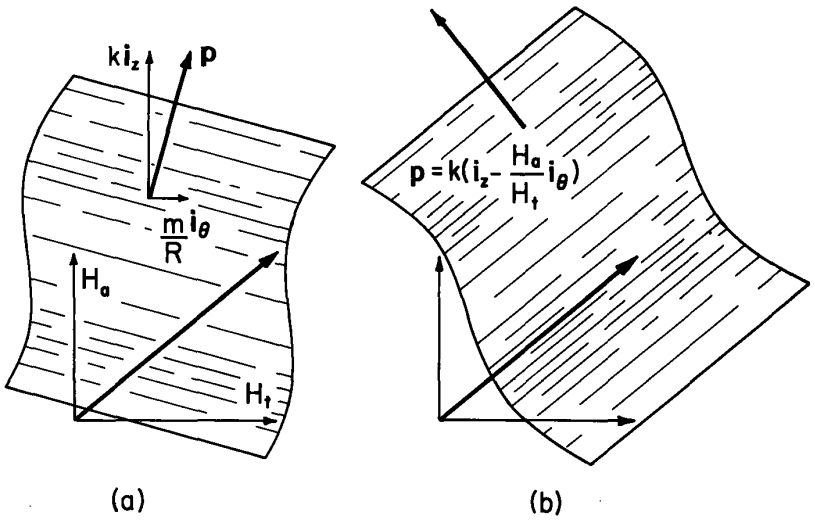

Fig. 8.12.3

(a) Equilibrium $\vec{H}$ and propagation vector in (Rθ,z) plane at r = R. (b) Exchange modes showing $\vec{p}\cdot\vec{n} = 0$ and hence lines of constant phase parallel to equilibrium $\vec{H}$.

of time. Experiments are illustrated by Fig. 8.12.2. From the hydromagnetic viewpoint, the stability of the theta pinch depends on effects not included here, such as the necessary curvature of the imposed fields if the column is closed on itself. Internal modes associated with volume distributions of current are thought to come into play in pinch devices and especially in the tokamaks. Such modes are taken up in Secs. 8.17-8.18. In any case, there are many other forms of instability associated with a highly ionized gas that are not described by a hydromagnetic theory.

One approach to stabilizing the equilibrium is to sense the position of the interface and feedback fields to a structure located on the outer wall. For example, in the limit of a continuum of samples and feedback stations, the normal magnetic field at the wall might be made proportional to the deflection of the interface at the same (θ,z) location, $\mathscr{H} = A\hat{\xi}$. With this expression introduced into Eq. 11, the revised dispersion equation follows. But, note that no matter what the nature of the feedback scheme, the last term in Eq. 11 has a factor $[(m/R)H_t + kH_a]$. No matter what the feedback, in the framework of this linear model, it will not couple to the exchange modes. The origins of this difficulty are clear from the stress balance, Eq. 10, which shows that field perturbations perpendicular to the imposed field result in no perturbation stress. This is true whether $\hat{\Psi}^c$ (Eq. 4b) is the result of the self-field (Eq. 7) or caused by the feedback at the outer wall.

8.13 Potential Conserving Stability of a Charged Drop: Rayleigh's Limit

Charged drops and droplets are exploited in devices such as ink jet printers that use electric fields to deflect and direct the ink, charged droplet scrubbers for air pollution control and electrostatic paint sprayers. Of possible importance in these applications is the limiting amount of charge that can be placed on a drop without producing mechanical rupture. It is this Rayleigh's limit,[1] determined as it is by considerations of stability, that is an objective in this section. The example gives the opportunity to put to work relations derived in Chaps. 2 and 7 in spherical coordinates.

The drop, perhaps of water, is assumed to be perfectly conducting and to have the equilibrium radius R and surface tension γ. Its interface has the radial position $r = R + \xi(\theta,\phi,t)$, as sketched in Fig. 8.13.1. The drop is initially in static equilibrium with a total charge, q, evenly distributed over its surface. Thus, an equilibrium electric field

$$\vec{E} = E_o\left(\frac{R}{r}\right)^2;\quad q = 4\pi\epsilon_o R^2 E_o \tag{1}$$

surrounds the drop with the radial electric surface force density $\epsilon E_o^2/2$ balanced by the jump in equilibrium pressure $\Pi_c - \Pi_d$ and the surface tension force density $-2\gamma/R$.

Surface deformations take the form

$$\xi = \mathrm{Re}\hat{\xi}P_n^m(\cos\theta)e^{j(\omega t - m\phi)} \tag{2}$$

1. Lord Rayleigh, "On the Equilibrium of Liquid Conducting Masses Charged with Electricity," Phil. Mag. 14, 184-186 (1882).

with normal vector and surface tension force density summarized in Table 7.6.2.

Bulk Relations: With the perturbation in electric field from that given by Eq. 1 represented by $\vec{e} = -\nabla\Phi$, the Laplacian nature of the fields surrounding the drop is represented by the flux-potential transfer relation, Eq. (d) of Table 2.16.3:

$$\hat{e}_r^c = \frac{(n+1)}{R}\hat{\Phi}^c \tag{3}$$

Similarly, the inviscid fluid within is represented by the pressure-velocity relation, Eq. (i) of Table 7.9.1 in the limit $\beta \to 0$,

$$\hat{p}^d = j\omega\rho F_n(0,R)\hat{v}_r^d = -j\omega\rho\frac{R}{n}\hat{v}_r^d \tag{4}$$

Boundary Conditions: The electrical boundary condition at the drop interface requires that there be no tangential electric field: $\vec{n} \times \vec{E} = 0$. This condition prevails if frequencies of interest are low compared to the reciprocal charge relaxation time of the drop. With the objective of evaluating the electric field at the perturbed position of the interface, note that to linear terms Eq. 1 is evaluated at the interface as

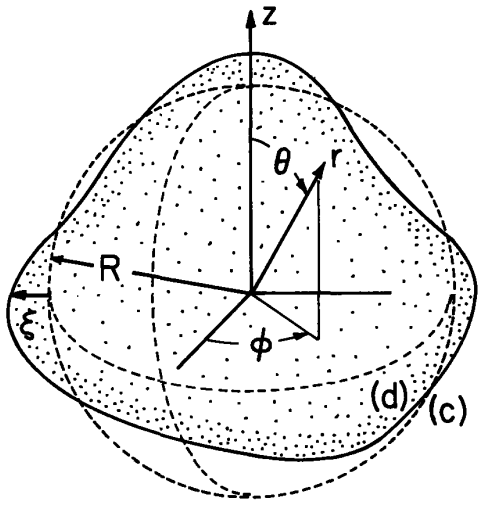

Fig. 8.13.1. Spherically symmetric equilibrium for a drop having total charge q uniformly distributed over its surface.

$$E_o\left(\frac{R}{r}\right)^2\Big|_{r=R+\xi} \simeq E_o\left(1 - \frac{2\xi}{R}\right) \tag{5}$$

Then, Eq. (e) of Table 7.6.1 is used to represent $\vec{n}$ and, to linear terms in ξ and hence $\vec{e}$, the boundary condition is written in terms of amplitudes evaluated at the unperturbed interfaces

$$\hat{\Phi}^c = E_o\hat{\xi} \tag{6}$$

Continuity requires that (Eq. 7.5.5 to linear terms)

$$\hat{v}_r^d = j\omega\hat{\xi} \tag{7}$$

Stress equilibrium for the interface, in general given by Eq. 7.7.3, is written with the perturbation pressure outside the drop ignored because the density there is negligible compared to that of the drop. Thus,

$$\Pi_c - \Pi_d - (p')^d = T_{rj}n_j + (T_s)_r \simeq \frac{1}{2}\varepsilon_o E_o^2 - \frac{2\varepsilon_o E_o^2}{R}\xi + \varepsilon_o E_o e_r^c + (T_s)_r \tag{8}$$

The equilibrium terms balance out, so that with the complex amplitude of $(T_s)_r$ given by Eq. (l) of Table 7.6.2,

$$-\hat{p}^d = -\frac{2\varepsilon_o E_o^2}{R}\hat{\xi} + \varepsilon_o E_o\hat{e}_r^c - \frac{\gamma}{R^2}(n-1)(n+2)\hat{\xi} \tag{9}$$

Dispersion Relation and Rayleigh's Limit: All terms in the stress balance, Eq. 9, are written in terms of $\hat{\xi}$ by using Eq. 6 in Eq. 3 for $\hat{e}_r^c$, and Eq. 7 in Eq. 4 for $\hat{p}^d$. The factor multiplying $\hat{\xi}$ in the resulting homogeneous equation is the dispersion equation:

$$\omega^2\rho R^2 = (n-1)n\left[\frac{\gamma}{R}(n+2) - \varepsilon_o E_o^2\right] \tag{10}$$

The surface deflections are pictured with the help of Table 2.16.3. Conservation of mass excludes the n = 0 mode. From Eq. 10, the two n = 1 modes are neutrally stable. These are pure translations, either along or transverse to the z axis.

The first modes to become unstable as E_o is increased are the three n = 2 modes. This is seen by solving Eq. 10 for the E_o that makes the term in brackets vanish and recognizing that this is first

true for the lowest allowed value of n, n = 2. Thus, because $E_o = q/4\pi\epsilon_o R^2$, it follows that Rayleigh's limit on the total drop charge consistent with a stable equilibrium is

$$q = 8\pi\sqrt{\epsilon_o \gamma R^3} \tag{11}$$

From this result, slowly increasing the net charge causes the drop to burst by fissioning into two drops. In most situations, the instability is dominated by the most rapidly growing of a spectrum of unstable modes with growth rates predicted by Eq. 10.

8.14 Charge Conserving Dynamics of Stratified Aerosols

If charge can relax instantaneously on the time scale of interest, an interface and even bulk material of fixed identity can preserve its potential. Examples are given in Secs. 8.13 and 8.7. In the opposite extreme are motions that conserve the charge density in the neighborhood of material of fixed identity. A physical example is the transport of submicron charged particles entrained in air. By virtue of applied or self-fields, these particles migrate according to the laws investigated in Sec. 5.6. But there, the gas flow was assumed to be known. What if the force transmitted to the gas by the charged particles results in a gas motion that dominates the migration of the particles relative to the gas? In fact, because of their extremely low mobilities, fine particles of high density can result in a sufficient force on the gas that the resulting fluid motions dominate over migration in determining the transport of the particles. Typically, what is observed is transport of particles by turbulent mixing with its origins in the electrohydrodynamic instability examplified in this section.

If fluid convection dominates over migration (or relaxation) in the transport of charged particles by an incompressible fluid, then the charge density is related to the fluid flow by

$$\frac{D\rho_f}{Dt} = 0 \tag{1}$$

In Sec. 7.2, this same statement was made for the mass density of an incompressible fluid. The general laws and relations subsequently developed in Secs. 7.8 and 7.9 bear on the motions of a mass density stratified fluid in a gravitational field much as does this section on motions of a charged fluid in an electric field. The discussion of gravity-capillary dynamics, Sec. 8.9, exemplifies the dynamics of fluids stratified in mass density, and is an example of how piecewise continuous models represent systems that are inhomogeneous in mass density.

At least as discussed here, where effects of self-gravitation are ignored, $\vec{g}$ in the gravitational force density is constant, whereas the electric field $\vec{E}$ in the electric force density is a function of the distribution of the field source, in this case ρ_f. But, in regions where the charge density is constant, say $\rho_f = q$, the force density transmitted to the fluid by the charged particles nevertheless takes the form of the gradient of a pressure:

$$\vec{f} = \rho_f\vec{E} = -\rho_f\nabla\Phi = -\nabla\mathcal{E};\quad \mathcal{E} \equiv q\Phi \tag{2}$$

Note that this statement prevails only where ρ_f is constant. It cannot be used to deduce a stress tensor at a boundary where ρ_f is discontinuous, for example.

That the force density in regions of uniform charge density is the gradient of a pressure effectively uncouples the bulk fluid mechanics from the electromagnetics. The inviscid equations of motion are as given in Sec. 7.8, with $\mathcal{E}$ as defined by Eq. 2. Thus, in the bulk, vorticity is conserved by a surface of fixed identity, and Eqs. 7.8.10 and 7.8.11 determine the velocity and pressure of motions initiated from a state of zero vorticity.[1]

Planar Layer: Suppose that a planar layer is embedded in a system in such a way that the equilibrium fields generated by the space charge are x-directed, as shown in Fig. 8.14.1. Because the following comments are general, for the moment consider the layer to have an equilibrium uniform translation in the z direction with velocity U. With $\mathcal{E}$ defined by Eq. 2, the pressure follows from Bernoulli's equation, Eq. 7.9.4, as

$$p = p_o(x) + p'(x,y,z,t);\quad \begin{cases} p_o(x) = -\frac{1}{2}\rho U^2 - q\Phi_o + \Pi - \rho g x \\ p' = \rho\left(\frac{\partial}{\partial t} + U\frac{\partial}{\partial z}\right)\Theta' - q\Phi' \end{cases} \tag{3}$$

---

1. The piecewise uniform approximation used here is developed in various geometries by M. Zahn, "Space Charge Coupled Interfacial Waves," Phys. Fluids 17, 343 (1974).

where primes indicate the time varying perturbation. A hybrid perturbation pressure is now defined,

$$\pi' \equiv p' + q\Phi' \tag{4}$$

It follows from Eq. 3 that π is related to the velocity potential by

$$\hat{\pi} = j\rho(\omega - k_z U)\hat{\Theta} \tag{5}$$

Thus, $\hat{\pi}$ now has the same relationship to the velocity potential as did $\hat{p}$ in Sec. 7.9 (Eq. 7.9.6). Here, as in Sec. 7.9, Θ satisfies Laplace's equation. Thus, the pressure-velocity relations of Table 7.9.1 apply with $\hat{p} \to \hat{\pi}$.

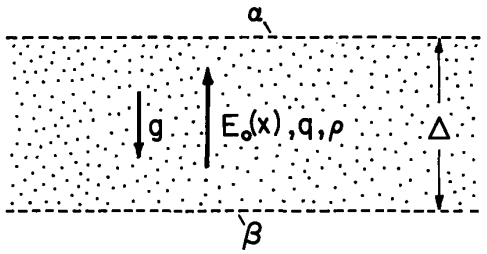

Fig. 8.14.1. Uniformly charged planar layer of charge conserving fluid.

On the electrical side, Poisson's equation must be satisfied at every point in the bulk. However, because ρ_f is constant, the equilibrium field equilibrates the charge density in Poisson's equation and perturbations in the potential must satisfy Laplace's equation. Thus, fields take the form

$$\Phi = \Phi_o(x) + \mathrm{Re}\hat{\Phi}\, e^{j(\omega t - k_y y - k_z z)}; \quad \frac{dE_o}{dx} = \frac{q}{\varepsilon_o}; \quad E_o = -\frac{d\phi_o}{dx} \tag{6}$$

where the flux-potential transfer relations of Table 2.16.1 apply to the perturbation, $\hat{\Phi}$.

Boundary Conditions: The electromechanical coupling occurs in the regions of singularity between layers of uniformly charged fluid. Interfacial boundary conditions representing the mechanical equations come from continuity, which requires that

$$\hat{v}_x = j\omega\hat{\xi} \tag{7}$$

and stress equilibrium. The charge density has a step discontinuity at the interface, but there is no surface charge. Further, there is no discontinuity in the permittivity at the interface. Thus, the surface force density, represented by the first term on the right side of Eq. 7.9.6, is zero. For layers of charged aerosol, it is appropriate to ignore the surface tension, so the boundary condition is simply

$$\vec{n}[\![p]\!] = 0 \tag{8}$$

In view of Eq. 3, this condition is represented by its x-component evaluated to linear terms on the interface at $x = \xi$ (say) to give

$$[\![qE_o - \rho g]\!]\hat{\xi} + [\![\hat{\pi}]\!] - [\![q\hat{\Phi}]\!] = 0 \tag{9}$$

where E_o is now the equilibrium electrical field evaluated at the unperturbed interface.

The potential must be continuous at the perturbed interface. Because there is no surface charge and no discontinuity in permittivity, it is also true that $[\![E_o]\!] = 0$, so this condition requires that

$$[\![\hat{\Phi}]\!] = 0 \tag{10}$$

Because there is no surface charge even on the perturbed interface, a further boundary condition reflecting Poisson's equations is that $\vec{n}\cdot[\![\varepsilon_o\vec{E}]\!] = 0$, so this condition requires that

$$[\![q]\!]\hat{\xi} + \varepsilon_o[\![e_x]\!] = 0 \tag{11}$$

where Eq. 6 is used to replace $d\varepsilon_o E_o/dx$ by (q). The four boundary conditions, Eqs. 7, 9, 10 and 11, are evaluated at the unperturbed position of the interface.

Stability of Two Charge Layers: As a specific example, consider the motions of the layers shown in Fig. 8.14.2. In the bulk, the mechanics in each layer is represented by Eqs. (c) of Table 7.9.1 with $\hat{p} \to \hat{\pi}$:

$$\begin{bmatrix} \hat{\pi}^c \\ \hat{\pi}^d \end{bmatrix} = \frac{j\omega\rho_a}{k}\begin{bmatrix} -\coth(ka) & \dfrac{1}{\sinh(ka)} \\ \dfrac{-1}{\sinh(ka)} & \coth(ka) \end{bmatrix}\begin{bmatrix} \hat{v}_x^c \\ \hat{v}_x^d \end{bmatrix} \tag{12}$$

$$\begin{bmatrix} \hat{\Pi}^e \\ \hat{\Pi}^f \end{bmatrix} = \frac{j\omega\rho_b}{k} \begin{bmatrix} -\coth(kb) & \frac{1}{\sinh(kb)} \\ \frac{-1}{\sinh(kb)} & \coth(kb) \end{bmatrix} \begin{bmatrix} \hat{v}_x^e \\ \hat{v}_x^f \end{bmatrix} \tag{13}$$

Similarly, the fields follow from Eqs. (a) of Table. 2.16.1:

$$\begin{bmatrix} \hat{e}_x^c \\ \hat{e}_x^d \end{bmatrix} = k \begin{bmatrix} -\coth(ka) & \frac{1}{\sinh(ka)} \\ \frac{-1}{\sinh(ka)} & \coth(ka) \end{bmatrix} \begin{bmatrix} \hat{\Phi}^c \\ \hat{\Phi}^d \end{bmatrix} \tag{14}$$

$$\begin{bmatrix} \hat{e}_x^e \\ \hat{e}_x^f \end{bmatrix} = k \begin{bmatrix} -\coth(kb) & \frac{1}{\sinh(kb)} \\ \frac{-1}{\sinh(kb)} & \coth(kb) \end{bmatrix} \begin{bmatrix} \hat{\Phi}^e \\ \hat{\Phi}^f \end{bmatrix} \tag{15}$$

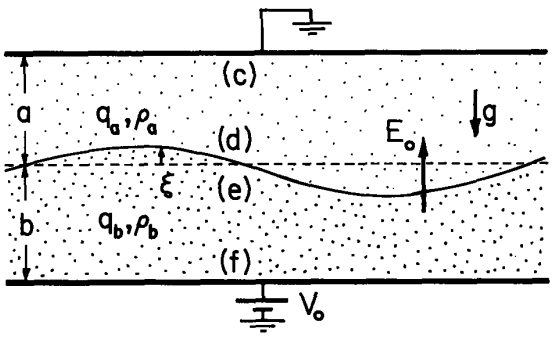

Fig. 8.14.2. Fluid layers of different uniform charge and mass densities have an interface, d-e, and are bounded by rigid electrodes.

Boundary conditions at the top electrode are

$$\hat{v}_x^c = 0 \tag{16}$$

$$\hat{\Phi}^c = 0 \tag{17}$$

at the interface are Eqs. 5, 7, 8 and 9:

$$\hat{v}_x^d = \hat{v}_x^e = j\omega\hat{\xi} \tag{18}$$

$$[E_o(q_a-q_b) - g(\rho_a-\rho_b)]\hat{\xi} + (\hat{\Pi}^d-\hat{\Pi}^e) - (q_a\hat{\Phi}^d-q_b\hat{\Phi}^e) = 0 \tag{19}$$

$$\hat{\Phi}^d - \hat{\Phi}^e = 0 \tag{20}$$

$$(q_a - q_b)\hat{\xi} + \varepsilon_o(\hat{e}_x^d - \hat{e}_x^e) = 0 \tag{21}$$

and at the bottom electrodes are

$$\hat{v}_x^f = 0 \tag{22}$$

$$\hat{\Phi}^f = 0 \tag{23}$$

It is a simple matter to substitute Eqs. 16-18,20,22, and 23 into the bulk relations. Substitution of the resulting Eqs. 14b and 15a into Eq. 21 then shows that

$$\hat{\Phi}^d = \hat{\Phi}^e = \frac{-(q_a-q_b)\hat{\xi}}{\varepsilon_o k[\coth(ka)+ \coth(kb)]} \tag{24}$$

The force-equilibrium boundary condition, Eq. 19, is finally evaluated using Eqs. 12b and 13a and Eq. 24 to obtain the dispersion equation

$$\frac{\omega^2}{k}[\rho_a\coth(ka) + \rho_b \coth(kb)] = g(\rho_b-\rho_a)+E_o(q_a-q_b) + \frac{(q_a - q_b)^2}{\varepsilon_o k[\coth(ka) + \coth(kb)]} \tag{25}$$

Remember that E_o is the equilibrium electric field evaluated at the unperturbed position of the interface. The equilibrium fields imply that the voltage V_o is related to E_o and the charge densities by

$$E_o = \frac{V_o}{b+a} + \frac{q_b b^2 - q_a a^2}{2\varepsilon_o (a+b)} \tag{26}$$

The last "self-field" term in Eq. 25 is positive regardless of the relative charge densities, and hence tends to stabilize all wavelengths. However, for short waves (ka >> 1 and kb >> 1) its contribution is negligible compared to the gravitational and "imposed field" term. Thus, a necessary and sufficient condition for all wavelengths to be stable is that the first two terms on the right in Eq. 25 be positive,

$$g(\rho_b - \rho_a) + E_o(q_a - q_b) > 0 \tag{27}$$

The static arguments used in Sec. 8.4 lead to a similar condition, Eq. 8.4.11, because instability is incipient at zero frequency.

If the inequality of Eq. 27 is not satisfied, Eq. 25 shows that the growth rate of instabilities increases linearly with the wave number. Actually, there is a wavelength for maximum rate of growth that would be predicted if the model included effects of viscosity (which come into play at short wavelengths) or recognized the finite structure of the discontinuity in charge density.

The model of a charge density that is frozen to the fluid is of course relevant only if the processes described take place on a time scale short compared to the migration time of the charged particles. To what physical situations might the model apply?

Suppose that the electromechanical waves are of interest and V_o is adjusted to make $E_o = 0$. For a fluid of uniform mass density ($\rho_a = \rho_b = \rho$), according to Eq. 25, short waves have the frequency

$$\omega = \frac{|q_a - q_b|}{\sqrt{4\varepsilon_o \rho}} \tag{28}$$

(Note that this is a reciprocal electro-inertial time.) For particles having charge q, number density n and mobility b, the self-precipitation time due to migration is $\tau_e = \varepsilon_o/nqb$) (Eq. 5.6.6). The frozen charge model is valid if the electro-inertial frequency given by Eq. 28 is high compared to the reciprocal of the self-precipitation time. That is, for $|q_a - q_b| \simeq nq$, it is valid if

$$\omega\tau_e = \frac{1}{2}\frac{\sqrt{\varepsilon_o/\rho}}{b} >> 1 \tag{29}$$

The summary of typical mobilities given by Table 5.2.1 makes it clear that the model does not apply to ions in a gas. However, it could apply to charged macroscopic particles in air[2] and to ions in liquids.[3,4] In fact, as a consequence of the electrohydrodynamic instability that prevails when Eq. 27 is not satisfied, the electrically induced convection can be a dominant charge transport mechanism.

The effect of the instability on transport of an aerosol is demonstrated by the experiment shown in Fig. 8.14.3.[5] Generated by dry ice immersed in water, the aerosol passes from left to right as a layer, bounded from below by an electrode and from above by clear air. Thus, the configuration is essentially that of Fig. 8.14.2 with the upper region uncharged. The aerosol is negatively charged by ion impact at the left. From the picture center to the right, the layer is subjected to a vertically applied electric field. In Fig. 8.14.3a, the applied field is upward and hence the configuration is stable. Some migration is observed, but little convection. In Fig. 8.14.3b, the field is reversed. Electrohydrodynamic instability is apparent in its contribution to the transport of charge out of the gas stream. For this experiment, $\sqrt{\varepsilon_o/\rho}/2b > 10$, so effects of convection are expected to be important.

---

2. R. S. Withers, J. R. Melcher and J. W. Richmann, "Charging, Migration and Electrohydrodynamic Transport of Aerosols," J. Electrostatics 5, 225-239 (1978)

3. P. K. Watson, J. M. Schneider and H. R. Till, "Electrohydrodynamic Stability of Space-Charge-Limited Currents in Dielectric Liquids," Phys. Fluids 13, 1955 (1970).

4. E. J. Hopfinger and J. P. Gosse, "Charge Transport by Self-Generated Turbulence in Insulating Liquids Submitted to Unipolar Injection," Phys. Fluids 14, 1671 (1971).

5. R. S. Colby, "Electrohydrodynamics of Charged Aerosol Flows," B.S. Thesis, Department of Electrical Engineering and Computer Sciences, Massachusetts Institute of Technology, Cambridge, Mass., 1978.

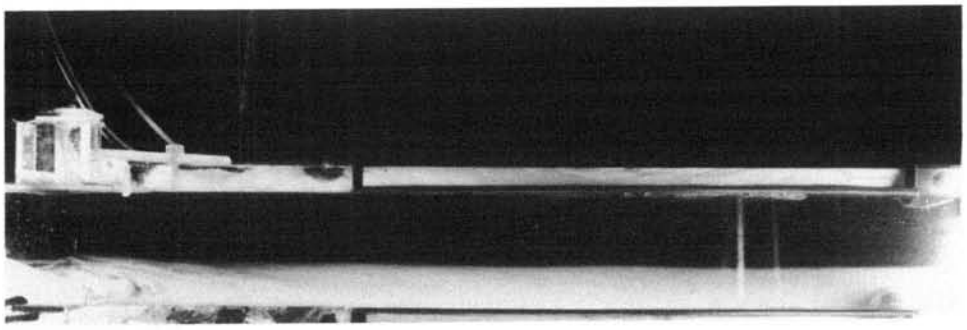

(a)

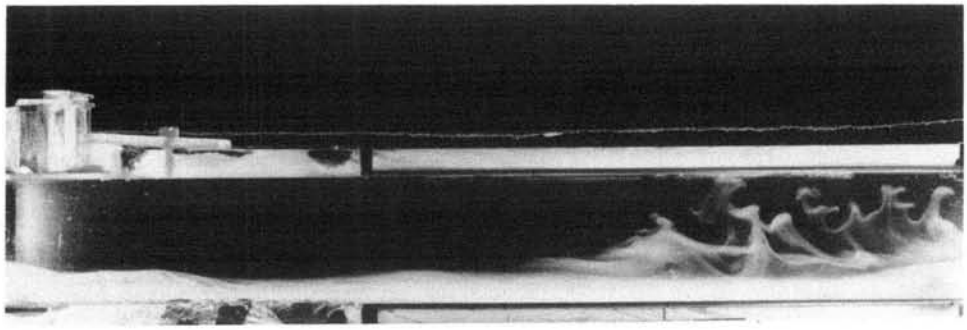

(b)

Fig. 8.14.3. Aerosol passed through ion-impact charging region at left and into region of applied electric field from the center to the right. The aerosol is charged negatively. (a) Stable configuration with applied field directed upward. (b) Unstable configuration with applied field reversed.

8.15. The z Pinch with Instantaneous Magnetic Diffusion

The model exemplified in this section pertains to the MQS dynamics of electrical conduction in the opposite extreme of that considered in Sec. 8.12. There time scales of interest were short compared to the magnetic diffusion time, so that the magnetic flux linked by a surface of fixed identity was conserved. In the opposite extreme considered here, the diffusion of magnetic field on the time scales of interest is instantaneous. In the magnetic diffusion equation, Eq. 6.2.2, the induction and "speed-voltage" terms are now negligible. That is, the magnetic diffusion time $\tau_m = \mu\sigma\ell^2$ is short compared to times of interest and the magnetic Reynolds number $R_m = \mu\sigma\ell v$ is small (Eq. 6.3.9).

In this limit of instantaneous magnetic diffusion, the effect of the material deformation on the magnetic field comes from the heterogeneity of the conductor. The distribution of $\vec{J}$ and hence $\vec{H}$ is determined by the geometry of the conductors. This is best emphasized by dealing with the current density rather than the magnetic field. Because $R_m \ll 1$, the effect of motion on the current density is ignorable. Thus

$$\vec{J} = \sigma\vec{E} \tag{1}$$

It follows from the law of induction, Eq. 6.2.3 with $\tau_m/\tau \ll 1$ and $R_m \ll 1$, that

$$\nabla \times \left(\frac{\vec{J}}{\sigma}\right) \simeq 0 \tag{2}$$

In the MQS approximation, the current density is also solenoidal:

$$\nabla\cdot\vec{J} = 0 \tag{3}$$

This is insured by Ampère's law, which represents $\vec{J}$ in terms of a "vector potential" which happens to be the magnetic field intensity:

$$\vec{J} = \nabla \times \vec{H} \tag{4}$$

In regions where σ and μ are uniform, it follows from Eqs. 2 and 4 and the solenoidal nature of $\vec{B}$ that

$$\nabla^2\vec{H} = 0 \tag{5}$$

which is of course the limit $\tau_m/\tau \ll 1$ and $R_m \ll 1$ of Eq. 6.2.6.

Liquid Metal z Pinch: The column of liquid metal shown in Fig. 8.15.1 initially has a uniform circular cross section and carries a longitudinal current density, $\mathcal{J}_o$, that is uniform over this cross section,

$$\vec{J} = \mathcal{J}_o\vec{i}_z \tag{6}$$

Thus, by contrast with the perfectly conducting pinch of Sec. 8.12 where the current is on the surface, the equilibrium magnetic field has completely diffused into the conductor. It assumes the linear distribution consistent with Ampère's law and Eq. 6:

$$\vec{H} = \begin{cases} \dfrac{\mathcal{J}_o r}{2}\vec{i}_\theta & r < R \\ \dfrac{\mathcal{J}_o R^2}{2r}\vec{i}_\theta & r > R \end{cases} \tag{7}$$

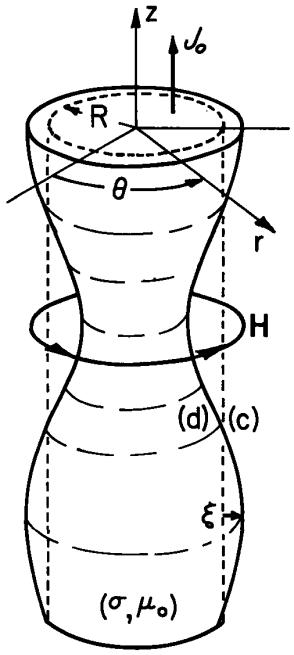

Fig. 8.15.1. Column of liquid metal has static equilibrium with $\xi = 0$ and uniform axial current density.

Static equilibrium prevails because the radial pressure distribution, p(r), just balances the associated radial magnetic force density and surface tension surface force density. With p defined as zero in the air surrounding the column,

$$p = -\frac{1}{4}\mu_o\mathcal{J}_o^2(r^2 - R^2) + \frac{\gamma}{R} \tag{8}$$

An experiment demonstrating the dynamics to be described (Ref. 2, Appendix C) makes use of a liquid jet of mercury. In the model now developed, the longitudinal streaming of the jet is ignored. Instabilities exhibiting a temporal growth here can be displayed as a spatial growth as a result of the streaming. Such effects of streaming are taken up in Chap. 11.

Bulk Relations: With the vector potential $\vec{A} \to \vec{H}$ and $\vec{B} \to \vec{J}$, the situation is formally the same as described by Table 2.18.1. Axisymmetric perturbations from this static equilibrium now considered can be described in terms of one component of the magnetic field, $H = H_\theta(r,z,t)\vec{i}_\theta$. Here, $H_\theta = \Lambda/r$ and in terms of $\Lambda(r,z,t)$, the perturbation current density is

$$\vec{J} = -\frac{1}{r}\frac{\partial\Lambda}{\partial z}\vec{i}_r + \frac{1}{r}\frac{\partial\Lambda}{\partial r}\vec{i}_z \tag{9}$$

The axisymmetric solutions of Eq. 5 in cylindrical coordinates are discussed in Sec. 2.19. Solutions are of the form of Eq. 2.19.10 with $\beta \to 0$:

$$\hat{\Lambda} = \hat{H}_\theta^d\frac{rJ_1(jkr)}{J_1(jkR)} \tag{10}$$

That is, the perturbation current density in the bulk is uncoupled from the mechanics and determined by the geometry of the interface, which will determine the coefficient $\hat{H}_\theta^d$.

By contrast, the mechanics is bulk coupled to the field distribution. The strategy in Sec. 8.14 was to represent the electromechanical bulk coupling in terms of a force density that was the gradient

of a pressure. Essentially, this attributes the coupling to interfaces. Here, part of the force density is rotational, so that matters are not so simple. It follows from Eqs. 6 and 7 that

$$\vec{F} = \vec{J} \times \mu_o \vec{H} = -\frac{\mu_o \mathcal{J}_o^2 r}{2} \vec{i}_r + \vec{J}' \times \frac{\mu_o \mathcal{J}_o r}{2} \vec{i}_\theta + \mathcal{J}_o \vec{i}_z \times \mu_o \vec{H}' \tag{11}$$

Thus, in view of Eq. 9, the force equation for the fluid becomes

$$\rho \frac{\partial \vec{v}}{\partial t} + \nabla \pi = -\frac{\mathcal{J}_o \mu_o \Lambda}{r} \vec{i}_r; \quad \pi \equiv p' + \frac{\mathcal{J}_o \Lambda}{2} \tag{12}$$

where the part of the force density that is the gradient of a pressure is lumped with the perturbation p'. Effects of gravity and viscosity are not included in Eq. 12. What is on the right in the force of Eq. 12 is the rotational part of the magnetic force density.

Because of this "one-way" coupling of the field to the fluid, it is necessary to rederive what amounts to the transfer relations for the fluid. The r and z components of Eq. 12, as well as the continuity condition $\nabla \cdot \vec{v} = 0$, give three relations for the mechanical perturbations:

$$j\omega\rho\hat{v}_r + \frac{d\hat{\pi}}{dr} = -\frac{\mathcal{J}_o \mu_o \hat{\Lambda}}{r} \tag{13}$$

$$j\omega\rho\hat{v}_z - jk\hat{\pi} = 0 \tag{14}$$

$$\frac{1}{r}\frac{d}{dr}(r\hat{v}_r) - jk\hat{v}_z = 0 \tag{15}$$

Elimination of $\hat{v}_z$ between Eqs. 14 and 15 gives an expression that can be solved for $\hat{\pi}$,

$$\hat{\pi} = \frac{\omega\rho}{jk^2}\frac{1}{r}\frac{d}{dr}(r\hat{v}_r) \tag{16}$$

Substitution of this expression into Eq. 13 gives

$$\frac{d^2\hat{v}_r}{dr^2} + \frac{1}{r}\frac{d\hat{v}_r}{dr} - \frac{\hat{v}_r}{r^2} - k^2\hat{v}_r = -\frac{jk^2 \mathcal{J}_o \mu_o}{\omega\rho}\frac{\hat{\Lambda}}{r} \tag{17}$$

In the absence of the bulk coupling, these last two expressions could be used to derive the pressure-velocity transfer relations of Table 7.9.1. Added to the homogeneous solutions of Eq. 17 (that comprise these transfer relations) is now a particular solution satisfying the equation with Eq. 10 substituted on the right. Substitution and recognition that $J_o(jkr)$ satisfies Eq. 2.16.19 with m = 0 shows that a particular solution is

$$\frac{\mathcal{J}_o \mu_o k \hat{H}_\theta^d}{2\omega\rho J_1(jkR)} r J_o(jkr) \tag{18}$$

where Eq. 2.16.26c has been used. Of the two homogeneous solutions, the one that is not singular at the origin is $J_1(jkr)$. The linear combination of particular and homogeneous solutions that makes $\hat{v}_r(R) = \hat{v}_r^d$ is

$$\hat{v}_r = \hat{v}_r^d \frac{J_1(jkr)}{J_1(jkR)} - \frac{\mathcal{J}_o \mu_o k \hat{H}_\theta^d}{2\omega\rho J_1(jkR)} \left[\frac{RJ_o(jkR)J_1(jkr)}{J_1(jkR)} - rJ_o(jkr) \right] \tag{19}$$

Thus, in view of Eqs. 12 and 16, the amplitude of the perturbation pressure is

$$\hat{p} = \frac{\omega\rho}{k}\frac{J_o(jkr)}{J_1(jkR)}\hat{v}_r^d - \frac{\mathcal{J}_o \mu_o \hat{H}_\theta^d}{2jkJ_1(jkR)} \left[\frac{jkRJ_o(jkR)}{J_1(jkR)} J_o(jkr) - 2J_o(jkr) + 2jkrJ_1(jkr) \right] \tag{20}$$

Boundary Conditions: The effect of the boundary condition on the distribution of current density, and hence magnetic field, is represented by the condition that at the interface, $\vec{n} \cdot \vec{J} = 0$. To linear terms, with $\vec{n}$ written in terms of $\xi(z,t)$ (Eq. (e) of Table 7.6.2),

$$\hat{J}_r^d + jk\mathcal{J}_o\hat{\xi} = 0 \tag{21}$$

The radial current density, J_r, is substituted into this expression using Eqs. 9 and 10 to show that

$$\hat{H}_\theta^d = -\mathcal{J}_o\hat{\xi}$$

This condition represents the effect of the mechanics (geometry) on the field.

The return effect of the field on the fluid is taken into account in writing stress equilibrium for the interface. Note that there is no singularity in the magnetic force density at the interface. That is, there is no surface current and no discontinuity in magnetizability of the material. Hence, the magnetic surface force density, $[\![T_{ij}^e]\!] n_j$, makes no contribution to the stress equilibrium, Eq. 7.7.6. Because the fluid surrounding the column is of considerably lesser density than the column, the perturbation pressure, $\hat{p}^c$, is ignored. Thus, the jump in total pressure evaluated at the perturbed position of the interface is balanced by the surface tension surface force density, Eq. (f) of Table 7.6.2:

$$-\{-\frac{1}{4}\mu_o\mathcal{J}_o^2[(R+\xi)^2 - R^2] + \frac{\gamma}{R} + p^d\} = \gamma[-\frac{1}{R} + \frac{\xi}{R^2} + \frac{\partial^2\xi}{\partial z^2}] \tag{23}$$

By design, the equilibrium part of this balance cancels out. In terms of complex amplitudes, the perturbation part is

$$\frac{1}{2}\mu_o\mathcal{J}_o^2 R\hat{\xi} - \hat{p}^d = \frac{\gamma}{R^2}[1 - (kR)^2]\hat{\xi} \tag{24}$$

Evaluated using Eqs. 20, 22 and the continuity condition $\hat{v}_r^d = j\omega\hat{\xi}$, this expression becomes the dispersion equation

$$\omega^2\frac{\rho R^3}{\gamma} = \frac{kRI_1(kR)}{I_o(kR)}\left\{\left[\frac{\mathcal{J}_o^2\mu_o R^3}{2}\right]\left[\frac{I_o^2(kR)}{I_1^2(kR)} - \frac{2I_o(kR)}{kRI_1(kR)} - 1\right] + [(kR)^2 - 1]\right\} \tag{25}$$

Rayleigh-Plateau Instability: The normalized frequency given by Eq. 25 is shown as a function of wave number by Fig. 8.15.2 with the magnetic pressure $\mu_o(\mathcal{J}_o R)^2/2$ normalized to the surface tension pressure γ/R as a parameter. Negatives of the quantities shown are also solutions. Note that even in the absence of an axial current, perturbations $kR < 1$ (wavelengths longer than $2\pi R$) are unstable. Any perturbation results in major radii of curvature that differ in sign. For a region that is necking off, the curvature associated with the axial dependence tends to restore the equilibrium whereas that caused by the circular cross section of the column tends to further neck off the column. For perturbations having wavelength $\lambda > 2\pi R$, the latter wins and the equilibrium is unstable. The wavelength for maximum rate of growth, given by $kR \simeq 0.7$, can be used to give a rough prediction of the size of drops formed from a liquid jet. According to the linear theory, a drop having radius r_o would have a volume equal to that of one wavelength of the jet, $\pi R^2 = 4/3(\pi r_o^3)$.

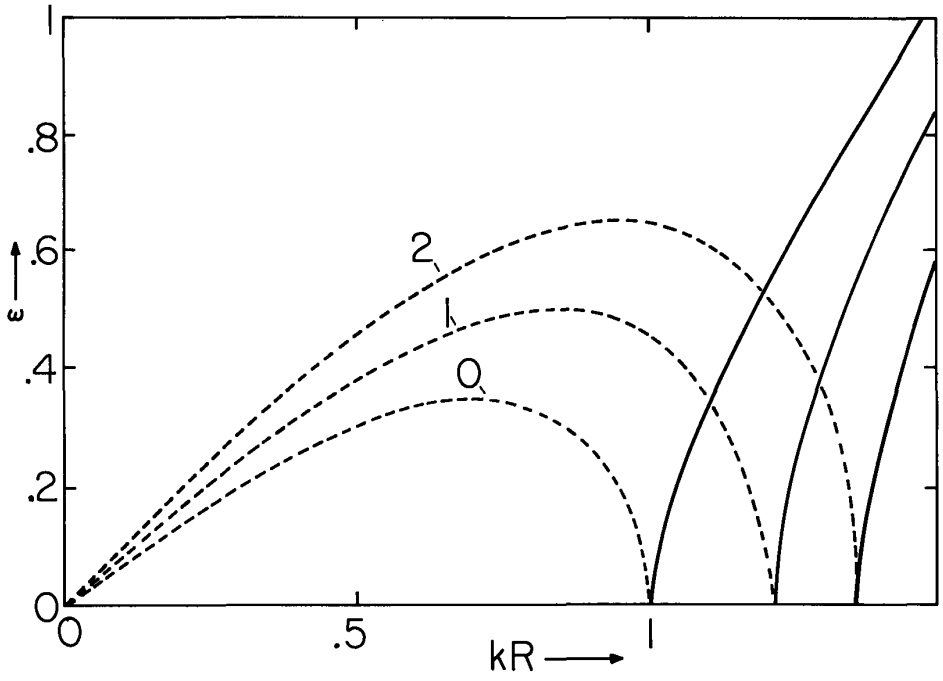

Fig. 8.15.2

Normalized frequency $\omega \equiv \omega\sqrt{\rho R^3/\gamma}$ as a function of wave number. --- ω_i, —— ω_r. The parameter is $\mathcal{J}_o^2\mu_o R^3/2\gamma$.

z-Pinch Instability: The general nature of the pinch instability is qualitatively similar to that found with the flux conserving pinch of Sec. 8.12. Because the current through the column must be conserved, both the current density and the magnetic field intensity in the fluid adjacent to the interface go up wherever the column tends to neck off. The result is an inward magnetic force density that tends to further encourage the necking off. Unless wavelengths are sufficiently short to be stabilized by surface tension, they are unstable. According to the model, it is only the inertia of the column that limits the rate of growth of the instability.

Finally, is the instantaneous magnetic diffusion model appropriate for the description of a mercury column having a radius of 1 cm or less? From Eq. 25 and Fig. 8.15.2 the frequency can be taken as of the order of $\sqrt{\gamma/\rho R^3}$. For the approximation to be justified, the product of this frequency (or growth rate) and the magnetic diffusion time (based here on the column radius) must be small:

$$\omega\tau_m = \sqrt{\frac{\mu^2\sigma^2\gamma R}{\rho}} \tag{26}$$

Typically, this number is less than 10^{-3}.

The major electromechanical effect that would be experimentally observed but not accounted for by this model is magnetic damping.

8.16 Dynamic Shear Stress Surface Coupling

It is a straightforward process to include the effects of viscosity in the piecewise homogeneous models developed in Secs. 8.9-8.15. The fluid mechanics is represented by the viscous diffusion transfer relations of Sec. 7.19 rather than the inviscid pressure-velocity relations of Sec. 7.11. With the viscosity come additional boundary conditions. At an interface, not only is the normal velocity continuous, but so also is the tangential velocity (Eq. 7.7.3). Also, the shearing stresses acting at an interface, Eq. 7.7.6, are not automatically balanced. In Secs. 8.9-8.15, the interfacial stress balance is for interfaces free of shearing surface force densities. Thus, any of these examples have stress balance equations in directions tangential to the equilibrium interface that are identically satisfied.

In this section, the example treated not only illustrates how viscosity is taken into account in piecewise homogeneous systems, but also involves an electric shearing surface force density. Hence, the viscous shear stresses are necessary for the formulation of a self-consistent model.

A highly insulating liquid, such as hexane, has a free surface which is bounded from above by a gas, as shown in Fig. 8.16.1. Perhaps by means of a very small radioactive source, some ion pairs are provided in the bulk of the liquid. By means of a potential applied between the planar electrodes, half of this charge is swept to the interface where it forms a monolayer of surface charge that shields the electric field from the liquid; thus, $\sigma_o = \varepsilon_o E_o$. Subjected to a tangential electric field, common interfacial ions migrate relative to the liquid at a rate that is negligible compared to that due to convection. A good model pictures the charge as frozen to the liquid interface. What are the modes of motion characterizing the adjustment of the interface to a perturbation field?

Because the fluids to either side of the interface have uniform permittivities and no free charge density, the electromechanical coupling is confined to the interface. In the following, it is assumed that the depth of the liquid and the distance to the upper electrode from the interface are large compared to typical perturbation wavelengths on the interface.

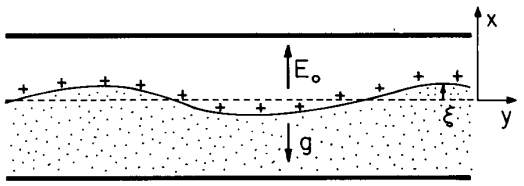

Fig. 8.16.1. Cross section of liquid-air interface supporting surface charge density σ_o. Charges are modeled as frozen to the liquid.

Static Equilibrium: With the interface flat and $\vec{v} = 0$, the electric field is

$$\vec{E} = \begin{cases} E_o\vec{i}_x = \dfrac{\sigma_o}{\varepsilon_o}\vec{i}_x; & x > 0 \\ 0 \quad\quad ; & x < 0 \end{cases} \tag{1}$$

and the pressure balances the gravitational force density in the liquid with a jump at the interface to equilibrate the surface force density $\varepsilon_o E_o^2/2$:

$$S_{xx} = -p = \begin{cases} -\Pi & ; \quad x > 0 \\ \rho g x + \dfrac{1}{2}\varepsilon_o E_o^2 - \Pi; & x < 0 \end{cases} \tag{2}$$

Bulk Perturbations: With the perturbation electric field represented by $\vec{e} = -\nabla\Phi$, the flux-potential relations describe the fields in the bulk regions. Application of Eqs. (a) from Table 2.16.1 in the limit $(k\Delta) \to \infty$ gives

$$\hat{e}_x^d = k\hat{\Phi}^d; \quad \hat{e}_x^e = -k\hat{\Phi}^e \tag{3}$$

for the regions above and below the interface respectively. Because the system is invariant to rotation about the x axis, there is no loss in generality if perturbations are taken as independent of z; Φ = Re exp j(ωt - ky).

For the half-space of liquid, the mechanical perturbation stress-velocity relations are given by Eq. 7.19.19, where $\gamma_V \equiv \sqrt{k^2 + j\omega\rho/\eta}$,

$$\begin{bmatrix} \hat{S}_{xx}^e \\ \hat{S}_{yx}^e \end{bmatrix} = \begin{bmatrix} \eta \dfrac{\gamma_V}{k}(\gamma_V + k) & -j\eta(\gamma_V - k) \\ j\eta(\gamma_V - k) & \eta(\gamma_V + k) \end{bmatrix} \begin{bmatrix} \hat{v}_x^e \\ \hat{v}_y^e \end{bmatrix} \tag{4}$$

Jump Conditions: Each of the laws prevailing in the bulk must be consistently represented in the highly singular neighborhood of the interface. The charge forms a monolayer, but not a double layer, and hence consistent with the irrotational nature of $\vec{E}$ is the condition that its tangential component is continuous. In writing this condition, note that $\hat{v}_x = j\omega\xi$ where $\vec{n}$ is given in terms of ξ by Eq. (a) of Table 7.6.2:

$$\hat{\Phi}^d - \hat{\Phi}^e = -\frac{jE_o}{\omega}\hat{v}_x^e \tag{5}$$

The remaining electrical laws are charge conservation, Eq. 23 of Table 2.10.1, and Gauss' law. Together, these require that

$$\frac{\partial\sigma_f}{\partial t} + \nabla_\Sigma\cdot(\sigma_f\vec{v}) = 0; \quad \sigma_f = \vec{n}\cdot[\![\varepsilon\vec{E}]\!] \tag{6}$$

To linear terms, Gauss' law and conservation of charge are then represented by

$$\omega(\varepsilon_o\hat{e}_x^d - \varepsilon\hat{e}_x^e) - k\sigma_o\hat{v}_y^e = 0 \tag{7}$$

For the mechanical jump conditions, continuity of the velocity components does not enter because the contributions of the upper fluid to the stress equilibrium is negligible. Stress equilibrium, represented by Eq. 7.7.5, includes the normal surface force density due to surface tension, γ (given by Eq. (d) of Table 7.6.2):

$$[\![S_{ij}]\!] n_j + [\![T_{ij}^e]\!] n_j - \gamma(\nabla\cdot\vec{n})n_i = 0 \tag{8}$$

Physically, the x component of this expression represents (to linear terms) the balance of stresses normal to the distorted interface. Note that the total normal stress, S_{xx}, is the sum of an equilibrium part and the perturbation:

$$S_{xx} = \Pi + \frac{1}{2}\varepsilon_o E_o^2 + \rho g x + \text{Re}\,\hat{S}_{xx}(x)\exp j(\omega t - ky) \tag{9}$$

Thus, because $\hat{\xi} = \hat{v}_x^e/j\omega$, the x component of Eq. 8 is

$$-\hat{S}_{xx}^e - \rho g\frac{\hat{v}_x^e}{j\omega} + \varepsilon_o E_o\hat{e}_x^d - k^2\gamma\frac{\hat{v}_x^e}{j\omega} = 0 \tag{10}$$

What is new is the shearing component, the y component, of Eq. 8. In linearizing this expression, remember that S_{yy} also has an equilibrium part. Above the interface, it is $-\Pi$, while below the interface it is $-\Pi + \frac{1}{2}\varepsilon_o E_o^2 + \rho g x$ (Eq. 2). Thus, to linear terms, $[\![S_{yy}]\!] n_y \simeq [-\Pi - (-\Pi + \frac{1}{2}\varepsilon_o E_o^2)](-\partial\xi/\partial y)$ and this adds to one of the two terms resulting from the electric stress contribution. Also, $\hat{e}_y = jk\hat{\Phi}$, so the shearing component of the stress equilibrium reduces to

$$-S_{yx}^e - \varepsilon_o E_o^2\frac{k\hat{v}_x^e}{\omega} + j\varepsilon_o E_o k\hat{\Phi}^d = 0 \tag{11}$$

Dispersion Equation: By using Eqs. 3, the components $(\hat{e}_x^d, \hat{e}_x^e)$ can be eliminated from the electric jump conditions, Eqs. 5 and 7, and these solved for $\hat{\Phi}^d$,

$$\hat{\Phi}^d = \frac{-j\varepsilon E_o \hat{v}_x^e + \sigma_o \hat{v}_y^e}{\omega(\varepsilon_o + \varepsilon)} \tag{12}$$

This expresses the effect of the mechanics on the fields.

The self-consistent electromechanics is now represented by the two stress conditions, Eqs. 10 and 11, written in terms of the velocity amplitudes $(\hat{v}_x^e, \hat{v}_y^e)$. The stress amplitudes are eliminated in favor of these variables using Eqs. 4, while $\hat{e}_x^d$ is written in terms of $\hat{\Phi}^d$ by using Eq. 3a, and $\hat{\Phi}^d$ in turn eliminated using Eq. 12. Thus, the two expressions are

$$\begin{bmatrix} \left[-\frac{\eta\gamma_V}{k}(\gamma_V+k)-(\rho g+k^2\gamma)\frac{1}{j\omega}+\frac{j\varepsilon k E_o^2}{\omega(1+\frac{\varepsilon}{\varepsilon_o})}\right] & \left[j\eta(\gamma_V-k)+\frac{\sigma_o E_o k}{\omega(1+\frac{\varepsilon}{\varepsilon_o})}\right] \\ \left[-j\eta(\gamma_V-k)-\frac{\varepsilon k E_o^2}{\omega(1+\frac{\varepsilon}{\varepsilon_o})}\right] & j\left[j\eta(\gamma_V+k)+\frac{\sigma_o k E_o}{\omega(1+\frac{\varepsilon}{\varepsilon_o})}\right] \end{bmatrix} \begin{bmatrix} \hat{v}_x^e \\ \hat{v}_y^e \end{bmatrix} = \begin{bmatrix} 0 \\ 0 \end{bmatrix} \tag{13}$$

Physical insights are more easily obtained by adding j times Eq. 13b to Eq. 13a, and writing both equations (each multiplied by ω) in terms of the variables $\hat{v}_x^e$ and $(-\hat{v}_x^e + j\hat{v}_z^e)$. Use is made of the definitions $\sigma_o = \varepsilon_o E_o$ and $\gamma_V^2 \equiv k^2 + j\omega\rho/\eta$:

$$\begin{bmatrix} -\left[\frac{j\omega^2\rho}{k}+4\eta k\omega-j(\rho g+k^2\gamma)+j\varepsilon_o k E_o^2\right] & [-2\eta k\omega] \\ [2j\eta k\omega] & \left[j\eta(\gamma_V+k)\omega+\frac{k\varepsilon_o E_o^2}{1+\frac{\varepsilon}{\varepsilon_o}}\right] \end{bmatrix} \begin{bmatrix} \hat{v}_x^e \\ -\hat{v}_x^e+j\hat{v}_y^e \end{bmatrix} = \begin{bmatrix} 0 \\ 0 \end{bmatrix} \tag{14}$$

The dispersion equation is obtained by setting either the determinant of the coefficients from Eq. 13 or from Eq. 14 equal to zero. But, written in the second form, it is clear that as the viscosity approaches zero, two modes can be distinguished. These have limiting dispersion equations given by setting the diagonal terms to zero. The frequencies resulting from the upper left and lower right terms, respectively, are then

$$\omega = j\left(\frac{2\eta k^2}{\rho}\right) \pm \omega_o; \quad \omega_o \equiv \left[\frac{k}{\rho}(\rho g + k^2\gamma - k\varepsilon_o E_o^2) - \left(\frac{2\eta k^2}{\rho}\right)^2\right]^{1/2} \tag{15}$$

$$\omega = \omega_c\left[\left(\frac{\sqrt{3}}{2}+\frac{j}{2}\right)\right]; \quad \omega_c \equiv \left[\frac{\sigma_o^2}{\sqrt{\eta\rho}}\frac{k}{(\varepsilon_o+\varepsilon)}\right]^{2/3} \tag{16}$$

The modes can be distinguished in this way only if the frequencies given by Eqs. 15 and 16 are disparate. In general, the higher order dispersion equation must be solved.

When Eq. 15 is satisfied, Eq. 14 shows that $\hat{v}_x^e \simeq j\hat{v}_z^e$, and similarly, if Eq. 16 holds, then the vertical motions are dominated by the horizontal ones, $\hat{v}_x^e \simeq 0$. Thus, the dispersion equation (Eq. 15) is identified with gravity-capillary like waves coupled to an electric field in much the same way as discussed in the latter part of Sec. 8.10.

The main effect of viscosity on the gravity-capillary modes is damping, represented by the imaginary term in Eq. 15. Perhaps a surprising feature of these modes in this low-viscosity limit is that the electric field has the same destabilizing effect as if the interface were perfectly conducting. For example, the condition for incipient instability is the same as given by Eq. 8.10.21, even though that result was derived for an equipotential interface. In this low-viscosity limit, the surface charge on the insulating interface is convected sufficiently rapidly to maintain the interfacial potential constant.

The electromechanical oscillations or shear waves, represented by Eq. 16, involve interfacial dilatations. If an interfacial region is horizontally compressed, self-fields give rise to horizontal

electric repulsion forces, much as if there were an elastic film on the interface. Because this electrical "film" is coupled to the inertia of the liquid below through the viscous shear stress, an initial horizontal dilatation of the interface results in oscillations. The oscillations are highly damped because the electrical "spring" is coupled to the "mass" only through the viscous "damper." The frequency ω_c typifies how rapidly nonuniformities in a charged interface can adjust, so that the interface is free of electrical shear stress. The motion stops when the interface is an equipotential.

SMOOTHLY INHOMOGENEOUS SYSTEMS AND THEIR INTERNAL MODES

8.17 Frozen Mass and Charge Density Transfer Relations

A static EQS equilibrium with mass density $\rho_o(x)$ and charge density $q_o(x)$ continuously varying with vertical position is shown in Fig. 8.17.1. The equilibrium vertical gravitational and electrical force densities are balanced by a vertical gradient in pressure. It is the objective in this section to describe small amplitude perturbations from this equilibrium.

The mass density and charge density are conserved by a fluid element of fixed identity,

$$\frac{D\rho}{Dt} = 0; \quad \frac{D\rho_f}{Dt} = 0 \qquad (1)$$

The fluid has uniform permittivity ε and it is inviscid.

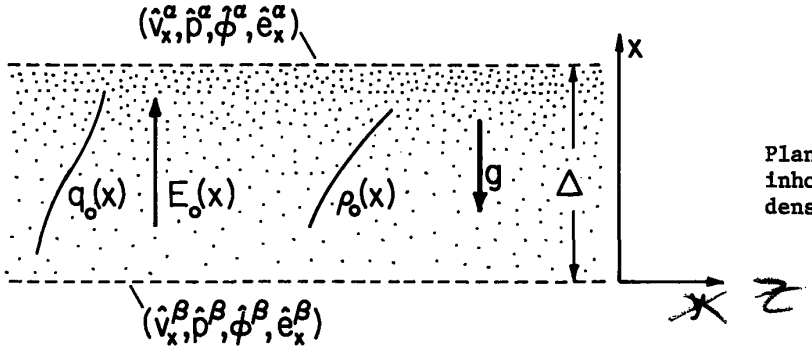

Fig. 8.17.1

Planar layer of fluid with vertical inhomogeneities in mass and charge densities.

It will be recognized that this system is a generalization of the piecewise homogeneous systems considered in Secs. 8.9 and 8.14. In principle, any distribution of $\rho_o(x)$ and $q_o(x)$ could be approximated by "stair-steps" representing stratified layers, with uniform densities, as illustrated in Fig. 8.17.2. The transfer relations for the homogeneous layers might then be used to represent the approximated system. With each interface goes a pair of modes, so that the piecewise homogeneous approximation represents the dynamics in terms of twice as many modes as interfaces. In the limit of a smooth distribution, an infinite number of modes are brought into play. Hence, it should come as no surprise that associated with the smoothly distributed inhomogeneities are an infinite number of "internal" modes. The objective in this and the next sections is to explore an approach that is an alternative to the piecewise homogeneous models.

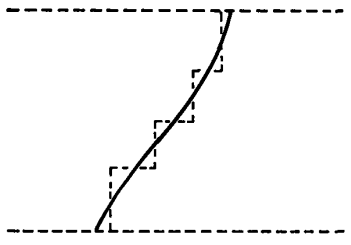

Fig. 8.17.2. Stair-step approximation to smooth inhomogeneity in $\rho_o(x)$ or $q_o(x)$.

In manipulations that follow, remember that ρ_o, q_o and E_o are functions of x. By Gauss' law, $DE_o = q_o/\varepsilon$, where $d(\ )/dx \equiv D(\ )$. Thus, in terms of complex amplitudes and $\hat{\xi} \equiv \hat{v}_x/j\omega$, Eqs. 1 relate perturbations in mass and charge density to the deformation

$$\hat{\rho} = -(D\rho_o)\hat{\xi}; \quad \hat{q} = -(Dq_o)\hat{\xi} \qquad (2)$$

The additional statements represent force balance, mass conservation, that the electric field is irrotational and Gauss' law. These are unraveled so as to obtain four first-order differential equations in $(\hat{v}_x, \hat{p}, \hat{\Phi}, \varepsilon\hat{e}_x)$.

The z-component of the force equation can be solved for $\hat{v}_z$ to obtain

$$\hat{v}_z = \frac{k}{\omega\rho_o}\hat{\pi} \qquad (3)$$

where the perturbation electric field $\vec{e} = -\nabla\Phi$ and $\hat{\pi} \equiv \hat{p} + q_o\hat{\Phi}$. Thus, the continuity equation, $\nabla\cdot\vec{v} = 0$,

requires that

$$D\hat{\xi} = \frac{k}{\omega}\hat{v}_z = \frac{k^2}{\omega^2\rho_o}\hat{\pi} \tag{4}$$

In view of Eqs. 2, the x component of the force equation requires that

$$D\hat{\pi} = (\omega^2\rho_o - E_oDq_o + gD\rho_o)\hat{\xi} + (Dq_o)\hat{\Phi} \tag{5}$$

where $\hat{e}_x$ is replaced by $-D\hat{\Phi}$ and p represented in terms of $\hat{\pi}$. That $\vec{e}$ is irrotational is also explicitly stated,

$$D\hat{\Phi} = -\frac{\not{\varepsilon}\hat{e}_x}{\not{\varepsilon}} \tag{6}$$

Finally, Gauss' law, together with Eq. 2b, gives

$$D(\varepsilon\hat{e}_x) = \hat{q} + jk\varepsilon\hat{e}_z = -Dq_o\hat{\xi} - k^2\varepsilon\hat{\Phi} \tag{7}$$

Given the amplitudes $(\hat{\xi}^\beta,\hat{p}^\beta,\hat{\Phi}^\beta,\varepsilon\hat{e}_x^\beta)$ at the lower extremity of the layer (say x = 0), these last four equations can be numerically integrated and the amplitudes evaluated at the upper extremity. Thus the relations

$$\begin{bmatrix}\hat{\xi}^\alpha\\ \hat{\pi}^\alpha\\ \hat{\Phi}^\alpha\\ \varepsilon\hat{e}_x^\alpha\end{bmatrix} = [B_{ij}]\begin{bmatrix}\hat{\xi}^\beta\\ \hat{\pi}^\beta\\ \hat{\Phi}^\beta\\ \varepsilon\hat{e}_x^\beta\end{bmatrix} \tag{8}$$

are obtained. For example, to compute the B_{ij}'s, the equations are integrated with $(\hat{\xi}^\beta,\hat{p}^\beta,\hat{\Phi}^\beta,\varepsilon\hat{e}_x^\beta) = (1,0,0,0)$. Then, $(B_{11},B_{12},B_{13},B_{14})$ are the computed values of $(\hat{\xi}^\alpha,\hat{p}^\alpha,\hat{\Phi}^\alpha,\varepsilon\hat{e}^\alpha)$, respectively.

Transfer relations in the form

$$\begin{bmatrix}\hat{\pi}^\alpha\\ \hat{\pi}^\beta\\ \varepsilon\hat{e}_x^\alpha\\ \varepsilon\hat{e}_x^\beta\end{bmatrix} = [C_{ij}]\begin{bmatrix}\hat{\xi}^\alpha\\ \hat{\xi}^\beta\\ \hat{\Phi}^\alpha\\ \hat{\Phi}^\beta\end{bmatrix} \tag{9}$$

follow by manipulating Eqs. 8. With the 4x4 matrix C_{ij} divided into four 2x2 submatrices, transduction between electrical and mechanical surface variables is represented by the upper right and lower left submatrices. In the absence of coupling (say, with $q_o = 0$), these entries should vanish. In this same limit, the upper left submatrix relates the pressure to the velocity amplitudes and these relations play the role of those derived in Sec. 7.9. Of course, here the layer has a nonuniform equilibrium mass density. Also in this limit, the lower right matrix relates the electric perturbation flux to the potentials. Because the layer has uniform electrical properties, these should become the same as the 2x2 entries in relations given by Eq. (a) of Table 2.16.1.

An alternative way of expressing Eqs. 4-7 results from combining the first three of these expressions to obtain

$$D(\rho_oD\hat{\xi}) + k^2\left(\frac{\mathcal{N}}{\omega^2} - \rho_o\right)\hat{\xi} = \frac{k^2Dq_o}{\omega^2}\hat{\Phi} \tag{10}$$

where $\mathcal{N} \equiv E_oDq_o - gD\rho_o$ and the last two to obtain

$$(D^2 - k^2)\hat{\Phi} = \frac{Dq_o\hat{\xi}}{\varepsilon} \tag{11}$$

This pair of second-order expressions can be used to determine $(\hat{\xi},\hat{\Phi})$ and the remaining pair of variables $(\hat{\pi},\varepsilon\hat{e}_x)$ then evaluated using Eqs. 4 and 6. The first of these expressions represents force equilibrium between the inertial force density and the gravitational and electric force densities. The "imposed-field" electric force density is on the right. The second expression is Poisson's equation.

On the right is the perturbation space charge generated by the convection of the nonuniform equilibrium charge density.

The driven response, spatial modes and temporal modes are illustrated in Sec. 8.18.

Weak-Gradient Imposed Field Model: Two approximations make it possible to obtain analytical expressions for the C_{ij}. First, the mass and charge densities are taken as being linear functions of x. Hence,

$$\rho_o = \rho_m + (D\rho_m)x; \quad q_o = q_e + (Dq_e)x \tag{12}$$

where $\rho_m, D\rho_m, q_e$ and Dq_e are constants and neither ρ_o nor q_o departs greatly from a mean value. Then, Eqs. 10 and 11 are approximated by

$$D^2\hat{\xi} + \gamma^2\hat{\xi} = \frac{k^2 Dq_e}{\omega^2\rho_m}\hat{\Phi}; \quad \gamma^2 \equiv (\frac{\mathcal{N}}{\rho_m\omega^2} - 1)k^2 \tag{13}$$

$$(D^2 - k^2)\hat{\Phi} = \frac{Dq_e}{\varepsilon}\hat{\xi} \tag{14}$$

Secondly, the field E_o is regarded as largely imposed by means of external sources. Then, not only is E_o approximated by a constant, but the coupling between fluid and field, represented by the terms on the right in Eqs. 13 and 14, is relatively weak. This breaks the electromechanical feedback loop.

First, to determine the mechanical response, the effect of the motion on the charge distribution is ignored in determining the potential distribution. With the term on the right in Eq. 14 set to zero,

$$\hat{\Phi} = \hat{\Phi}^\alpha \frac{\sinh(kx)}{\sinh(k\Delta)} - \hat{\Phi}^\beta \frac{\sinh k(x-\Delta)}{\sinh(k\Delta)} \tag{15}$$

This potential is used as a "drive" to evaluate the right-hand side of Eq. 13. By inspection, the solution satisfying the boundary conditions that $\hat{\xi}$ is $\hat{\xi}^\alpha$ and $\hat{\xi}^\beta$ at the respective planes is

$$\hat{\xi} = \left[\hat{\xi}^\alpha - \frac{k^2 Dq_e\hat{\Phi}^\alpha}{\omega^2\rho_m(k^2+\gamma^2)}\right]\frac{\sin(\gamma x)}{\sin(\gamma\Delta)} + \left[-\hat{\xi}^\beta + \frac{k^2 Dq_e\hat{\Phi}^\beta}{\omega^2\rho_m(k^2+\gamma^2)}\right]\frac{\sin\gamma(x-\Delta)}{\sin(\gamma\Delta)}$$
$$+ \frac{k^2 Dq_e}{\omega^2\rho_m(k^2+\gamma^2)}\left[\hat{\Phi}^\alpha\frac{\sinh(kx)}{\sinh(k\Delta)} - \hat{\Phi}^\beta\frac{\sinh k(x-\Delta)}{\sinh(k\Delta)}\right] \tag{16}$$

To find the approximate electrical response, the procedure is reversed. Given that $\hat{\xi}$ is $\hat{\xi}^\alpha$ and $\hat{\xi}^\beta$ at the respective planes, solution of Eq. 13 with the term on the right ignored gives

$$\hat{\xi} = \hat{\xi}^\alpha\frac{\sin(\gamma x)}{\sin(\gamma\Delta)} - \hat{\xi}^\beta\frac{\sin\gamma(x-\Delta)}{\sin(\gamma\Delta)} \tag{17}$$

In turn, the solution of Eq. 14 is

$$\hat{\Phi} = \left[\hat{\Phi}^\alpha + \frac{Dq_e\hat{\xi}^\alpha}{\varepsilon(\gamma^2+k^2)}\right]\frac{\sinh(kx)}{\sinh(k\Delta)} - \left[\hat{\Phi}^\beta + \frac{Dq_e\hat{\xi}^\beta}{\varepsilon(\gamma^2+k^2)}\right]\frac{\sin k(x-\Delta)}{\sin(\gamma\Delta)}$$
$$- \frac{Dq_e}{\varepsilon(\gamma^2+k^2)}\left[\hat{\xi}^\alpha\frac{\sin(\gamma x)}{\sin(\gamma\Delta)} - \hat{\xi}^\beta\frac{\sin\gamma(x-\Delta)}{\sin(\gamma\Delta)}\right] \tag{18}$$

where coefficients are determined by inspection so that the boundary conditions on $\hat{\Phi}$ are satisfied at the respective planes. The covariables $(\hat{\pi}, \varepsilon\hat{e}_x)$ follow from Eqs. 4 and 6 and are evaluated at the respective boundaries to give the transfer relations, Eqs. 9, with

$$C_{11} = -C_{22} = \frac{\omega^2 \rho_m \gamma}{k^2} \cot(\gamma\Delta)$$

$$C_{21} = -C_{12} = \frac{\omega^2 \rho_m \gamma}{k^2 \sin(\gamma\Delta)}$$

$$C_{13} = -C_{24} = -C_{31} = C_{42} = \frac{Dq_e}{k^2 + \gamma^2} [k \coth(k\Delta) - \gamma \cot(\gamma\Delta)] \tag{19}$$

$$C_{14} = -C_{23} = -C_{32} = C_{41} = \frac{Dq_e}{k^2 + \gamma^2} \left[\frac{\gamma}{\sin(\gamma\Delta)} - \frac{k}{\sinh(k\Delta)}\right]$$

$$C_{33} = -C_{44} = -\varepsilon k \coth(k\Delta)'$$

$$C_{34} = -C_{43} = \frac{\varepsilon k}{\sinh(k\Delta)}$$

Although the weak coupling approximation is sufficient to give the mechanical response to an electrical drive or the electrical response to a mechanical drive, the electrical-to-electrical response, represented by C_{33}, C_{34}, C_{43} and C_{44} is devoid of any of the electromechanics. Electromechanical effects on the transfer between electrical signals depend on there being a "two-way" interaction.

Reciprocity and Energy Conservation: That some coefficients, C_{ij}, in the transfer matrix have equal magnitudes suggests that basic relations exist between off-diagonal coefficients even with arbitrary gradients and fields. The frozen charge model is free of dissipation and allows for energy storage in electrical, kinetic and gravitational forms. With variables as defined in Eq. 9, this requires that the submatrix representing the hybrid pressure responses to electrical excitations is the negative of that representing the electrical flux responses to mechanical deformations. It also requires that mutual electrical and mutual mechanical coefficients are respectively negatives. The proof is a generalization of that developed in Sec. 2.17 for a region storing only electric energy.

Incremental changes in the total electrical, kinetic and gravitational energy stored by a system having volume V enclosed by a surface S are respectively

$$\delta w_e = \int_V \Phi \delta \rho_f dV - \oint_S \Phi \delta \vec{D} \cdot \vec{n} da \tag{20}$$

$$\delta w_k = \int_V \rho_f \vec{E} \cdot \delta \vec{\xi} dV - \oint_S p \delta \vec{\xi} \cdot \vec{n} da + \int_V \rho \vec{g} \cdot \delta \vec{\xi} dV \tag{21}$$

$$\delta w_g = \int_V (-\vec{g} \cdot \vec{r}) \delta \rho dV \tag{22}$$

The electrical contribution is familiar from Sec. 2.13 (Eq. 2.13.4). The kinetic statement exploits Newton's law and the incompressibility condition to state that all work done by the electrical, mechanical and gravitational subsystems goes into the creation of kinetic energy (Eq. 7.17.3). The gravitational energy storage is familiar as a specialized analogue of the electric one. The scale is small enough that gravitational self-fields are neglected and g is constant. Thus, by contrast with the potential ϕ for the electrical system, the gravitational potential is "imposed" and is simply $-\hat{g} \cdot \hat{r}$.

Charge migration is negligible, so the charge carried by fluid of fixed identity is conserved. Because $\nabla \cdot \delta\vec{\xi} = 0$, it follows (from Eq. 3.7.5 with $\alpha_i \to q$) that

$$\delta q = -\nabla q \cdot \delta \vec{\xi} \tag{23}$$

Similarly, the mass density of fluid of fixed identity is conserved,

$$\delta \rho = -\nabla \rho \cdot \delta \vec{\xi} \tag{24}$$

These expressions are now used in writing the sum of Eqs. 20-22 as

$$\delta(w_e + w_k + w_g) = -\oint_S \Phi \delta \vec{D} \cdot \vec{n} da - \oint_S p \delta \vec{\xi} \cdot \vec{n} da - \int_V (\Phi \nabla q + q \nabla \Phi) \cdot \delta \vec{\xi} dV$$
$$-\int_V [\rho \nabla(-\vec{g} \cdot \vec{r}) + (-\vec{g} \cdot \vec{r}) \nabla \rho] \cdot \delta \vec{\xi} dV \tag{25}$$

where use has also been made of the relations $\vec{E} = -\nabla\Phi$ and $\vec{g} = \nabla(\vec{g}\cdot\vec{r})$. The volume integrals are converted to surface integrals by first using a vector identity to contract the integrands [$\Phi\nabla\Psi+\Psi\nabla\Phi=\nabla(\Psi\Phi)$] and then exploiting the fact that $\nabla\cdot\delta\vec{\xi} = 0$ to make the integrands take the form of perfect divergences ($\nabla\Psi\cdot\vec{A} = \nabla\cdot\Psi\vec{A} - \vec{A}\cdot\nabla\Psi$). From Gauss' theorem, it follows that

$$\delta(w_e + w_k + w_g) = -\oint_S \Phi\delta\vec{D}\cdot\vec{n}da - \oint_S [p + \Phi q + (-\vec{g}\cdot\vec{r})\rho]\delta\vec{\xi}\cdot\vec{n}da \tag{26}$$

The desired reciprocity relations are between perturbation quantities, now designated by primes to distinguish them from the zero-subscripted equilibrium variables. Thus, incremental changes $\delta\vec{D}\cdot\vec{n}$ and $\delta\vec{\xi}\cdot\vec{n}$ on S lead to changes in the total energy given by Eq. 26 expressed up to quadratic terms in the perturbations as

$$\delta(w_e + w_k + w_g) = -\oint_S \Phi_o\delta\vec{D}_o\cdot\vec{n}da - \oint(\Phi_o\delta\vec{D}' + \Phi'\delta\vec{D}_o + \Phi'\delta\vec{D}')\cdot\vec{n}da$$

$$- \oint_S [p_o + \Phi_o q_o + (-\vec{g}\cdot\vec{r})\rho_o]\delta\vec{\xi}'\cdot\vec{n}da - \oint_S [p' + \Phi_o q' + q_o\Phi' + (-\vec{g}\cdot\vec{r})\rho']\delta\vec{\xi}'\cdot\vec{n}da \tag{27}$$

The surface S is now made one enclosing a section of the planar layer shown in Fig. 8.17.1 that has the wavelengths $2\pi/k_y$ and $2\pi/k_z$ in the y and z-directions, respectively. Because $\vec{D}_o$ is x-directed, the first term makes contributions only on the α and β surfaces. Perturbations are assumed to take the complex-amplitude form $\xi = \mathrm{Re}\xi\ \exp(-jk_y - jk_z z)$, where k_y and k_z are real. The spatial periodicity in the y and z directions insures that contributions to the surface integrations from the second and third terms only come from the α and β surfaces. Moreover, because the integrands of these terms are linear in the perturbation quantities, they "average out" and make no contribution. The quadratic perturbation terms from the last intergral, which are also periodic and hence make contributions only on the α and β surfaces, can be represented using the space-average theorem, Eq. 2.15.14:

$$\delta(w_e + w_k + w_g) = -(\Phi_o^\alpha\delta D_{xo}^\alpha - \Phi_o^\beta\delta D_{xo}^\beta) - \frac{1}{2}\mathrm{Re}[\tilde{\Phi}^\alpha\delta(\tilde{D}_x^\alpha)^* - \tilde{\Phi}^\beta\delta(\tilde{D}_x^\beta)^*]$$

$$- \frac{1}{2}\mathrm{Re}[\tilde{p}^\alpha\delta(\tilde{\xi}^\alpha)^* - \tilde{p}^\beta\delta(\tilde{\xi}^\beta)^*] - \frac{1}{2}\mathrm{Re}[\Phi_o^\alpha\tilde{q}^\alpha\delta(\tilde{\xi}^\alpha)^* - \Phi_o^\beta\tilde{q}^\beta\delta(\tilde{\xi}^\beta)^*] \tag{28}$$

$$- \frac{1}{2}\mathrm{Re}[q_o^\alpha\tilde{\Phi}^\alpha\delta(\tilde{\xi}^\alpha)^* - q_o^\beta\tilde{\Phi}^\beta\delta(\tilde{\xi}^\beta)^*] - \frac{1}{2}\mathrm{Re}(-\vec{g}\cdot\vec{r})[\tilde{\rho}^\alpha\delta(\tilde{\xi}^\alpha)^* - \tilde{\rho}^\beta\delta(\tilde{\xi}^\beta)^*]$$

With the understanding that the incremental variations are made with the equilibrium potentials Φ_o held fixed on the transverse boundaries, the first terms on the right become perfect differentials, $\Phi_o\delta D_{xo} \rightarrow \delta(\Phi_o D_{xo})$, so these equilibrium terms are moved to the left side of the equation.

In the remaining terms, it is now assumed that all complex amplitudes are real. It is entirely possible to proceed without making this assumption by treating the real and imaginary parts of the variables ($\tilde{\xi}^\alpha,\tilde{\xi}^\beta,\tilde{\Phi}^\alpha,\tilde{\Phi}^\beta$) as independent. However, there is little to be learned from this generalization because it is obvious from Eqs. 4-7 (which, provided ω^2 is real, have real coefficients) that the coefficients C_{ij} are real. Hence, given that the amplitudes ($\tilde{\xi}^\alpha,\tilde{\xi}^\beta,\tilde{\Phi}^\alpha,\tilde{\Phi}^\beta$) are real, the amplitudes of the conjugate variables are clearly real.

In the forth and sixth terms of Eq. 28, Eqs. 2 are used to substitute

$$\Phi_o\tilde{q}\delta\tilde{\xi} = -\Phi_o Dq_o\tilde{\xi}\delta\tilde{\xi} = -\frac{1}{2}\delta(\Phi_o Dq_o\tilde{\xi}^2) \tag{29}$$

$$(-\vec{g}\cdot\vec{r})\tilde{\rho}\delta\tilde{\xi} = -(-\vec{g}\cdot\vec{r})D\rho_o\tilde{\xi}\delta\tilde{\xi} = -\frac{1}{2}\delta[(-\vec{g}\cdot\vec{r})D\rho_o\tilde{\xi}^2] \tag{30}$$

respectively. The second equalities are based on recognition that if variations in the $\tilde{\xi}$'s and $\tilde{D}_x$'s result in variations of Dq_o or $D\rho_o$, the latter can be neglected, because the terms in which they appear are already quadratic in the perturbations. With the substitution of Eqs. 29 and 30, the fourth and sixth terms also become perfect differentials and are therefore moved to the left side of Eq. 28. Finally, in the second term on the right the transformation $\tilde{\Phi}\delta\tilde{D}_x = \delta(\tilde{\Phi}\tilde{D}_x) - \tilde{D}_x\delta\tilde{\Phi}$ is made and the perfect differential moved to the left-hand side. Thus, the energy statement becomes

$$\delta w' = -\frac{1}{2}(\tilde{\pi}^{\alpha}\delta\tilde{\xi}^{\alpha} - \tilde{\pi}^{\beta}\delta\tilde{\xi}^{\beta}) + \frac{1}{2}(\tilde{D}_x^{\alpha}\delta\tilde{\Phi}^{\alpha} - \tilde{D}_x^{\beta}\delta\tilde{\Phi}^{\beta}) \tag{31}$$

where

$$w' \equiv w_e + w_k + w_g + \frac{1}{2}(\tilde{\Phi}^{\alpha}\tilde{D}_x^{\alpha} - \tilde{\Phi}^{\beta}\tilde{D}_x^{\beta}) - \frac{1}{4}[\Phi^{\alpha}Dq_o^{\alpha}(\tilde{\xi}^{\alpha})^2 - \Phi_o^{\beta}Dq_o^{\beta}(\tilde{\xi}^{\beta})^2]$$

$$- \frac{1}{4}(-\vec{g}\cdot\vec{r}\,)[D\rho_o^{\alpha}(\tilde{\xi}^{\alpha})^2 - D\rho_o^{\beta}(\tilde{\xi}^{\beta})^2] + (\Phi_o^{\alpha}\delta D_{xo}^{\alpha} - \Phi_o^{\beta}\delta D_{xo}^{\beta})$$

and

$$\tilde{\pi} \equiv \tilde{p} + q_o\tilde{\Phi}$$

Now, with the assumption that w' is a state function $w'(\tilde{\xi}^{\alpha},\tilde{\xi}^{\beta},\tilde{\Phi}^{\alpha},\tilde{\Phi}^{\beta})$, the incremental change $\delta w'$ can also be written as

$$\delta w' = \frac{\partial w'}{\partial\tilde{\xi}^{\alpha}}\delta\tilde{\xi}^{\alpha} + \frac{\partial w'}{\partial\tilde{\xi}^{\beta}}\delta\tilde{\xi}^{\beta} + \frac{\partial w'}{\partial\tilde{\Phi}^{\alpha}}\delta\tilde{\Phi}^{\alpha} + \frac{\partial w'}{\partial\tilde{\Phi}^{\beta}}\delta\tilde{\Phi}^{\beta} \tag{32}$$

Because the variables $(\tilde{\xi}^{\alpha},\tilde{\xi}^{\beta},\tilde{\Phi}^{\alpha},\tilde{\Phi}^{\beta})$ are independent, it follows from Eqs. 31 and 32 that corresponding coefficients must be equal:

$$\tilde{\pi}^{\alpha} = -2\frac{\partial w'}{\partial\tilde{\xi}^{\alpha}}\,; \quad \tilde{\pi}^{\beta} = 2\frac{\partial w'}{\partial\tilde{\xi}^{\beta}} \tag{33}$$

$$\tilde{D}_x^{\alpha} = 2\frac{\partial w'}{\partial\tilde{\Phi}^{\alpha}}\,; \quad \tilde{D}_x^{\beta} = -2\frac{\partial w'}{\partial\tilde{\Phi}^{\beta}} \tag{34}$$

The reciprocity relations follow by taking cross-derivatives of these relations. For example, in view of Eqs. 33a and 34b together with Eq. 9,

$$\frac{\partial\tilde{\pi}^{\alpha}}{\partial\tilde{\Phi}^{\beta}} = \frac{\partial\tilde{D}_x^{\beta}}{\partial\tilde{\xi}^{\alpha}} \Rightarrow C_{14} = C_{41} \tag{35}$$

Thus, if C_{ij} is broken into four 2x2 matrices K, L, M and N such that

$$C_{ij} = \begin{bmatrix} K & L \\ M & N \end{bmatrix} \tag{36}$$

where K and N are each antisymmetric and L is the negative of M.

The next section exemplifies the implications of the transfer relations, both found by numerical integration and approximated by the weak-gradient imposed-field model.

8.18 Internal Waves and Instabilities

The frozen charge and mass density transfer relations derived in Sec. 8.17 are now applied to the study of space-charge gravity waves excited in the sinusoidal steady state from transverse boundaries. Also discussed are the temporal and spatial modes. Instability conditions are exemplified and a general proof given that the principle of exchange of stabilities is satisfied. With the objective of both gaining physical insight for this type of dynamics and for ways in which it can be represented, two models are developed and compared. First, the weak-gradient imposed-field approximation of Sec. 8.17 is used to obtain an analytical representation of the response. Then, as a recourse that is applicable for an arbitrary distribution of charge and mass density, numerical integration is used to determine the response. Because one of these representations depends on numerical procedures, it is convenient to normalize variables at the outset.

Configuration: The stratified layer shown in Fig. 8.18.1 is bounded from above by fixed excitation electrodes upon which a spatially and temporally periodic potential is imposed. From below, it is bounded by a conducting rigid electrode, essentially constrained in potential to the constant equilibrium value V_o.

Normalization: To be specific about the distributions in charge and mass density, they are taken as linear and written in terms of the constants defined in Fig. 8.18.1:

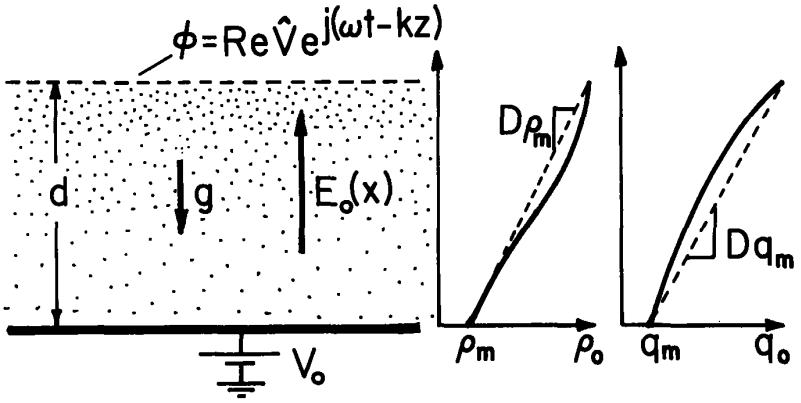

Fig. 8.18.1

Cross section of system in which internal space-charge gravity waves are excited.

$$\underline{q}_o \equiv \frac{q_o(x)}{q_e} = 1 + \frac{\underline{D}q_e}{q_e}\underline{x}; \quad \underline{\rho}_o \equiv \frac{\rho_o}{\rho_m} = 1 + \frac{\underline{D}\rho_m}{\rho_m}\underline{x} \tag{1}$$

In terms of these quantities, variables are normalized such that

$$\begin{aligned} x &= \underline{x}d & \hat{\xi} &= \hat{\underline{\xi}}d \\ k &= \underline{k}/d & \hat{\pi} &= \hat{\underline{\pi}}|Dq_e||v_o|d \\ \omega^2 &= \frac{\underline{\omega}^2|V_o||Dq_e|}{\rho_m d} & \hat{\Phi} &= \hat{\underline{\Phi}}|V_o| \\ \hat{V} &= \hat{\underline{V}}|V_o| & \hat{d}_x &= \varepsilon\hat{e}_x = \hat{\underline{d}}_x|Dq_e|d^2 \end{aligned} \tag{2}$$

For other equilibrium distributions, the same normalization could be used with the quantities ρ_m and $|Dq_e|$ defined as mean values.

From the one-dimensional form of Gauss' law and the equilibrium potential boundary conditions, the equilibrium distribution of electric field is written in terms of the normalized variables as

$$E_o = \frac{|V_o|}{d}\left\{\frac{V_o}{|V_o|} + S\left[\frac{q_e}{|\underline{D}q_e|}\left(\underline{x} - \frac{1}{2}\right) + \frac{1}{2}\frac{\underline{D}q_e}{|\underline{D}q_e|}\left(\underline{x}^2 - \frac{1}{3}\right)\right]\right\} \tag{3}$$

where $S \equiv |\underline{D}q_e|d^2/\varepsilon|V_o|$ represents the influence of the space charge on the imposed field.

Driven Response: Boundary conditions reflect electrode constraints on the normal motion of the fluid and on the potential:

$$[\hat{\xi}^a, \hat{\xi}^b, \hat{\Phi}^a, \hat{\Phi}^b] = [0, 0, \hat{V}, 0] \tag{4}$$

Given the electrical excitation at the upper boundary, what is the mechanical and electrical response of the fluid, and in particular, what perturbation pressure and normal electric field would be expected on instruments embedded in the lower electrode? These follow from Eq. 8.17.9 as

$$\frac{\hat{\pi}^b}{\hat{V}} = C_{23}; \quad \frac{\hat{d}_x^b}{\hat{V}} = C_{43} \tag{5}$$

In the weak-gradient imposed-field approximation, it is possible to evaluate the C_{ij}'s by using Eqs. 8.17.19. Thus normalized, Eq. 3 becomes

$$\frac{\hat{\pi}^b}{\hat{V}} = C_{23} \equiv \frac{C_{23}}{d|Dq_e|} = \frac{-1}{k^2 + \gamma^2}\left(\frac{\gamma}{\sin\gamma} - \frac{k}{\sinh k}\right) \tag{6}$$

$$\frac{\hat{d}_x^b}{\hat{V}} = C_{43} \equiv \frac{C_{43}|V_o|}{|Dq_e|d^2} = -S^{-1}\frac{k}{\sinh k} \tag{7}$$

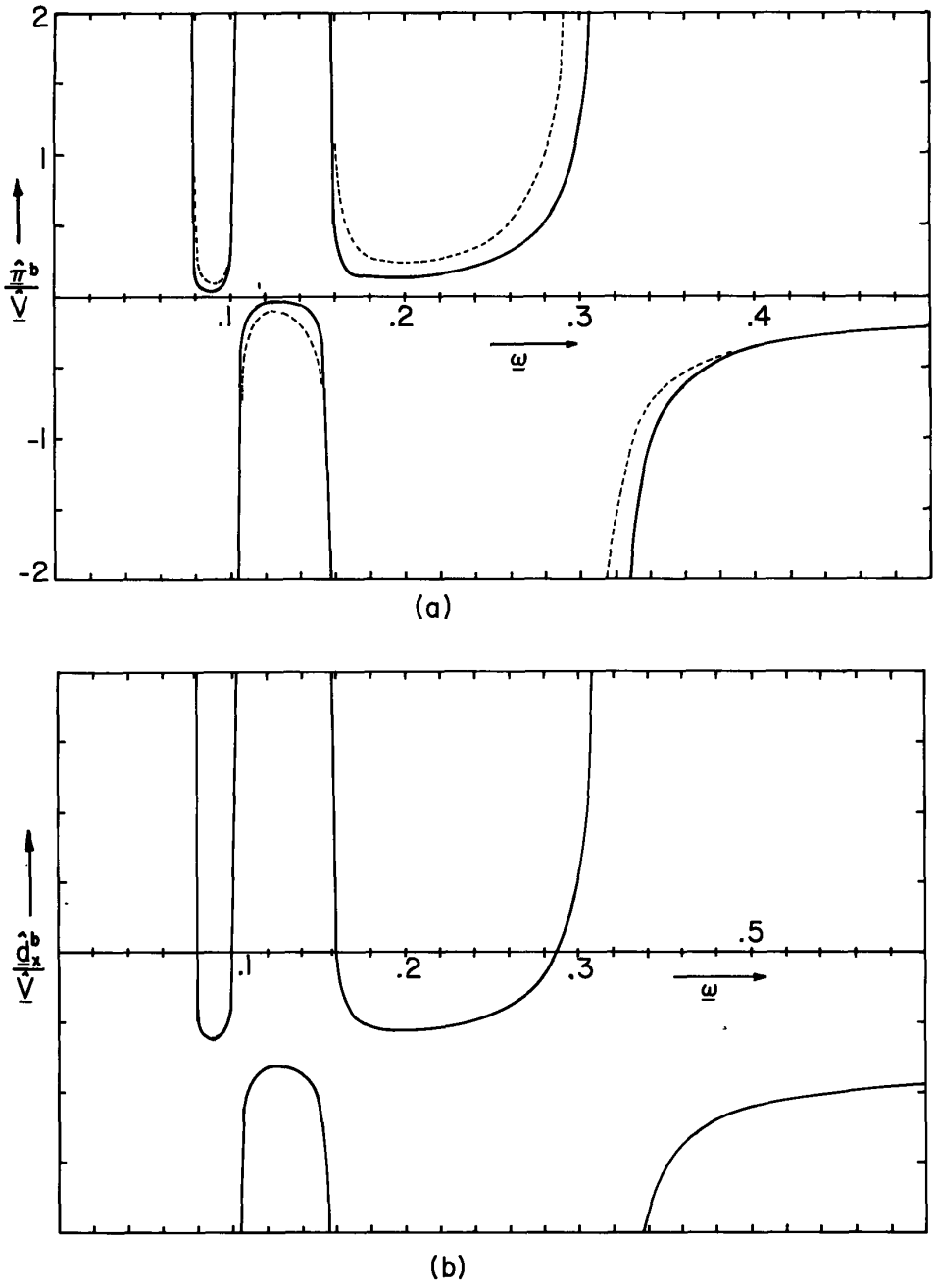

Fig. 8.18.2. Driven response of charged layer showing prediction of weak-gradient imposed-field model (broken line) for comparison with numerically determined response (solid line). The response below $\underline{\omega} = 0.08$ is not shown because it displays an infinite number of resonances crowded toward the origin. In both cases, $\underline{k} = 1$ and $\underline{V}_o$ and $\underline{D}q_e$ are both positive or both negative so that equilibrium is stable. The solid numerically predicted curves are for $\underline{D}q_e/q_e = 1$ and $S = 1$. (a) Hybrid pressure response at lower electrode as a function of frequency for electrical excitation at upper electrode. (b) Electric flux at lower electrode.

where

$$\gamma \equiv k\sqrt{\pm\frac{1}{\omega^2}\left(1-\frac{gD\rho_m d}{V_o Dq_e}\right)-1} \tag{8}$$

The upper sign applies if V_o and Dq_e are both positive or both negative. The lower sign is to be used if V_o and Dq_e have opposite signs.

The weak-gradient imposed-field driven responses are illustrated as a function of frequency in Fig. 8.18.2. Because of approximations inherent to this model, the electrical-to-electrical response is no more than that of the layer without the charged fluid. This result will be refined to include the electromechanical effects shortly. The resonances in the hybred pressure response that dominate the picture reflect the electromechanical coupling. In this loss-free system, they serve notice that the natural frequencies of the stable temporal modes are real and that there are an infinite number of spatial modes having real wave numbers. The conditions for the resonances follow from Eq. 6:

$$\sin\gamma = 0 \Rightarrow \gamma = n\pi, n = 1,2,\cdots \tag{9}$$

Thus, the resonance frequencies are found by evaluating γ in Eq. 8 and solving for ω,

$$\omega^2 = \frac{k^2 \mathcal{N}}{k^2 + (n\pi)^2}\ ;\ \mathcal{N} = \frac{\frac{V_o}{d}Dq_e - gD\rho_m}{\frac{|V_o|}{d}|Dq_e|} \tag{10}$$

The associated distributions, $\hat{\xi}(x)$, in the neighborhood of a resonance follow from Eq. 8.17.17 as being $\sin(n\pi\underline{x})$. These are pictured by the broken curves of Fig. 8.18.3. Implicit to the discussion thus far is the presumption that $\mathcal{N} > a$.

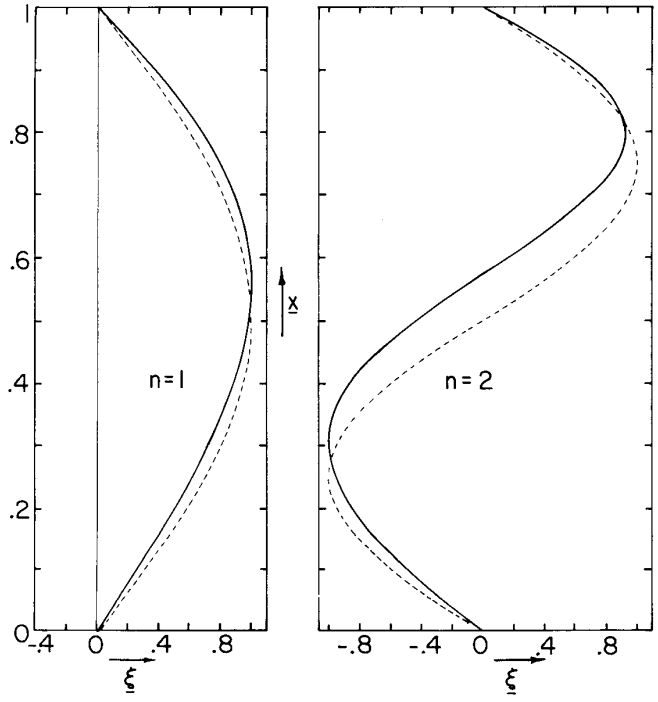

Fig. 8.18.3

Vertical displacement of fluid as a function of vertical position. Response is shown in the neighborhood of first and second resonances, and hence represents first and second temporal eigenmodes. Solid curves are predicted numerically using parameters of Fig. 8.18.2, while broken curves are weak-gradient imposed-field approximation.

Consider now the more general approach of numerically integrating Eqs. 8.17.4-7 to find the transfer relations. Normalized, these equations are

$$D\hat{\xi} = \frac{k^2}{\omega^2\rho_o}\pi \tag{11}$$

$$D\pi = (\omega^2\rho_o - \mathcal{N})\hat{\xi} + \frac{Dq_o}{|Dq_e|}\hat{\Phi} \tag{12}$$

$$D\Phi = -Sd_x \tag{13}$$

$$Dd_x = -\frac{Dq_o}{|Dq_e|}\hat{\xi} - \frac{1}{S}k^2\hat{\Phi} \tag{14}$$

These expressions are applicable with arbitrary charge and mass distributions. For the specific linear distributions, ρ_o is given by Eq. 2, $Dq_o = Dq_e$ and

$$\zeta = \left\{\frac{V_o}{|V_o|} + \frac{Dq_e}{|Dq_e|}S\left[\frac{q_e}{Dq_e}(x - \tfrac{1}{2}) + \tfrac{1}{2}(x^2 - \tfrac{1}{3})\right]\right\}\frac{Dq_e}{|Dq_e|} - \frac{gdD\rho_m}{|V_o||Dq_e|} \tag{15}$$

The coefficients required to evaluate the responses, Eqs. 3, follow by converting the transfer relations of Eq. 8.17.8 to those of Eq. 8.17.9. The coefficients needed here are

$$C_{23} = -B_{14}/D; \quad C_{43} = B_{12}/D; \quad D \equiv B_{12}B_{34} - B_{14}B_{32} \tag{16}$$

Coefficients in the transfer relations have been normalized so that $\underline{C}_{ij}$ and $\underline{B}_{ij}$ relate normalized veriables. The $\underline{B}_{ij}$'s are determined by numerical integration of Eqs. 11-14 following the procedure indicated following Eq. 8.17.8. (Numerical integration of systems of first-order differential equations written in the form of Eqs. 11-14 is conveniently carried out using standard library subroutines. Used here was the IMSLIB Routine DVERK.)

For purposes of comparison, the numerically determined frequency responses are shown with those predicted by the weak-gradient imposed-field model in Fig. 8.18.2. For the numerical case shown, $Dq_e/q_e = 1$ and $S = 1$, so both the weak-gradient and the imposed-field approximations are somewhat invalid. Note that the electrical-to-electrical response now displays the characteristic resonances of the internal waves. The numerically determined mechanical displacement and potential distributions with the frequency in the neighborhood of the first and of the second resonances are shown in Fig. 8.18.3.

Spatial Modes: Still in the sinusoidal steady state, these modes satisfy homogeneous transverse boundary conditions and are needed to make the total solution obey longitudinal boundary conditions. (Spatial modes are introduced in Sec. 5.17.) For example, what is the response to a drive at some z plane with the duct walls free of excitations?

From the weak-gradient imposed-field driven response of Eq. 6, the dispersion equation is $D(\omega,k) = \sin\gamma = 0$. This has roots that are the same as for the resonance conditions, Eq. 10. Here, however, interest is in complex k for a real driving frequency ω,

$$k = \pm\frac{n\pi\omega}{\sqrt{\mathcal{N} - \omega^2}} \tag{17}$$

Under the assumption once again that $\mathcal{N} > 0$, the dispersion equation is typified by Fig. 8.18.4. Note that all modes have the same cut-off frequency $\underline{\omega} = 1$. With $\underline{\omega} < 1$, all modes are propagating, whereas with $\underline{\omega} > 1$, all modes are evanescent.

The resonances below $\underline{\omega} = 1$ in the driven frequency response, Fig. 8.18.2, result from a coincidence of the imposed wave number and the purely real wave number of the propagating spatial modes.

Temporal Modes: When t = 0, initial conditions are spatially periodic in the z direction, with wave number k. What modes are to be superimposed in representing the ensuing transient? (Temporal modes are introduced in Sec. 5.15.)

A mode $\hat{\xi}_n(x)$ has the eigenfrequency $j\omega_n \equiv s_n$. Without being specific as to the charge and density distributions, it can be deduced from Eqs. 8.17.10 and 8.17.11 together with the boundary conditions that these eigenfrequencies are either purely real or purely imaginary so s_n^2 is real. Equation 8.17.10 is multiplied by $\hat{\xi}_n^*$ and integrated over the cross section. The first term is then integrated by parts to obtain

$$\rho_o\hat{\xi}_n^*D\hat{\xi}_n]_o^d - \int_o^d \rho_o D\hat{\xi}_n D\hat{\xi}_n^* dx - k^2\int_o^d (\rho_o + \frac{\mathcal{N}}{s_n^2})\hat{\xi}_n\hat{\xi}_n^* dx = -k^2\int_o^d \frac{Dq_o\hat{\Phi}_n^*\hat{\xi}_n^*}{s_n^2}dx \tag{18}$$

Similarly, the complex conjugate of Eq. 8.17.11 is multiplied by $k^2\varepsilon\hat{\Phi}_n$ and integrated over the cross section. Again, the first term is integrated by parts to obtain

$$k^2\varepsilon\hat{\Phi}_n D\hat{\Phi}_n^*]_o^d - k^2\varepsilon\int_o^d D\hat{\Phi}_n(D\hat{\Phi}_n)^* dx - k^4\varepsilon\int_o^d \hat{\Phi}_n\hat{\Phi}_n^* dx = k^2\int_o^d Dq_o\hat{\xi}_n^*\hat{\Phi}_n dx \tag{19}$$

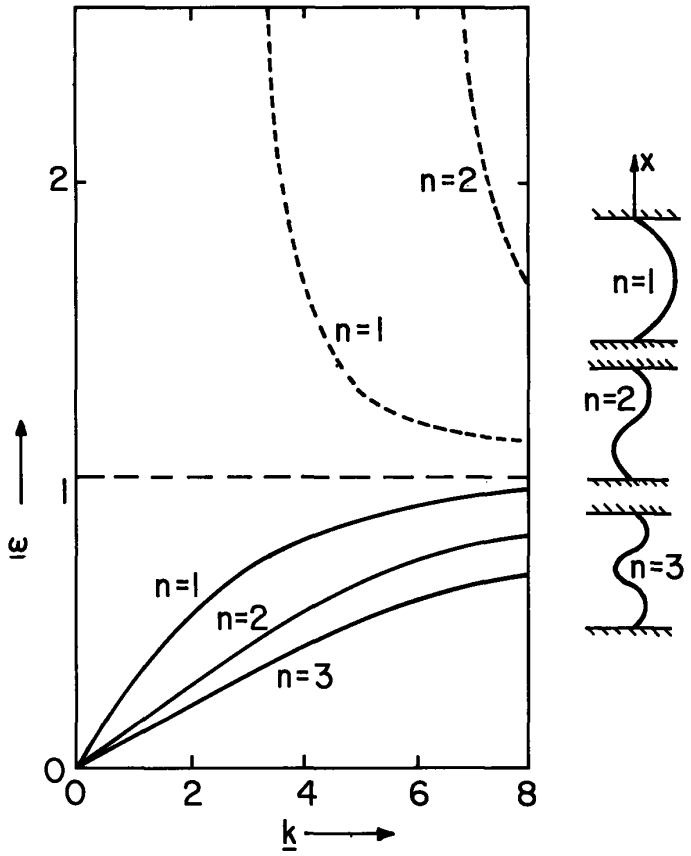

Fig. 8.18.4

Complex normalized frequency as function of real longitudinal wave number for spatial modes in weak-gradient imposed-field approximation. $\underline{\omega}_r$ ——, $\underline{\omega}_i$ ----. All modes have common asymptotic frequency at $\underline{\omega} = 1$, above which they are evanescent.

The point of these manipulations is to obtain positive definite integrands and to make the right-hand sides of these expressions negatives. Because of the boundary conditions on $\hat{\xi}_n$ and $\hat{\Phi}_n$, the terms evaluated on the boundaries vanish. Thus, the last two expressions give

$$\int_o^d (\rho_o |D\hat{\xi}_n|^2 + \rho_o k^2 |\hat{\xi}_n|^2)\, dx = -\frac{k^2}{s_n^2} \int_o^d [\mathcal{N} |\hat{\xi}_n|^2 + \epsilon(|D\hat{\Phi}|^2 + k^2 |\hat{\Phi}|^2)] dx \tag{20}$$

This expression can be solved for the square of the eigenfrequency, s_n^2,

$$s_n^2 = \frac{-k^2 \int_o^d [\mathcal{N} |\hat{\xi}_n|^2 + \epsilon(D\hat{\Phi} D\hat{\Phi}^* + k^2 \hat{\Phi}\hat{\Phi}^*)] dx}{\int_o^d [\rho_o (|D\hat{\xi}_n|^2 + k^2 |\hat{\xi}_n|^2)\, dx} \tag{21}$$

Terms on the right are real, and it therefore follows that s_n^2 is real. Moreover, because terms in the denominator are positive definite, as is $k^2|\hat{\xi}_n|^2$ in the numerator, it is clear that if $\mathcal{N}$ is everywhere positive, the eigenmodes are all stable:

$$\mathcal{N} \equiv E_o D q_o - g D \rho_o > 0 \tag{22}$$

Similarly, if $\mathcal{N}$ is everywhere negative, the eigenmodes have an exponential dependence, half of them decaying and half of them growing in time.

Using the weak inhomogeneity imposed-field approximations, the eigenfrequencies follow from Eq. 10 where this time k is a given real number. These are shown as a function of $\underline{k}$ in Fig. 8.18.5. According to this model, in the unstable configuration ($\mathcal{N} < 0$) the n = 1 mode is the most rapidly growing.

It is worthwhile to make a comparative study of the discretely and smoothly stratified charge layers. The condition of Eq. 22 plays a role relative to the smoothly inhomogeneous system that is played by Eq. 8.14.25 for the piecewise homogeneous system of Sec. 8.14.

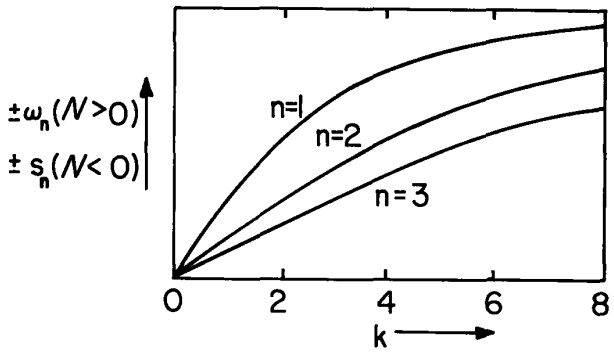

Fig. 8.18.5

Weak-gradient imposed-field eigenfrequencies of temporal modes as a function of wave number. For $N > 0$, all modes are stable and purely oscillatory. For $N < 0$, they are either exponentially growing or decaying with time.